KINESIN: DIRECTIONAL PROPERTIES, STRAIN COORDINATION AND NANOTECHNOLOGY APPLICATIONS

by

Ming-Tse Kao

A dissertation submitted in partial fulfillment
of the requirements for the degree of
Doctor of Philosophy
(Biomedical Engineering)
in The University of Michigan
2009

Doctoral Committee:

Professor Edgar Meyhöfer, Chair
Associate Professor Alan J. Hunt
Associate Professor Katsuo Kurabayashi
Associate Professor Shuichi Takayama
Associate Professor Kristen J. Verhey

To Jiayin and Selina

ACKNOWLEDGEMENTS

I would like to take this opportunity to express my appreciation to all the people who help me during the years for prosuing my Ph.D degree in the University of Michiagn.

As an engineer in semi-conductor industry for several years, I have never though that I will come back to school again until I studied the properties of proteins. With high throughput, higt selivity and property of self assembly, proteins are amazing machines for an engineer. I started my journey in the United State and would like to study motor proteins which, as I considered, have more similarities to eengineering machines than any other proteins. I would like to thank my advisor, Dr. Edgar Meyhöfer, who brough me into this whole new world of studying molecular motor kinesin. Beside the experimental details, he trained me the way of scientific thinking and taught a lot of knowledge of ethics in science field.

In my early years in the University of Michigan, I worked with several groups for designing molecular motor powered devices. It is a very interesting experience to combine my previous knowledge of micro-fabrication and the new skills in kinesin motors. From the discussion with my cocowkers, I learned a lot in the integrating technologies and have a good time to work with them. I would like to thank Dr. Chih-Ting Lin, Dr. Katsuo Kurabayashi, Dr. Li-Jing Chen, Dr. L. Jay Guo, Dr. Taesung Kim and Dr. Ernst F. Hasselbrink.

I would like to thank Dr. Dawen Cai and Dr. Kristen J. Verhey who helps me a lot when I encounter problems on biology field which I am not samiliar with. They enrich me with the knowledge of cell biology. They are always my emergency supplier for my experiments.

I am thankful to many students in my group, who have helped me in many aspects. Special thank to Dr. Stefan Lalämper who tougsht me the molecular cloning technique such that I have an opened new window on my cuerrent and future work.

I would like to express my special thanks to my committee members, Dr. Edgar Meyhöfer, Dr.Katsuo Kurabayashi, Dr. Alan J. Hunt, Dr. Shuichi Takayama and Dr. Kristen J. Verhey fro their advices on my current work.

Finally, I would like to thank my wife, Jiayin Li. With her company, my journey has turned to a much more colorful one.

TABLE OF CONTENTS

LIST OF FIGURES

LIST OF TABLES

ABSTRACT

Kinesin motors are nanometer-scale biological motor proteins that evolved for a range of biological transport functions in cells. They move along microtubules, long filaments that are part cell's cytoskeleton, by hydrolyzing ATP. The small size and robustness of movement *in vitro* provide tremendous advantages for using kinesin in engineering application compared to many artificial motors. Moreover, kinesin's efficiency and ability to readily utilize chemical energy from their ambient environment simplify microdevice design and eliminate the requirement of large external power supplies. In this dissertation, I present three micro- and nano-devices into which kinesin motors are integrated. Two of the devices efficiently rectify the mechanical power produced by multiple kinesins into designated directions by mechanically guiding the movement of microtubules with micro- and nano-structures. The third device leverages the previously developed techniques of directioning the motion of microtubules and integrates antibody to achieve highly sensitive bio-molecule sorting. These devices demonstrate that kinesin-powered devices are practical and have significant potential for future applications in modern microfluidic devices.

To enhance future technological application, it is important to understand the molecular mechanisms of kinesin. Kinesin has been intensively studied for decades; however, many of the detaileds of its molecular mechanisms remain poorly understood.

One major gap in our understanding relates to the mechanism(s) that control the direction of movement of kinesin motors along microtubules. Regardless of the structural similarity of the head domain, the structural domain for force production and energy transduction, kinesins with head domain in N-terminus (N-terminal kinesins) are microtubule plus-end directed motors. C-terminal kinesins on the other hand, which have their head domain at the C-terminal end, are minus-end directed kinesins. Here, I used mutagenesis to investigate which structural domains determine the directionality of conventional kinesin and Ncd, the two major kinesin models most frequently used for directionality studies. The result suggests that structural components that control kinesins' directionality are also directly involved generating the motor's motility. Therefore, it is challenging to alter kinesins' directionality and simuteneously keeping their motility intact. My data are consistant with a model where both kinesin and Ncd use components close to their head domains for controlling their directionality: the structural components that may control kinesins' direction are neck-linker and C-terminal neck domain for plus-end directed kinesin and minus-end directed kinesin, respectively.

An important physiological property of conventional kinesin is its ability of single motor molecules to take a large number of uninterrupted, sequential steps along the surface lattice of the microtubule without detachment. This processive hand-over-hand motion is believed to be based on a coordinated, alternate catalysis of the two head domains. One frequently cited hypothesis postulates that this coordination is based on intra-molecular mechanical strain. However, little work has directly investigated the

intra-molecular strain coordination of kinesin's processive movement. To test this intra-molecular strain hypothesis I inserted a set of flexible residues at the junction between kinesin's neck domain and neck-linker. The single molecular motor gliding assays show that the wild-type and mutated kinesins move in vitro with the same velocity, but the run lengths of mutants decrease. These biophysical properties of these kinesin mutants suggest that the strain coordination mechanism is not essential and kinesins may use different mechanism(s) other than the mechanical strain to coordinate their processive movement.

CHAPTER 1

INTRODUCTION

1.1 Kinesin

1.1.1 Molecular motors

Molecular motors or motor proteins are poly-peptide which can convert chemical energy to mechanical work inside the cells. Because of this unique property, they are responsible for various mechanical roles in living organisms. For example, the F_0F_1-ATPase, a rotary motor, consists of 12 different types of polypeptides and can convert the energy of a proton ion gradient to mechanical work which in turn is used to form a high energy molecule ATP. Kinesin-1, a linear motor, has 4 polypeptide chains and uses the energy available from the hydrolysis of ATP to transport organelles inside the cells. For an engineering or mechanical point of view, these motors can be divided into rotary motors and linear motors. For instance, the F_0F_1-ATPase is a torque generating rotary motor while the kinesin and myosin are linear motors because they move unidirectionally along their substrates, and do not generate torque or rotary motion. The other difference between the rotary motors and linear motors is that linear molecular motors move or produce force on their own substrate. One example of linear

motor is DNA polymerase, it moves along a DNA template strand to synthesize a complementary copy. Another example is myosin, a large family of motors which are involved in the transport of cargos along actin filaments and the production of contractile forces in the muscle cells. Among these linear molecular motors, three types of motor, known as cytoskeletal motors, use cytoskeleton as their substrate and have similar functions; they are actin-based myosin motors, and microtubule-based kinesin and dynein motors. All of these three motors are responsible for different kind of intracellular transportation and force production. For instance, myosin II can produce force in muscle fibers and cause muscle contraction(Fujiwara and Pollard, 1976; Mabuchi and Okuno, 1977; Robinson and Spudich, 2004) whereas myosin V is responsible for secretory vesicle transportation(Johnston et al., 1991; Schott et al., 1999). Another motor, kinesin, for example, kinesin-1 and kinesin-2 have function on intracellular transportation(Aizawa et al., 1992; Cole et al., 1993; Hirokawa and Noda, 2008; Kondo et al., 1994) and Eg5, a kinesin from kinesin-5 family, can produce force to establish and maintain bipolar spindle(Cochran et al., 2004).

1.1.2 Kinesin

Among the cytoskeletal motors, the members of the kinesin family have the simplest structure as indicated by its smaller size, lower molecular weight and apparent fewer components compared to other families. The first kinesin was discovered only 2 decades ago from the transporting of squid giant axon(Allen et al., 1982; Brady, 1985; Brady et al., 1982; Vale et al., 1985a; Vale et al., 1985b; Vale et al., 1985c; Vale et al.,

1985d). This kinesin is generally referred to as conventional kinesin and belongs to kinesin-1 family(Brady, 1985; Lawrence et al., 2004; Vale et al., 1985a). After systematic search using ATP binding and microtubule binding consensus sequences, kinesin antibodies and bioinformatics tools, about hundred different kinesins were identified, and based on their structures, they are now categorized into 14 families (Lawrence et al., 2004).

1.1.3 The functions of kinesin

The function roles of kinesin motors inside cells are wildly assumed to be related to organelle and molecular transport and movement and force generation in mitosis. The members of kinesin superfamily which are responsible for intracellular transport are kinesin-1, kinesin-2, kinesin-3, kinesin-4 and kinesin-6 whereas kinesin-4 and kinesin-6 also participate in mitosis. The other kinesin families, in contrast, all have function in mitosis(Hirokawa and Takemura, 2004). For example, members of Kinesin-1 family are responsible for transporting organelles and macromolecular complex, such as mitochondria(Tanaka et al., 1998), lysosomes(Hollenbeck and Swanson, 1990; Nakata and Hirokawa, 1995), tubulin oligomers(Terada et al., 2000), mRNA complex(Brendza et al., 2000; Carson et al., 1997) while members in kinesin-2 family transport vesicles and macromolecules in axons of mammalian neurons(Takeda et al., 2000) and play important roles in the molecular assembly of cilia and flagella (Cole, 1999a; Cole, 1999b; Cole, 2005; Cole et al., 1998). On the contrary, kinesins from kinesin-5 and kinesin-13 families are important in mitosis where they generate

forces or movement to position anti-parallel microtubules(Bannigan et al., 2007; Kapitein et al., 2005; Sharp et al., 1999).

1.1.4 Kinesin and diseases

As mentioned above, member of kinesin family are mostly responsible for intracellular transport and mitosis. Consequently, kinesin related diseases can be classified as intracellular transportation malfunction, non-physiological cargo transportation and disease linked to uncontrollable cell proliferation(Goldstein, 2001; Mandelkow and Mandelkow, 2002). One example related to intra-cellular transport malfunction of kinesin is Charcot-Marie-Tooth (CMT) 2A disease. The cause of CMT is that KIF1B, a member of kinesin-3 family, is mutated in its motor domain, and synaptic vesicle precursors are not properly transported to the required synaptic termini. This malfunction leads to a progressive atrophy of distal muscles(Zhao et al., 2001). Another example is relevant to kinesin-2 which is responsible to supplying protein component for cilia and flagella(Goldstein, 2001; Hirokawa, 2000; Pazour and Rosenbaum, 2002). Defect in kinesin-2 related transport cause polycystic kidney disease by affecting sensory cilia in the kidney(Qin et al., 2001), retinitis pigmentosa in which the transport for photoreceptors is malfunctioning(Marszalek et al., 2000) and Kartagener's syndrome is characterized by abnormal sperm flagella, bronchial cilia and nodal cilia(Marszalek et al., 1999; Nonaka et al., 1998).

The second category of kinesin linked disease is non-physiological cargo transport. This non-physiological cargo transport involves certain viruses, bacteria or parasites. These pathogens hijack kinesin-dependent transport system to transport their

compartment back to cell membrane(Sodeik, 2000). For example, vaccinia requires kinesin-1 motor to transport viral protein A36R(Rietdorf et al., 2001), and herpes viruses interact with kinesin-1 for long distance transport from cell body to axon terminals(Diefenbach et al., 2002). The third category of kinesin-related diseases is uncontrollable cell proliferation. The uncontrollable cell proliferation or cancer requires multiple mitosis steps to duplicate the cells. It is clear that number of kinesins involve in mitosis (Bannigan et al., 2007; Kapitein et al., 2005; Sharp et al., 1999); therefore, one possible strategy to treat such cancers is to develop drug that target kinesin for chemotherapy. For example, the compound adociasulfate-2 can block kinesin-dependent motility and mitosis(Sakowicz et al., 1998) whereas another compound, monastrol, can inhibit Eg5, a member of kinesin-5 group of motors, and cause defect in cell division(Kapoor et al., 2000). Since these molecules can inhibit or modulate kinesin's function, they offer significant potential for future clinical applications.

1.1.5 The structure of kinesin

Common to all kinesins is its head domain which consists of about 320 amino acid residues. The head domain has a nucleotide binding pocket and a microtubule binding site. The nucleotide binding pocket binds ATP and hydrolyzes it in this pocket whereas the microtubule binding site allows kinesin to bind in a stereo-specific manner to microtubules in order to produce directed forces and movement(Woehlke et al., 1997). Thus, the head domain is the force generate domain and truncated kinesins from which all but the head domain has been eliminated can convert energy from ATP to mechanical power without the interaction of other domains(CHAPTER 3). Besides, the

position of the head domain classifies kinesins into three categories: N-terminal motor, C-terminal motor and M-kinesin. The N-terminal motor has kinesin's head domain in the N-terminal of poly-peptide; the C-terminal motor's head domain is in the C-terminus of the peptide; in M-type kinesins, the head domain is located between two ploy-peptides(Hirokawa and Noda, 2008). One interesting observation with regard to these three classes of motors is that all N-terminal motors are plus-end directed motors whereas all C-terminal motors are minus-end directed(Woehlke and Schliwa, 2000a).

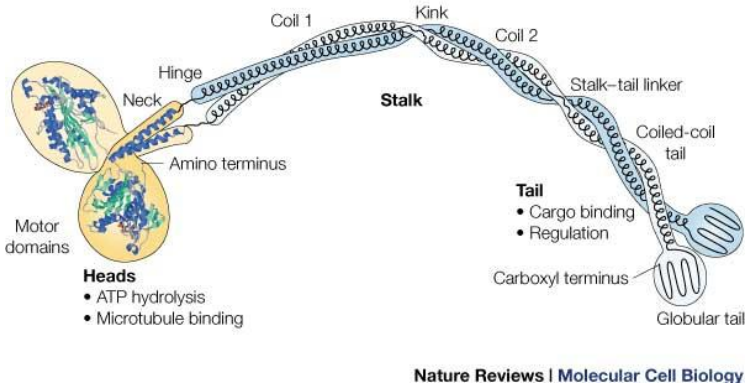

Figure 1-1: Structure of kinesin heavy chain (KHC) of conventional kinesin. Conventional kinesin is a tetramer consisting two kinesin heavy chains and two kinesin light chains (KLC). Each kinesin heavy chain has a head domain in its N-terminal following by a coiled-coil neck domain and a stalk domain. A tail domain extended from stalk domain C-terminally. The kinesin light chains binding to the tail domains of KHC forms a kinesin tetramer. Picture is taken from Woehlke and Schliwa(Woehlke and Schliwa, 2000b).

The first kinesin, convention kinesin, is an N-terminal motor(Kozielski et al., 1997; Vale et al., 1985a). Conventional kinesin is a heterotetramer(Figure 1-1). It has two kinesin heavy chains (KHC) and two kinesin light chain (KLC). The KHC has a head domain in its N-terminus, a coiled-coil neck domain and a stalk domain extended

C-terminally from its head domain and a tail domain in KHC's C-terminus. This coiled-coil neck domain and stalk domain dimerize two kinesin heavy chains such that kinesin becomes a functional dimer with two head domains. Besides its role in dimerization, it has been suggested that the neck domain interacts with the microtubule increase the distance that individual kinesin motors move along microtubules(Thorn et al., 2000)and increase the speed of movement(Kallipolitou et al., 2001). The stalk domain contains several flexible hinge structures which facilitate the interactions of the tail domain of KHC with the head domain(Coy et al., 1999a; Wong et al., 2009). The tail domains are located C-terminally from the stalk domain and interact with the head domain and inactivate the catalytic activity of kinesin. This inactivation is a physiological adaption of kinesin to prevent futile consuming of ATP(Coy et al., 1999a; Wong et al., 2009). Each tail domain binds to a light chain (KLC). There is significant evidence that the light chains bind scaffolding proteins, JIPs, to facilitate kinesin's cargo binding(Verhey et al., 2001).

1.1.6 Properties of kinesin:

Kinesin is a force generating enzyme and can directly transform chemical energy (ATP) to mechanical work. Kinesin-1 (from animal cells) has speed about 0.3-0.8 μm/s which is the unloaded speed of kinesin measured in multiple motor kinesin gliding assay (Howard et al., 1989), optical tweezers experiments (Svoboda et al., 1993) and single kinesin gliding assay (Funatsu et al., 1997).

In addition, biochemical measurements indicate that Kinesin-1 has a maximal turnover rate about 40 ATP molecules per head per second in the presence of

microtubules (k_{cat}= $40s^{-1}$) (Hackney, 1995; Jiang et al., 1997). For wild type Kinesin-1, because it is dimeric motor, this means that it will turnover approximately 80 ATP per molecule per second. Considering that the step size of Kinesin-1 is about 8nm (Coppin et al., 1996; Hua et al., 1997; Ray et al., 1993; Schnitzer and Block, 1997; Svoboda et al., 1993), and that Kinesin-1 takes one step per each ATP molecule it hydrolyzes (Coy et al., 1999b); Kinesin-1 has a predicted speed about 0.64 μm /s which is consistent with the speed measurements from *in vitro* gliding experiments.

Furthermore, the force generated by kinesin is about 5-7 pN *in vitro* experiments (Hunt et al., 1994; Kojima et al., 1997; Meyhofer and Howard, 1995; Schnitzer et al., 2000; Svoboda and Block, 1994; Svoboda et al., 1993; Visscher et al., 1999)which can easily overcome the drag force produced by moving micro size beads(Block et al., 1990; Gelles et al., 1988) and, thus, kinesin is well adapted for its proposed cellular transport roles and it becomes a motor suitable for power micro- and nanotechnology applicatrions to power micro devices(Bull et al., 2005; Clemmens et al., 2004; Hess et al., 2004a; Hess et al., 2005; Hess and Vogel, 2001; Ionov et al., 2005; Jia et al., 2004; Li-Jing Cheng 2005; Nitta and Hess, 2005; van den Heuvel et al., 2005a; van den Heuvel et al., 2005b).

In each diffusional encounter with a microtubule, from biochemical in solution measurement, each kinesin turns over about 120 to 200 ATP molecules (Gilbert et al., 1995; Hackney, 1995; Jiang et al., 1997) which also suggests that the processivity is larger than hundred steps for moving along a microtubule (Asbury et al., 2003; Funatsu

et al., 1997; Lakamper et al., 2003; Vale and Milligan, 2000; Yildiz and Selvin, 2005; Yildiz et al., 2004)

1.1.7 Kinesin and nanotechnology

Kinesin is a biological machine that evolved to handle the cell's nano- and microscale transport challenges. Interestingly, kinesin's nano-meter size, easy accessibility to its energy source, ATP, from ambient environment, high thermodynamic efficiency and self-assembly properties also give it tremendous advantages in engineering applications compare to any artificial motors. Therefore, several research groups have focused on the integration of kinesin-microtubule system with micro-devices(Clemmens et al., 2003b; Dennis et al., 1999; Hess et al., 2004b; Hess et al., 2002; Hess et al., 2003; Ramachandran et al., 2006; Stracke et al., 2002; van den Heuvel et al., 2005c; van den Heuvel et al., 2006; van den Heuvel and Dekker, 2007; Verma et al., 2009; Yokokawa et al., 2004). Since the force produced by single kinesin is insufficient to overcome the inertia, friction or drag associated with many of the current micro-devices, a large number of motor molecules must be integrated into the devices such that they can work collectively to overcome the mechanical challenges in micro-device applications. One simple solution for arranging a large number of kinesins for productive interactions with microtubules is to essentially utilize multiple motor kinesin gliding assay. In this assay kinesins in bound to the surface of the test chamber in a high density in such a way that multiple motors can bind and productively interact with a single microtubule and support high fidelity motion of this microtubule. However, the direction of moving microtubule is not unique which is not efficient for

artificial devices; therefore, controlling the moving direction of the microtubules inside the micro-devices is essential for such kinesin based device application. Several studies have shown that the moving direction of the microtubules can be successfully controlled by nano- and micro-structure and external fields(Kim et al., 2007a; Kim et al., 2008; van den Heuvel et al., 2006). In some cases there device configurations have now been advanced to the point where they could be successfully used for first proof-of –concept applications in biomolecules detection and sorting devices(Bachand et al., 2006; Fischer et al., 2009; Jia et al., 2004; Lin et al., 2006; Ramachandran et al., 2006; van den Heuvel et al., 2006; van den Heuvel and Dekker, 2007).

1.2 Overview

The work presented in this dissertation summarizes my research in integrating kinesin motors into engineering applications and fundamental studies of kinesin's functions. Integrate kinesin motors into engineering devices, as mentioned before, could provide sophisticate power to drive devices while more fundamental knowledge of molecular motors can be obtained by using technological devices as platforms. Moreover, more scientific knowledge of kinesin's functions will not only provide the understanding of nature's design on molecular motors but also promote future enhanced technological applications.

In Chapter 2, three kinesin-based micro- and nano-technology devices are presented. One of the micro-devices is a circular microfluidic channel which can rectify more than 90% of the microtubules to a unique moving direction. The other device is a nanometer-size structure of parallel barriers which can direct 99% of microtubules

moving along a designated course. These two devices show that different microstructures can efficiently control the motion of microtubules and redirect microtubule into a single direction which is essential for applying kinesin motors in nanotechnology. The third device is the kinesin-powered, high efficiency molecular sorter which incorporates previous design features to control the direction of microtubules and integrates antibodies and microscale trapping structures to achieve ultra-sensitive bio-molecule sorting. This device has an ability to sort specific analyte molecules presented in very low concentration from a complex mixture of molecules and concentrate the analyte molecules by about 2000-fold to a designated location in less than an hour. This ability indicates that this device has the potential to enhance existing bio-molecule detector, and demonstrates that the idea that integrate the kinesins into micro-engineered is practical and can have applications in modern instruments.

To enhance future technological application, it will be important to understand the molecular mechanism by which the directional movement of molecular motors is controlled. Toward this goal research summarized in chapter 3 is directed at figuring out the directional determinant of both plus-end and minus-end directed kinesins. To achieve this goal, a series of kinesin mutants was constructed. The directional properties results of these kinesin mutants and the results from previous reports, together, suggest that both plus-end and minus-end directional kinesins use structural components close to their head domains to control their directionality. For plus-end directed kinesin like conventional kinesin, it is the neck linker that may direct kinesin's

hand-over-hand movement toward the plus end. On the contrary, the head-proximal end of the neck domain may control the direction of minus-end directed kinesin Ncd. This finding provides not only the information on control of kinesins' directionality, but also illustrates additional detail on the motile mechanism in general.

During recent years, the mechanism of kinesin's processive movement has become a hotly contested research problem. Most of researchers hypothesized that a coordination mechanism should exist between two heads of the processive kinesins and this mechanism should be a mechanical force or strain. However, little work has been directed at directly investigating this strain dependence and the influence of intra-molecular force of the processive stepping kinesin. In chapter 4, the hypothesis that the strain coordinates kinesin's two heads is examined. To test the hypothesis, I constructed a set of kinesin mutants with different length of flexible inserts at the junction of the neck-linker and neck domains. The biophysical properties of these kinesin mutants suggest that this strain coordination mechanism may be not essential, and kinesin may use different mechanism(s) other than the mechanical strain to coordinate their processive movement.

Finally, in chapter 5, I will provide the conclusions of my researches and some future research directions.

CHAPTER 2

NANOTECHNOLOGY APPLICATIONS OF KINESIN MOTORS

2.1 Introduction

MEMS (Microelectromechanical system) and microfluidic devices utilize engineered microscale structures, such as tiny fluid channels, switches, cantilevers or electrodes, to integrate various advanced analytical or measurement techniques into fully functional microscale devices. More complex versions, integrating multiple devices on a single chip are frequently referred to as Lab-on-a chip (LOC), and recently significant efforts have been made to extend these technical developments to the nano-scale(Kim and Meyhofer, 2008; Lindquist et al., 2009). The general idea behind this miniaturization is that the small scale confers some superior cost and performance characteristics to this new technology that the instruments using traditional approaches do not have the ability to compete with. For example, LOC devices offer the advantages of low reagent consumption and fast response time (because of their small size), high throughput (because they are small and can be made in array form), biocompatible and low cost (ideally suited for mass production by nano- or microfabrication techniques). Although these devices *per se* are small, they require significant external equipment in

order to generate pressure and fluid motion or provide electrical power to the devices. Therefore, the complete technical solution is not small at all. Moreover, the power consumption of many devices is large for facilitating the motion, and since the devices are tiny this may causes significant heat dissipation problems. Without sufficient heat dissipating, the temperature of the devices may be so high that it exceeds the tolerance of biological systems. These challenges associated with the required power sources diminish the potential impact of MEMS and microfluidic devices.

In contrast, the nature completely avoids these problems in cellular transport systems. Here, molecular motors are responsible for powering the transport of organelles and other molecular constituents, as well as the motility and contraction of entire cells. They facilitate from several piconewton forces required vesicle transportation inside the cells to hundred tons of whale's swimming by a large number of motors collectively acting in muscle contraction. The size of these motors is much smaller (about 1,000 to 100 times smaller) than any existing MEMS or microfluidic devices; thus they can be integrated into the micro-devices. They are obviously biocompatible and they do not need any enormous external power source, because they utilize the energy of ATP present in their ambient aqueous environment. Although molecular motors have plenty of advantages for MEMS microfluidic devices, the force produced in any single molecular motor (maximally about 5 – 7 piconewtons) is insufficient to propel the motion of complete, existing micro-devices. These devices need a large number of motors to collectively work in a coordinated way. Fortunately such coordinated interactions of many molecular motors are also required in nature in

order to generate macroscopic forces. In skeletal muscle, thousands of billions of myosin II motors and actin filaments form array like structures (sacromeres) and generate forces on the order of tens to hundreds of newtons. Coincidently, the ability to arrange components into array like structure is one of the strengths of MEMS and microfluidic devices. Therefore, it should be possible to combine the desirable properties of molecular motors, and MEMS and microfluidic devices by functionally integrating molecular motors into microengineered device structures.

In this chapter, I present three major research projects that used the molecular motor kinesin in microfluidic devices. Because of the interdisciplinary research challenges of this work, I collaborated closely with other graduate students to carry out this work. I worked with Chih-Ting Lin(Kurabayashi Lab) to develop a device which can efficiently rectify the direction of movement of microtubules propelled by surface-attached kinesin motors (section 2.2). In section 2.3, I present a fluidic device that guides the motion of microtubules in nanoscale tracks (work in collaboration with Li-Jing Cheng, Guo lab). Finally, in section 2.4, I present a molecular motor--powered, molecular sorter, which uses kinesin motors to efficiently separate, sort and concentrate molecules (collaboration with Li-Jing Cheng and Taesung Kim, Hasselbrink lab).

I also participated in several other studies using kinesin to power molecular sorting and concentrating, utilizing MEMS and microfluidic devices to facilitate scientific questions related to the biophysical properties of microtubules and the external control of the directional movement of kinesin-powered microtubules. All of

these materials are published(Kim et al., 2007a; Kim et al., 2008; Kim et al., 2007b; Lin et al., 2008) and will not be described here.

2.2 Efficient designs for powering microscale devices with nanoscale biomolecular motors[1]

2.2.1 Abstract

Current MEMS and microfluidic designs require external power sources and actuators, which principally limit such technology. To overcome these limitations we developed a number of microfluidic systems into which we seamlessly integrate a biomolecular motor, kinesin, that transports microtubules by extracting chemical energy from its aqueous working environment. Here we establish that our microfabricated structures, the self-assembly of the bio-derived transducer, and guided, unidirectional transport of microtubules are ideally suited to create engineered arrays for efficiently powering nano- and microscale devices.

2.2.2 Introduction

In biological systems, cellular activities such as intercellular mass transport, cell division and various forms of cell motility and contractility are all driven by biomolecular motors. Among various biomolecular motors, conventional kinesin (now referred to as kinesin-1) holds significant potential for nanotechnology applications because it is compact (the actual motor domains are < 10 nm), efficient (~ 50%), moves

[1] Lin, C.T., M.T. Kao, K. Kurabayashi, andE. Meyhofer. 2006. Efficient designs for powering microscale devices with nanoscale biomolecular motors. *Small* 2(2):281-287.

robustly in *vitro*, and extracts chemical energy from its aqueous working environment(Brady, 1985; Vale et al., 1985d).Kinesin generates linear, stepwise motion along microtubules (a filamentous cytoskeletal polymer) toward their plus-end by alternately advancing its two motor domains in a hand-over-hand manner(Asbury et al., 2003; Yildiz et al., 2004). Each of the resulting 8-nanometer steps is coupled to the binding and hydrolysis of one molecule of adenosine triphosphate (ATP)(Hua et al., 1997).

Of particular significance for future nanotechnology applications of biomolecular motors are strategies to effectively interface with and extract sufficient mechanical power from this nanometer-scale machine. However, the force generated by a single kinesin molecule is miniscule (~ 5 - 6 pN) and needs to be scaled up to drive man-made microstructures. In nature, cells generate large forces and substantial mechanical power by utilizing highly ordered arrays of motor proteins. For example, in skeletal muscle cells myosin motors and actin filaments are precisely aligned in the nearly crystalline structure of the sarcomere to harness the collective forces (up to one hundred newton) and motion (up to 10 m/s) from a very large number ($>10^{13}$) of individual motor molecules. We need to follow nature's strategy and develop new technology to selectively pattern and functionally integrate kinesin molecules and microtubules into engineered microstructures. As the direction of motion of kinesin motors along microtubules is determined by the structure (polarity) of the microtubule and directed towards its plus-end, the most critical and challenging requirement is to uni-directionally guide, sort and align microtubules such that they can serve

simultaneously for many motors as nanoscale tracks. Accordingly, micrometer-scale structures may be driven by kinesins along such aligned microtubule tracks to generate meaningful motion and mechanical power.

Simple physical confinement of gliding microtubules by sidewalls has been demonstrated(Jia et al., 2004; Limberis and Stewart, 2000) using a linear microchannel patterned on a kinesin-coated glass substrate. Unfortunately, the guided motion in this earlier work was not uni-directional, and gliding microtubules frequently detached from the channel tracks. To achieve uni-directional microtubule sorting, Hiratsuka(Hiratsuka et al., 2001) introduced arrow-shaped structures into their microchannels and used experimental conditions to selectively adsorb motor proteins into the channels. This approach demonstrated that it was feasible to arrange microtubules by using a proper structural design, however, the design still suffered from frequent detachment of microtubule and unsatisfactory sorting performance. For instance, only about 70% of total microtubules were guided in the proper direction. To address some of these limitations, another group(Hess et al., 2003) introduced channel overhangs to reduce microtubule loss, but this technique makes it impossible for any other (microfabricated) structures to engage with the microtubules for power extraction. Yet another group(Yokokawa et al., 2004) used an external flow field to obtain uni-directional microtubule movement. While improved microtubule alignment was achieved, the method is not suitable for microscale fluidic systems or arrays because the large scale of the required external flow does not permit local control of microtubule movement. In addition, previous studies usually relied on photoresist as structural material for the

microfluidic channels. But alternative materials are more desirable as photoresist rapidly swells in an aqueous environment.

The long term goal of our work is to develop autonomous nano- to microscale transport systems that extract power from kinesin molecules and translocate microfabricated shuttle structures with molecular precision along defined pathways of complex microfluidic systems (Figure 2-1). To extract collective force and mechanical power from a group of kinesin molecules moving on microtubule tracks, the microfluidic channel design needs to allow for (i) efficient collection and retention (self-assembly) of microtubules, (ii) satisfactory uni-directional microtubule sorting, (iii) physical access to external micro-mechanical device structures or components, and (iv) stability in the aqueous environments. In this paper we present a new microfluidic channel design that meets these requirements as shown in Figure 1 (A), and on the basis of quantitative experimental observations we develop a mechanistic understanding of the guided sorting and assembly of microtubule tracks in our devices.

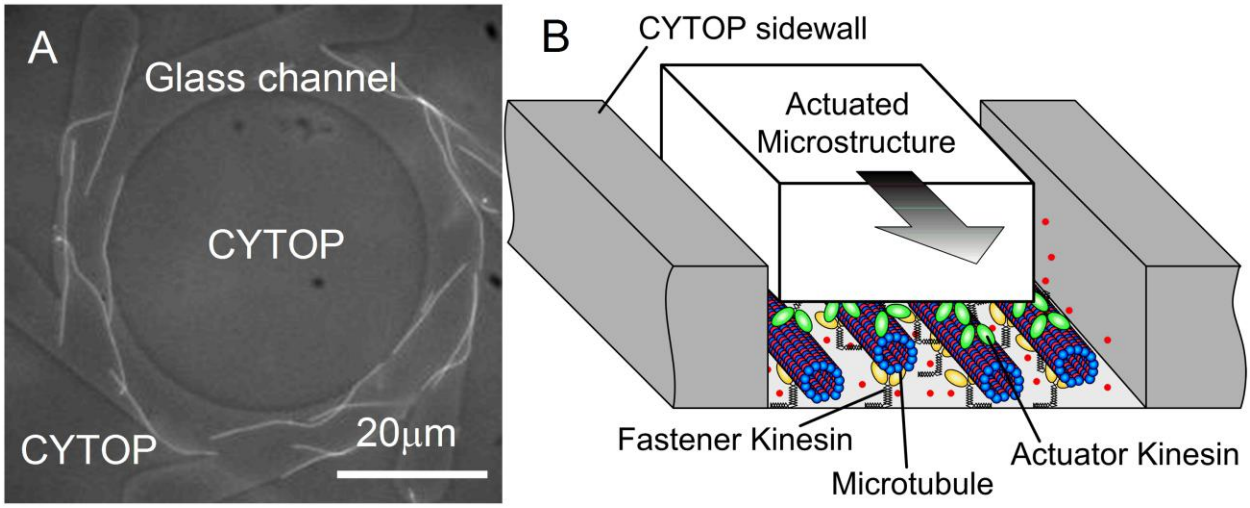

Figure 2-1: (A) Optical image of a microfluidic channel design for effective uni-directional sorting of microtubules. A fluorocarbon polymer (CYTOP) pattern forming the channel sidewalls achieves selective microtubule motility. (B) Design concept for powering microscale structures with nanoscale biomolecular motors. The fastener kinesin (yellow) is first used to align microtubules in the microfluidics channels, subsequently it is exploited to permanently immobilize, via a chemical crosslink, aligned microtubules (blue) onto the microfliuidic channel surface. The actuator kinesin (green) drives the transport of man-made microstructures by hydrolyzing ATP (red dots) from the microfludics environment requiring no external power source.

2.2.3 Results and discussions.

We used three different circular microfluidic channel designs (Figure 2-2) to study the influence of channel shape and geometry on the sorting performance. Each of the designs consists of a few micrometer-wide (5 μm for Design 1 and Design 2; 6 μm for Design 3) circular channel with differently shaped motion rectifiers, which are supposed to change the direction of motion of microtubules such that all microtubules in a channel rotate in the same direction.

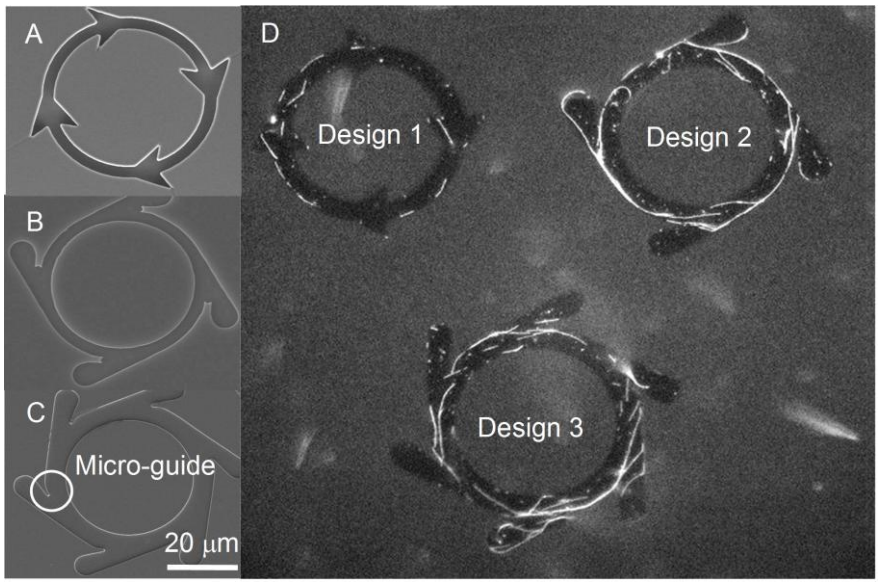

Figure 2-2: SEM images of channel (A) Design 1, (B) Design 2, and (C) Design 3. The micro-guide structure of Design 3 can be clearly shown in (C). (D) Fluorescence microscopy image of the microfluidic-channel designs operated under identical conditions in a single device structure. All three designs support uni-directional motility of sorted microtubules, but under identical conditions Design 2 and 3 contain more microtubules than Design 1.

Design 1 has four motion rectifiers with a sharp arrow-head shape. Experimental observations of the poor turning and detachment behavior of microtubules in the sharp corners of the arrow heads and theoretical predictions of the guiding of microtubules in micro-channels on the basis of a statistical mechanics model (described below) motivated Designs 2 and 3 with rounded rectifier corners to reduce the bending energy of microtubules following channel sidewalls. Design 3 has two additional rectifiers and a microstructural feature (see Figure 2-2 and Figure 2-3), which we call "micro-guide", to influence to the distribution of microtubules within the microchannel. Figure 2D shows a fluorescence light microscopy image of the three microchannel designs and

labeled microtubules during self-assembly and directional sorting. We used long image sequences of such events to characterize the functional properties of the different designs. All three microchannel designs support motility and upon sorting microtubules move, as expected, clockwise in Design 1 and counterclockwise in Designs 2 and 3.

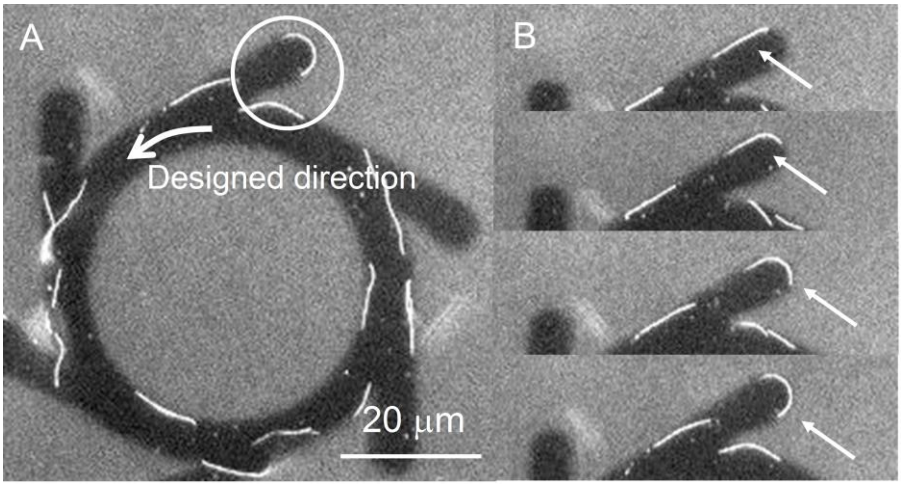

Figure 2-3: Turning of a microtubule to the designed direction in a rectifier. (A) Optical image of channel design 3; (B) image sequence of a microtubule redirected in the rectifier pattern

The total number of microtubules assembled in a channel at steady state is determined by the equilibrium between the rates of landing in and detaching form the channel. The high concentration of microtubules in the motility buffer and the large buffer volume ensure that the free microtubule concentration remains unaffected during our observations. It is therefore reasonable to assume that the landing rate of microtubules, *k* (the number of microtubules landing and moving inside the entire channel surface per unit time, number per minute) stays constant throughout the sorting process.

Following this assumption, the governing equation for the total number of microtubules as a function of time, $N_{MT}(t)$, is given by

$$\frac{dN_{MT}(t)}{dt} = k - pN_{MT}(t) \tag{1}$$

where p (min^{-1}) is the microtubule detachment probability per unit time. The solution to Eq. (1) is

$$N_{MT}(t) = \frac{k}{p}\ 1 - \exp(-pt) \tag{2}$$

Obtaining the two rates k and p from experimental data allows us to quantitatively assess the performance of each channel design. Figure 4 shows how the number of the microtubules collected in the channel and the fitted theoretical curves change as a function of time for each design. For reference, the same measurements were performed for an unprocessed bare cover glass surface. We included only microtubules longer than 1.5 μm in length in this analysis to avoid double counting, as some of the shorter microtubules are fragments detached from much longer microtubules moving in the microfluidics channel.

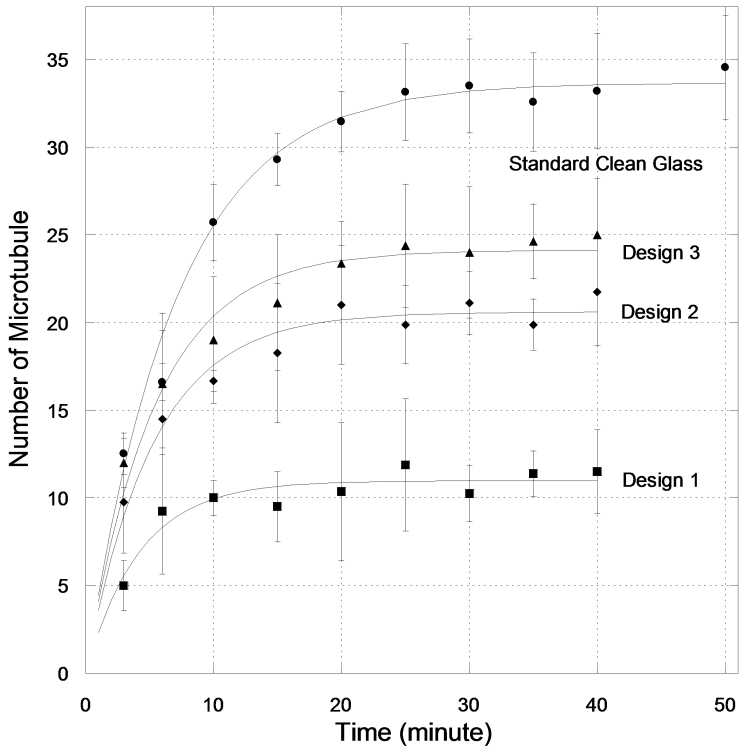

Figure 2-4: Total number of microtubules gliding within the different micro-channel designs as a function of time during the sorting process. The dashed lines show theoretical curves obtained from Eq. (2) with the key parameters fitted to the experimental data.

The experimentally measured landing and detachment rates for each design are summarized in Table 1. The larger initial slopes of the curves for Designs 2 and 3 are consistent with their higher microtubule landing rates. The larger landing rate and lower lift-off probability of Designs 2 and 3 explain the larger number of collected microtubules at steady state.

Table 2-1: Landing and lift-off rates measured for more 160 samples of the various channel designs and cover glass surfaces. We expect landing and detachment rates on flat, geometrically unconstrained cover glasses to represent (optimal) reference rates. Parameters for cover glass were normalized to an equivalent surface area as compared to the microfluidic channel designs.

	Design 1	**Design 2**	**Design 3**	**Cover glass**
landing rate *k* (number·min^{-1} per channel)	**2.601 ±0.378**	**3.948 ±0.333**	**4.483 ±0.376**	**4.787 ±0.155**
detachment rate *p* (min^{-1} per channel)	**0.237 ±0.038**	**0.1916 ±0.018**	**0.1858 ±0.018**	**0.1422 ±0.005**
The difference of landing rate *k* (compared to cover glass)	**-2.186**	**-0.839**	**-0.304**	**0**
The difference of lift-off rate *p* (compared to cover glass)	**0.0813**	**0.0345**	**0.0348**	**0**

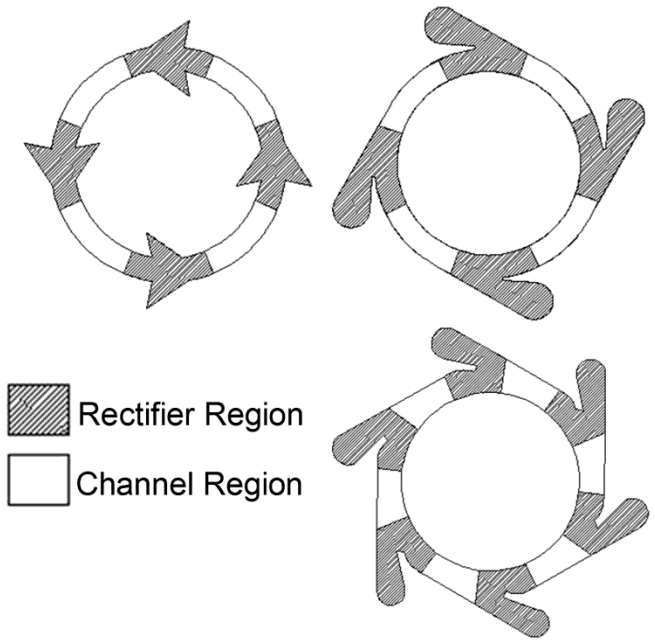

Figure 2-5: Rectifier and channel regions as defined by the angular symmetric configuration of the different designs.

To understand the detailed mechanisms responsible for the above results, we divide our microchannel structures into a rectifier region and a circular channel region as illustrated in Figure 2-5. Figure 2-6A compares the microtubule landing events measured for these regions. It is clear that landing events occur more frequently in the rectifier region. Figure 2-6B shows a particular microtubule landing event at the wider channel area near the *Y*-shaped junction between the rectifier pattern and circular channel of Design 3. We repeatedly observed that landing primarily occurred in this part of the channel. Also, the wider channel cross section of Designs 2 and 3 in the rectifier portion is responsible for the higher landing rate of these designs. This can be understood by calculating the probability of a microtubule landing and moving in the different micro-channel designs. Assuming that microtubules behave as rigid rods (a

reasonable assumption as the persistence length of a microtubule is several millimeters), randomly diffusing into the channel from solution and move upon contact with the kinesin-coated floor (but not the CYTOP sidewalls), a wider channel provides more incident directions for a microtubule with less geometric constraint, leading to a higher local landing probability. Our simple calculations predict, in agreement with the experimental observations, that the landing rate in the rectifier region of Design 2 is about 2-fold higher than that of Design 1. As Design 3 offers the least geometrical constraints for microtubules to diffuse into this micro-channel we predict landing rates that are about 1.5-fold higher than those of Design 2.

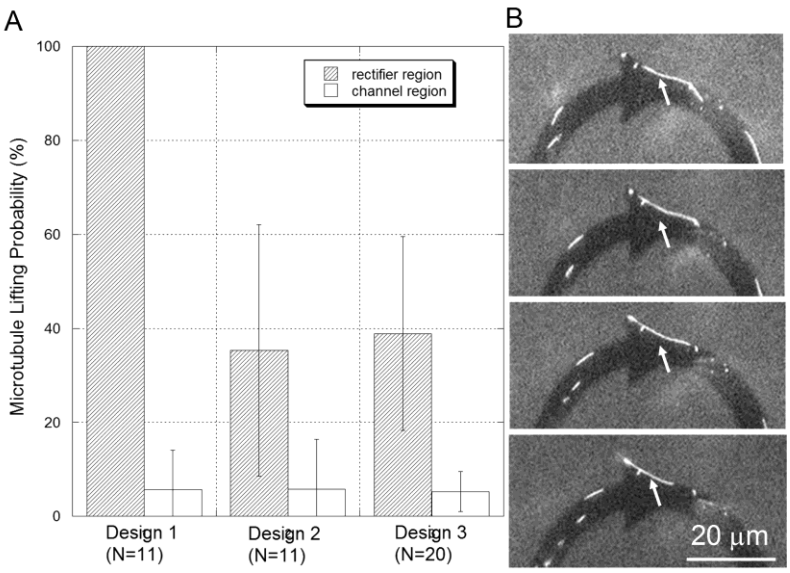

Figure 2-6: (A) Experimental data showing the distribution of landing events in the channel and rectifier regions of the different channel designs. The wider local channel areas of Designs 2 and 3 are result in the higher landing ratio. Design 1 does not have any locally wider channel area. (B) Microtubule landing sequence near the rectifier pattern of Design 3 channel

In addition to the landing rate, the number of microtubules in our microfluidics devices is decisively influenced by the detachment or lift-off of microtubules. Figure 2-7A summarizes our experimental observations on microtubule detachment events observed in the rectifier and circular channel regions of the three designs. Clearly, lift-off events most frequently occur in the rectifier region and are directly related to the mechanical guiding of the microtubule by the channel sidewall. To quantitatively understand the detachment of microtubules from the microfluidics channel we developed a (statistical mechanics) model that computes the probability of microtubule detachment.

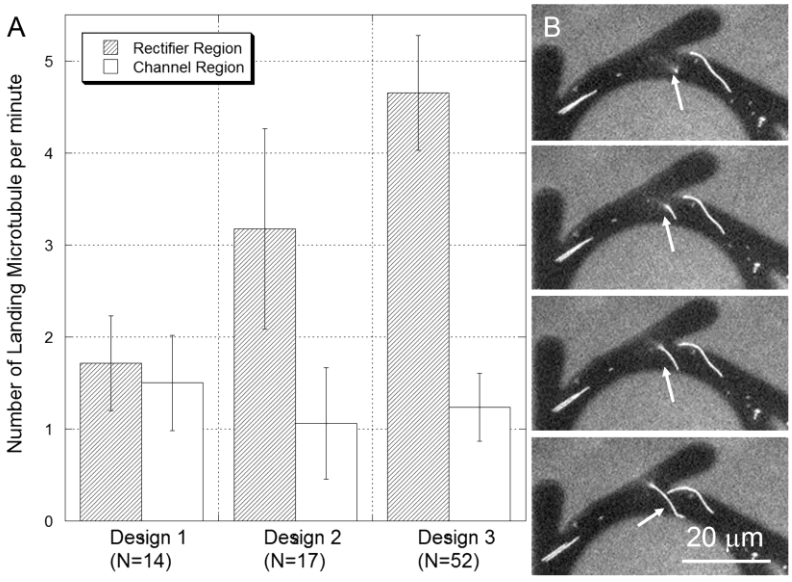

Figure 2-7: (A) Experimental data showing the microtubule detachment probability in two channel regions for various channel designs. The probability was calculated from detaching and total number of microtubules in specific region. The majority of the detachment events occurred in the rectifier region because of the large bending energy required for the microtubule to turn in the region. It should be noted that the detachment probability of the Design 1 rectifier region is 100%, because an extremely large bending energy is needed to guide microtubules along

this structure. (B) Microtubule detachment sequence at the sharp edge of the rectifier patter of Design 1 channel.

During normal gliding on the bottom surface of the microfluidic channels microtubules are prevented from detaching by kinesins that maintain continuous physical contact with the microtubules as they are pushed forward. When microtubules encounter a sidewall during the gliding process they are mechanically redirected and locally bent to accept the shape (bending angle θ) of the sidewalls. The energy for this process is provided by the cumulative action of many kinesin molecules leading to potentially large mechanical bending energy storage in the microtubule. In our model detachment will occur if the bending energy of the microtubule exceeds the binding energy of the kinesin-microtubule complex. We presume that microtubules are elastic rods guided by channel sidewalls with a perfectly smooth surface. When bending occurs, each microtubule stores energy given by(Clemmens et al., 2003a; Clemmens et al., 2003b; Hess et al., 2002):

$$U = \frac{EI}{2L}\theta^2 \tag{3}$$

where E is the Young's modulus of the microtubule, I is the moment of inertia of the microtubule, L is the length of the microtubule, and θ is the bending angle determined by the local channel curvature. Assuming a flexural rigidity EI of 1.9×10^{-24} N-m^2 (Felgner et al., 1996), an average spacing of functional kinesins of 100 nm and a kinesin-microtubule binding energy of half of the free energy of ATP hydrolysis

(~$50x10^{-21}$J), our calculations predict microtubule bending energies of 1.05×10^{-17} J, 9.26×10^{-20} J , and 8.42×10^{-21} J for a microtubule following the rectifier of design 1, the rectifier of designs 2 and 3, and the circular channel region respectively. Because of the sharp turning angle in the rectifier of Design 1, the bending energy for a microtubule to follow the sharp channel shape is much larger than for the others design, and it is also much larger than the energy available from the hydrolysis of ATP (about 5×10^{-20}J) during the stepwise motion of kinesin. We expect that the large bending energies in the microtubules could be generated by the concerted action of many kinesin, but during the mechanical interaction of the microtubule with the CYTOP sidewall this large bending energy inevitably leads to an upward directed force component. This unzippers the microtubule from kinesins at its leading end, because the bending energy of the microtubule is much larger than the maximum binding energy available from a single kinesin-microtubule interaction, resulting in the extremely high lifting probability in the arrow-shaped region. Consequently, our model predicts, that microtubules will not be able to turn in the sharp corner of the design 1 rectifier, there is a small, but significant detachment probability in the round rectifier of designs 2 and 3, and a very low detachment probability when a microtubule follows the channel region of the tested devices. These predictions are in good agreement with our experimental data (Figure 2-7, Table 1) suggesting that our model is well suited to predict the microtubule detachment behavior and should be used to guide design improvements of future devices.

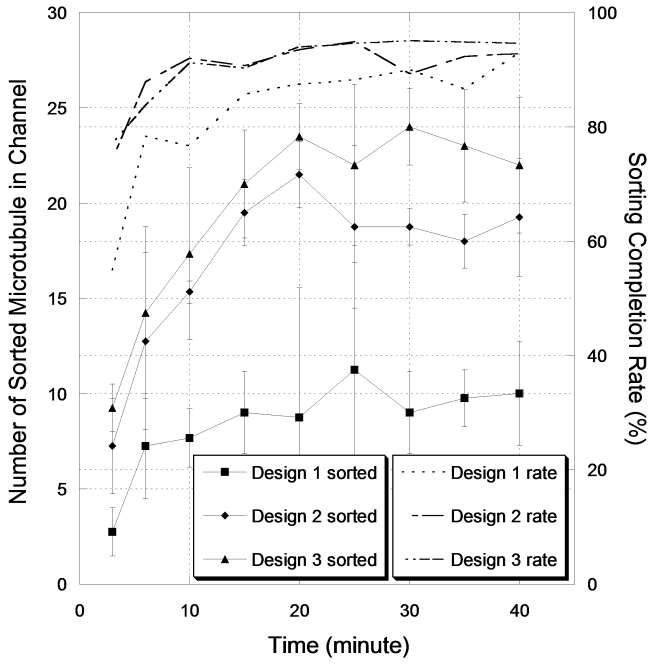

Figure 2-8: Time dependence of the total number of sorted microtubules and sorting ratio for various channel designs. All of the channel designs achieve a 90% sorting ratio after 25 minutes. The actual number of the sorted microtubules for Design 1 is much smaller than those for Designs 2 and 3.

Next, we have studied how many microtubules among those captured are uni-directionally sorted in these channels. Figure 2-8 shows the number of microtubules gliding in the designed direction and the ratio of sorted microtubules as functions of time for each design. This process reaches steady state after about 25 minutes achieving sorting ratio slightly above 90% regardless the design. While there is no obvious difference in the time variation of the sorting ratio among the designs, the largest number of sorted microtubules is always achieved in the same amount of time by Design 3. At steady state, both the landing and detachment of microtubules continues to occur while the total number of microtubules in the microfluidic channel stays

constant. Some of the (previously) sorted microtubules escape from the channel while new microtubules from solution land in the channel and of which initially one half glide in the reverse direction. As a result, the steady-state sorting ratio never reaches 100%. In a control experiment we removed the free microtubules by washing with a buffer solution without microtubules and repeated the above experiment (Design 3). Under these conditions we achieve sorting ratios of > 98%, consistent with our previous conclusions.

Finally, we have examined the spatial distribution of the sorted microtubules across the channel for each design. The gliding microtubules tend to approach the outer channel sidewall. This can also be explained by considering the bending energy state of the gliding microtubules. The gliding along the outer channel sidewall results in a minimum bending curvature, thus providing the lowest energy path for the microtubules. However, our future goal is to extract mechanical power from sorted microtubules. This requires the microtubules to engage with other external microscale mechanical components. For this purpose, a design leading to a uniform cross-channel microtubule distribution is highly desirable. To redirect the microtubules away from the outer channel sidewall, we introduced the micro guide structure as shown in Figure 2-9A and Figure 2-9B to channel Design 3. Due to its inwards-oriented curved shape, this structure redirects gliding microtubules towards the inner channel sidewall (Figure 2-9C). Figure 10 shows the cross-channel spatial distribution of microtubules at various times. It clearly shows that the distribution remains fairly uniform in Design 3 while the two other designs exhibit a larger number of microtubules near the outer channel

sidewall as time increases. This result indicates a significant impact of the micro-guide structures on the resulting cross-channel microtubule distribution.

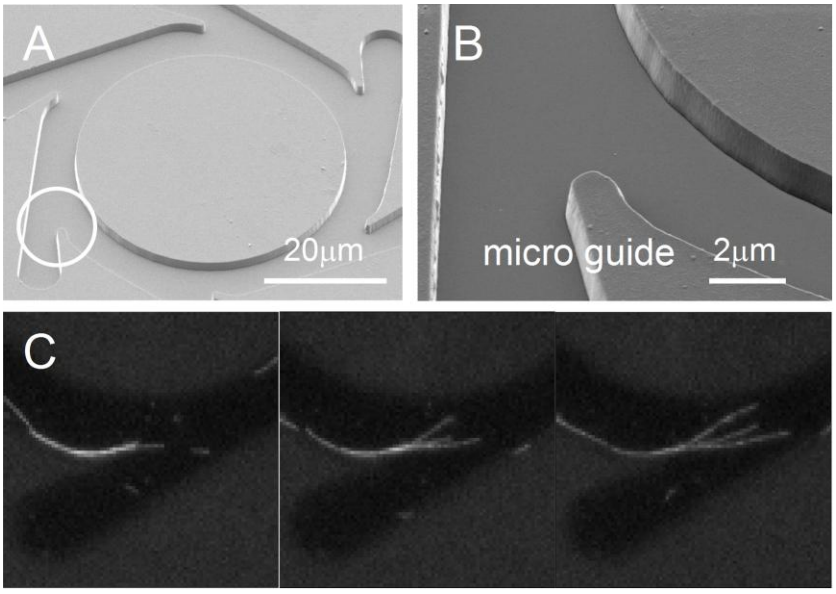

Figure 2-9: (A) SEM pictures of a design 3 microfluidic channel. (B) Micro-guide structure in the channel of a design 3 device. (C) Sequential optical images illustration the redistribution of microtubules within the micro-channel by the micro-guide.

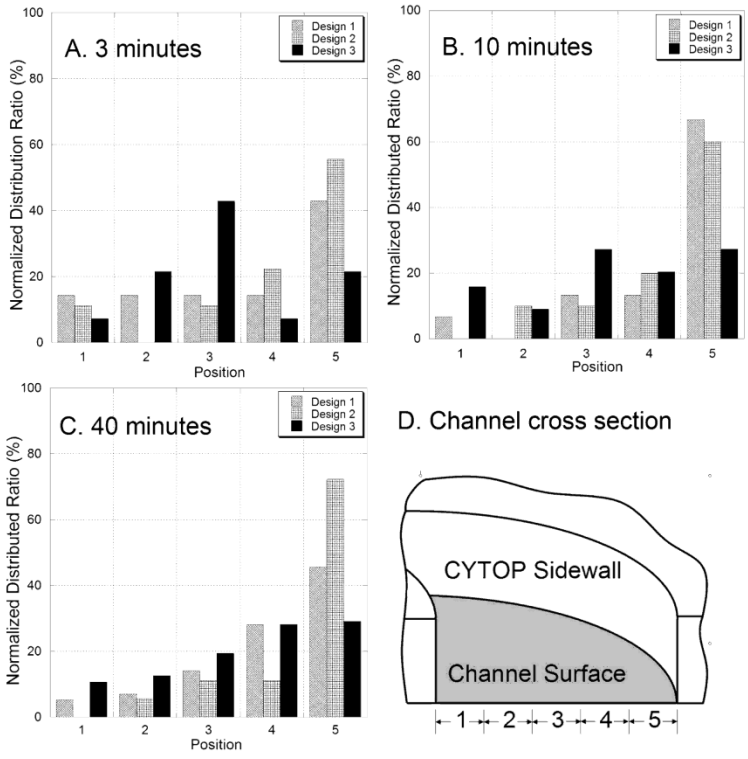

Figure 2-10: Microtubule positional distribution across channel for each design after (A) 3 minutes, (B) 10 minutes, (C) 20 minutes, and (D) schematic view of microfluidic channel cross section. The position coordinate is taken across the channel from the inner side to the outer side. The origin is located at the edge of the inner channel sidewall. Initially, the microtubules are relatively uniformly distributed across channel due to the randomness of the landing process. After the sorting process, a majority of the microtubules are located close to the outer sidewall in Designs 1 and 2. The micro-guide structure helps microtubules to uniformly stay more uniform distributed across the channel for Design 3.

2.2.4 Conclusion

In summary, we have designed, fabricated, experimentally tested and modeled microtubule uni-directional sorting mechanisms that make possible efficient integration

of nanoscale biomolecular motors and microengineered device structures. Future devices based on the finding presented here will be suitable for powering MEMS and microfluidic devices without external power sources at unprecedented low power levels. We are currently exploring implementations for sorting molecules and extracting mechanical power for the actuation of microscale mechanical devices and fluids.

2.2.5 Experimental Section

The micro channels utilized for our work consist of a circular pattern etched into a layer of fluorocarbon polymer, CYTOP, deposited on a glass substrate. The thickness of the CYTOP layer is typically 1.5 μm. Previous work(Nicholson et al., 1999) indicates that the CYTOP coating suppresses nonspecific protein binding. We have found a very large contrast between the numbers of gliding microtubules on bare and CYTOP-coated glass surfaces in a gliding assay. We believe that this differential in motility is due to the selective adsorption or selective functionality of kinesin on the exposed glass surface of the channel bottom. To fabricate these channels, we first prepared a cover glass substrate using piranha clean and diluted HF (1:20) surface treatment. A CYTOP film was spun on the cleaned glass substrate at 1500 rpm followed by a 30-minute curing step at 180^{o}C in an oven. Following standard photoresist lithography we patterned the channels in the CYTOP film by plasma etching using a SF_6 gas at a 20 mTorr pressure, an RF etching power of 120 W and a gas flow rate of 20 sccm (Standard Cubic Centimeters per Minute). Finally, the cover glass substrate with the micro-channel patterns was treated by NH_4OH (NH_4OH:H_2O_2 = 1:1) for 5 minutes. These fabrications reproducibly yield channels with surface

properties that allow kinesin binding and microtubule affinity and motility similar to those of control experiments on unprocessed glass surface. Furthermore, the walls of microfabricated channels processed in this manner are steep enough to prevent rapid loss (detachment) of microtubules from the microfluidic channels.

For our experiments we used a bacterially expressed kinesin motor, NKHK560cys. This motor consists of the head and neck domain of *Neurospara crassa* kinesin (amino acids 1-433) and stalk of *Homo sapiens* kinesin (residues 430 to 560) and a reactive cysteine at C-terminal end(Kallipolitou et al., 2001; Lakamper et al., 2003; Vale et al., 1996). The NKHK560cys gene was ligated into the pT77 plasmid and expressed in E. coli BL21 cells using TPM medium with 50 μM ampicllin at 37°C. Expression was induced by adding 0.1 mM IPTG at a cell density corresponding to an OD of 0.6-0.8 and continued over night at 22°C. Cells were centrifuged and resuspended in lysis buffer containing protease inhibitors, DNAse and lysozyme followed by sonification. The supernatant of this was loaded on SPFF ion exchanger(SP Fast Flow, Amersham Biosciences, Piscataway, NJ, USA) and kinesin was eluted by a step gradient to protocol. Tubulin and TMR-labelled tubulin were obtained by standard procedures. Birefly, tubulin was purified from cow brain by three cycles of microtubule polymerization and depolymerization followed by phosphocellulose ion exchange chromatography to eliminate microtubule associate protein. Tubulin was labeled with TMR(5-6carboxytetramethylrhodamine, Molecular Probs, Eugene, OR, USA) by reacting polymerized microtubules with a 20 folds excess of dye at room temperature for 30 minutes. Competent, labeled tubulin was purified

from this mixture by repeated depolymeriztion and polymerization. For experiments, microtubules were polymerized by incubating 2 mg/ml tubulin (equal ratios of TMR-labeled and unlabeled tubulin) 1mM GTP and 4 mM $MgCl_2$ in BRB80 buffer at 37°C for 20 minutes. Microtubules were stabilized by the addition of 10 µM taxol. Flow chambers were constructed from microscope slides and microfabricated cover glasses containing the microfluidic channels separated by 75 µm thick glass spacers. Where indicated, flow chambers were first pretreated with 100 µl of an 2 mg/ml aqueous solution of Pluronic (Pluronic® F108 Prill,BASF, NJ, USA) and then washed with 200 µl de-ionized water followed by 100 µl BRB80 buffer. Protein loading procedure was identical to that for standard kinesin gliding assays: Chambers were loaded with kinesin (47µg/ml casein and 1.4 µM kinesin in BRB80 buffer) and incubated for 5 minutes. Subsequently, microtubules in a BRB80 buffer containing 1 mM ATP and an oxygen scavenger system (4 µg/ml microtubules, 2 mM $MgCl_2$, 10 mM glucose, 100 µg/ml glucose oxidase, 80 µg /ml catalase, 10mM DTT, and 47µg/ml casein) were loaded. Samples were observed with an inverted fluorescence microscope (ZEISS Axiovert 200, 40x/ 1.3 NA Plan Neofluar objective) and images were recorded with a digital CCD camera (Orca II, Hamamatsu, Japan).

2.3 Highly efficient guiding of microtubule transport with imprinted CYTOP nanotracks[2]

2.3.1 Introduction

There has been increasing interests among the scientific community to explore natural biomaterials and biomolecules for engineering applications. Kinesins, a family of biomolecular motor proteins, are nanoscopic engines that utilize the free energy from the hydrolysis of ATP molecules to move along microtubules (MTs). Within cells, the kinesin-microtubule system is responsible for intracellular transport of proteins, organelles and vesicles throughout the cytosol. This system can also be exploited in *in vitro* environments to achieve certain useful functionalities, which may pave the way for complex artificial micro- and nanosystems. One of the important examples is nanoscale transport in which microtubules carrying designated target molecules glide along kinesin-coated tracks towards a destination, which can form the basis of novel chemical transport and separation systems. To produce controlled microtubule transport, it is necessary to immobilize kinesin motor proteins in the form of linear tracks by, for instance, protein patterning, physical confinement, or a combination of both. In this regard, a recently developed nanoscale protein patterning technique offers great potential(Hoff et al., 2004). Several previous studies proposed to control microtubule transport in microscale tracks made of or generated by lithographically patterned photoresist barriers(Hess et al., 2002; Hiratsuka et al., 2001; Jia et al., 2004). However,

[2] Li-Jing Cheng , M.-T.K., Edgar Meyhöfer, L. Jay Guo. 2005. Highly Efficient Guiding of Microtubule Transport with Imprinted CYTOP Nanotracks. Ibid. 11(4):409-414.

high guiding efficiency has not been achieved. The mechanisms of microtubule guiding in such artificial tracks have been analyzed in several papers(Clemmens et al., 2003a; Clemmens et al., 2003b). The reason for the observed low guiding efficiency and high MT detaching rate can be explained by the fact that in microscale tracks, the microtubules tend to reach the track barriers at large approach angle, which often leads to escape from kinesin tracks or permanent attachment at the site of contact with the barrier. These results imply that decreasing track width should significantly enhance the efficiency of microtubule guidance. Prior work by Dennis *et al.* has demonstrated that the motion of microtubules can be directed in oriented nanoscale protein tracks formed by rubbing a poly(tetrafluoroethylene) (PTFE)-coated glass substrate(Dennis et al., 1999). However, rubbed topographies lack micro- or nanoscale design and the barrier height, typically less than 30nm, was too small to prevent kinesin proteins from projecting out over the barriers, which makes it possible for MTs to frequently switch to adjacent tracks. Also, the low barrier height provides poor physical confinement for the gliding MTs. As a result, MTs continue to move randomly on the substrate.

2.3.2 Results and discussions

To solve all these problems, we have developed a very effective method to achieve highly efficient guiding of MT transported by kinesin motors that are immobilized within polymer nanotracks created by nanoimprint lithography (NIL). As illustrated in Figure 2-11, nanoscale protein tracks constrained by polymer barriers prevent the gliding microtubules from swaying and compel the microtubules to approach the track edge at glancing angles, thus restraining them from moving out of

the tracks. Furthermore, the barriers are chemically modified to have protein-nonadhesive properties, which effectively prevents microtubules from either climbing up the barriers or randomly gliding over the top surface of barriers. By combining these two strategies, we have obtained high-efficiency and high-density of controlled microtubule transport. Fluorescence microscopy-based microtubule motility assays showed that high densities of microtubules glide exclusively (close to 100%) along the imprinted nanotracks. The average gliding distance of microtubule before detaching from the surface is about 2.5 mm.

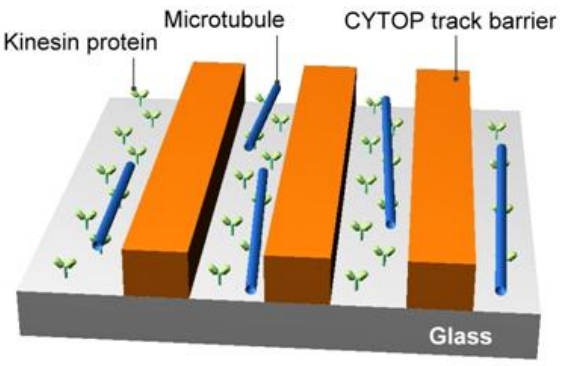

Figure 2-11: Kinesin motor proteins immobilized within CYTOP nanotracks on a glass coverslip. Microtubules propelled by the kinesin motors are physically confined by the CYTOP track barriers, leading to precision guided transport along the nanotracks.

We developed several novel techniques for forming such nanotracks to guide the motion of kinesin-propelled microtubules. For our experiments we used a bacterially expressed kinesin motor, NKHK560cys. Details on the biochemical techniques used for kinesin and MT preparation can be found in the experimental section. The nanotracks on glass substrates were fabricated through direct

nanoimprinting of a cyclized perfluoropolymer called CYTOP^{TM} (**Asahi Glass Co., Tokyo, Japan**), followed by CYTOP surface hydrophobicity enhancement that is based on sulphur hexafluoride (SF_6) reactive ion etching (RIE). The CYTOP track barriers are further treated with a Pluronic® triblock copolymer that forms a Poly(ethylene oxide) (PEO) monolayer on its surface, which or dramatically reduces protein adsorption.. Then a simple flow cell is constructed which is filled with kinesin protein. Kinesin protein is preferentially adsorbed on the glass surface, but not on modified CYTOP barriers. Kinesin motor protein immobilized on the coverslip in the form of nanotracks propels microtubules exclusively along the patterned nanotracks.

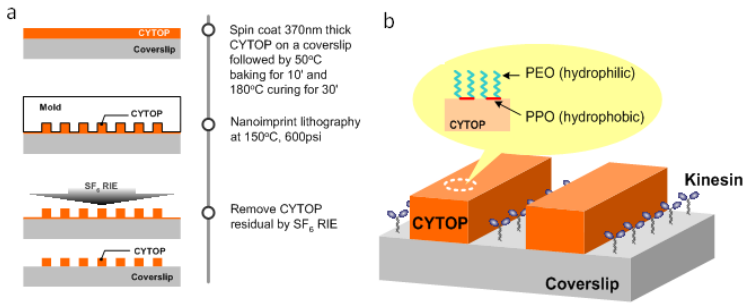

Figure 2-12: (a) Process flow of creating CYTOP nanotracks by NIL. (b) Schematic of Pluronic treatment of CYTOP surface to prevent adsorption of kinesin proteins on track barriers.

As illustrated in Figure 2-12a, CYTOP gratings were created using nanoimprint lithography (NIL). NIL provides the capability of creating large-area nanoscale patterns with high yield, high throughput and high reproducibility(Chou et al., 1997). CYTOP thin films are especially suitable as an imprinting material: the glass transition temperature (T_g) of CYTOP (105 ^{o}C) is well suited for the imprinting process and

CYTOP has very low surface energy which greatly facilitates the demolding process after NIL. These key material properties lead to very low defects in the imprinted CYTOP nanostructures. Low defect density is important to obtain controlled MT transport over long distances. The scanning electron microscope (SEM) image of the CYTOP grating in Figure 2-13 shows the uniform nanoscale tracks with very straight side walls. Imprinted CYTOP gratings of such quality perform extremely well in physically confining and guiding the motion of microtubules.

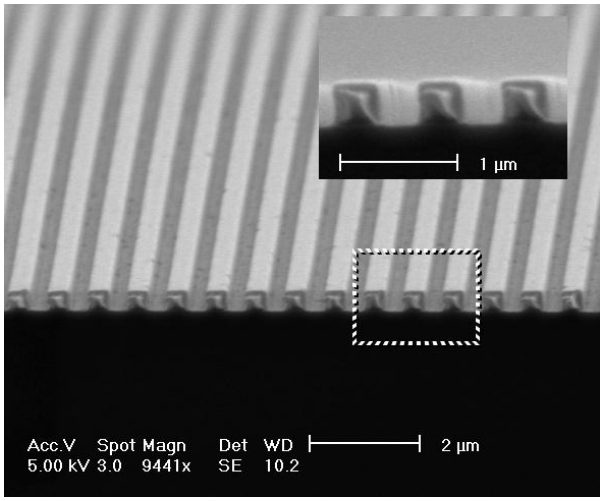

Figure 2-13: SEM image of nanoimprinted CYTOP grating.

CYTOP has previously been shown to significantly reduce nonspecific binding of certain types of proteins (such as BSA) at low concentration (< 1µg/ml)(Nicholson et al., 1999). Nevertheless, we found that untreated CYTOP surfaces was not effective in preventing the kinesin binding that leads to undesirable motility on the surface of the grating. Therefore, we chemically treated the hydrophobic CYTOP surfaces to further

reduce protein adsorption which makes it possible to selectively immobilize the motor protein kinesins on the exposed glass surface only. We used Pluronic® F-108 (PEO129-PPO56-PEO129 triblock copolymer) to coat the CYTOP surface, where PPO stands for poly(propylene oxide). The hydrophobic PPO domains bind with high affinity on the hydrophobic CYTOP surface while leaving the hydrophilic PEO domain extending out into the aqueous environment in the assay experiment (Figure 2-12b). PEO is known to have protein repelling properties. After the Pluronic treatment, CYTOP surfaces can effectively suppress the binding of kinesin motors. We found that the Pluronic treatment works well on the as-deposited and imprinted CYTOP surface, but the dry etching process necessary for removing the residual CYTOP layer after NIL unavoidably degrade the hydrophobicity of the imprinted CYTOP surface. Typically in NIL oxygen plasma RIE is used to remove the residual layers after nanoimprint. But O_2 plasma etching turns CYTOP surface hydrophilic, which significantly hinders the following Pluronic treatment. We found that baking at an elevated temperature can help to partially recover the hydrophobicity of etched CYTOP surface. However, since a temperature over the T_g of CYTOP is necessary to obtain sufficient hydrophobicity, such baking temperature can cause reflow of CYTOP material or even destroy the imprinted CYTOP nanostructures.

To overcome this problem, we replaced the oxygen RIE with a sulphur hexafluoride (SF_6) RIE process. It was reported previously that the surface fluorination by SF_6 plasma can significantly enhance the hydrophobicity of certain polymers, such as polyurethane, silicone and poly(tetrafluoroethylene) (PTFE)(Rangel et al., 2003).

The phenomenon of hydrophobicity enhancement was also observed in our experiment on the SF_6 RIE etched CYTOP surface. Figure 2-14 compares the results of water contact angle measurements performed on different RIE etched and/or chemically treated CYTOP. Oxygen RIE reduces the hydrophobicity of CYTOP, and baking (120^oC) can partially recover the hydrophobicity. In contrast to O_2 etching, SF_6 RIE actually improves the contact angle of CYTOP surfaces. In addition, it does not affect the binding of kinesin to glass surfaces as compared with the samples cleaned by our standard process. Based on these observations, we conclude that using CYTOP as track barriers, and employing SF_6 RIE to remove CYTOP residuals to expose glass surface for protein binding is an effective combination to achieve high contrast in kinesin binding.

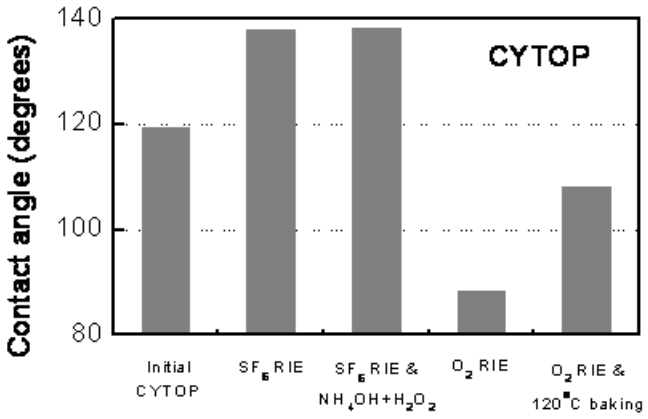

Figure 2-14: Water contact angle measurements on CYTOP substrates etched under different plasmas etching conditions and/or treated with different chemicals.

We performed microtubule motility assays that were evaluated by fluorescent microscopy. Flow chambers were constructed from microscope slides and

microfabricated glasses with 75µm cover glasses (**Menzel, Germany**) as spacers. Samples were observed with an inverted fluorescence microscope (ZEISS Axiovert 200, 40x/ NA 1.3 Plan-Neofluar objective) and images were recorded with a digital CCD camera (**Orca II, Hamamatsu, Japan**). The statistical results of MT density obtained on microtubule gliding assay shown in Figure 2-15 agree with our expectations. Pluronic treatment works very effectively on SF_6 RIE etched CYTOP samples and significantly reduces the binding of kinesin and hence the density of microtubules. The result indicates that the PEO coated CYTOP surface provides almost no kinesin adsorption, and therefore no microtubule gliding on it. Besides SF_6 RIE, chemical treatment in ammonia hydrogen peroxide mixtures was applied for 5 minutes and was observed to improve kinesin binding on glass surface. The reason of the improvement is not entirely clear at this moment. Further work is currently underway to understand the effect of chemical treatment on both glass and CYTOP surface.

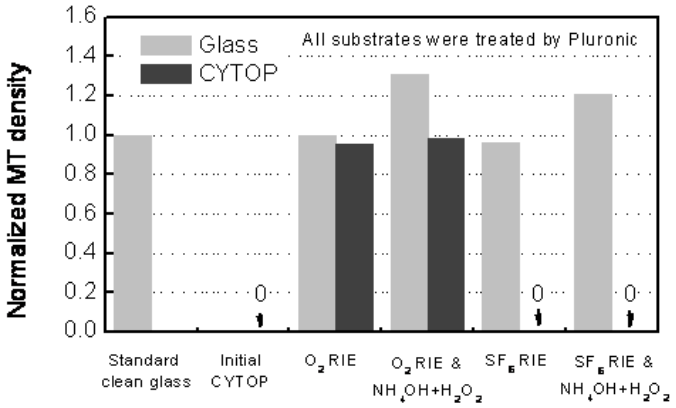

Figure 2-15: MT gliding assay on substrates generated under various plasma etching conditions and treated by different chemicals. The MT density of each sample is normalized to that of standard process-cleaned glass.

When the track width is reduced to nanoscale dimensions, PEO treatment of CYTOP surfaces is of vital importance. Without Pluronic treatment, CYTOP nanotracks have poor control over MT guiding. Figure 2-16a shows a large number of microtubules gliding *across* nanotracks that were not chemically treated with Pluronic copolymer. Since the closely-spaced CYTOP grating surface is not kinesin free, a large number of microtubules glides randomly on the top surface of CYTOP barriers. Also, those traveling in the track frequently climb over the track barriers to either switch between different tracks or detach and diffuse into the solution. Conversely, for the sample that has been treated with Pluronic F-108, high densities of microtubules are exclusively guided along the PEO-coated CYTOP grating shown in Figure 2-16b. In this image, the few microtubules oriented at an angle relative to the grating actually were not gliding but on their way diffusing onto surface searching for available kinesin proteins to bind. A short video of well-guided MT transport along the nanotracks can be found in the supporting materials.

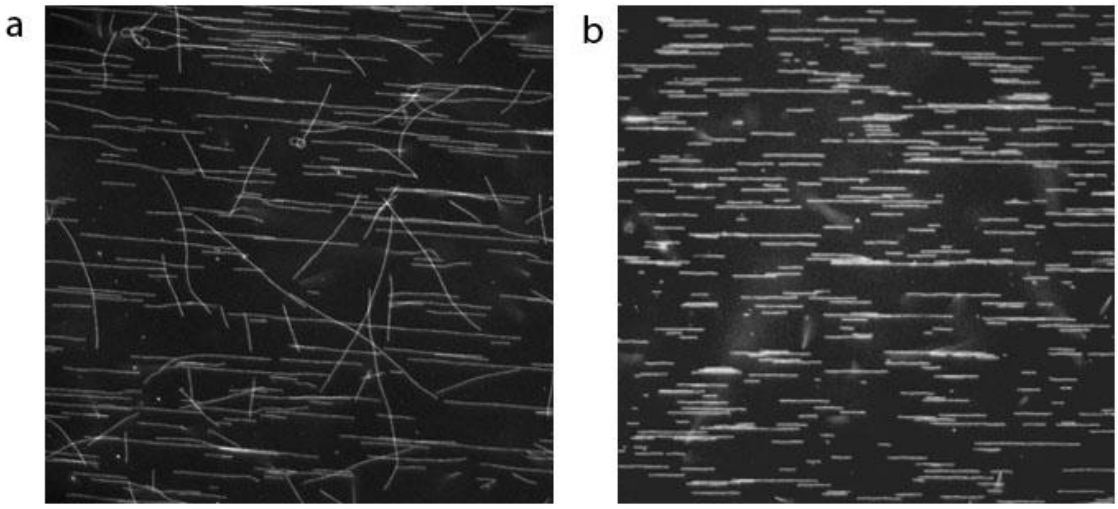

Figure 2-16: The influence of Pluronic treatment on guiding microtubule becomes significant for CYTOP nanotracks. Gliding assays were performed on the CYTOP grating without (a) and with (b) Pluronic treatment. Each image is 160μm×160μm in size.

Because of the physical confinement and chemical treatment, microtubules can glide in nanoscale tracks for a long distance before they detach. We managed to trace a large group of microtubules for about 1mm along the nanotracks. We only observed extremely small number (less than 1%) of microtubules escaping from the tracks within the 1mm travel distance. In order to better estimate the average length MTs can glide in nanotracks before detaching, we collected time-sequence data of microtubule bindings on CYTOP grating to determine the dissociation rate of microtubules from the nanotracks. The number of microtubule gliding on CYTOP nanotracks is plotted as a function of time in Figure 2-17. Since almost 100% of microtubules move in CYTOP grating we conclude that there is little kinesin available on the PEO-coated CYTOP surface to support microtubule motility.

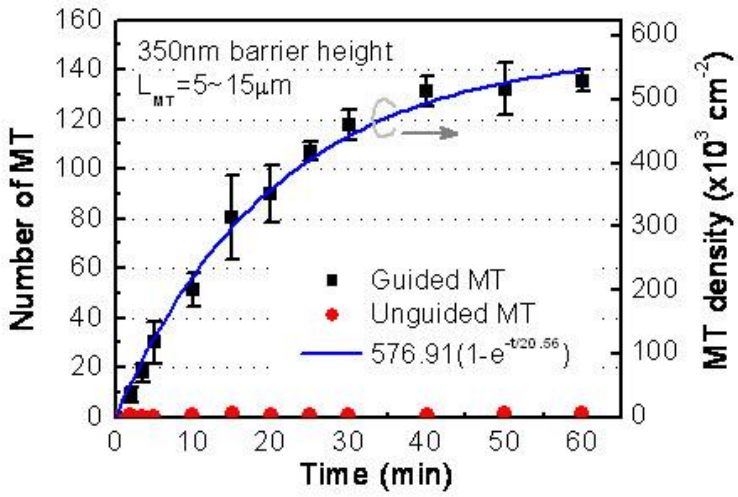

Figure 2-17: Time-sequence data of MT binding to kinesin proteins on the glass substrate covered with Pluronic treated CYTOP gratings.

We developed a simple MT binding kinetics model to estimate the dissociation rate, which can be used to infer the distance that microtubules travel on average before they detach from the nanotracks. Detailed analysis can be found in the Appendix. We first confirmed that, under our experimental conditions, the microtubule binding rate to the kinesin coated surface is much smaller than the diffusive flux, and therefore the diffusion process can be neglected when considering the MT surface binding kinetics. Under this condition, the binding rate of a single MT onto kinesin coated surface, *Ms*, can be shown to have a simple form:

$$Ms(t) = \frac{k_{on}}{k_{off}} M_b (1 - e^{-k_{off} \cdot t}),$$

where k_{on} and k_{off} are binding and dissociation rate constants, respectively, and M_b, is the constant concentration of freely difussing MTs in the buffer solution. This equation is used in fitting the experimental data presented in Figure 2-17 to obtain the MT dissociation rate. The fitting curve yields $1/(k_{off})$ to be ~ 21 minutes. Since the average MT gliding speed is ~ 2μm/sec, this implies that MTs translocate within the nanotracks an average distance of about 2.5 mm before detaching from the surface. In comparison, the average run-length of MTs traveling in microscale tracks defined by photoresist barriers was only a few tens of μm. This difference highlights the effectiveness of our method of combining nanoscale physical confinement with highly selectively patterning of kinesin within the CYTOP channels. The long average distance of translocation of microtubules achieved in this study has important implications for the development of biomolecular motor-based nanotechnology, because the combined speed and travel distance make it now possible to transport target molecules over significant distances and overcome the normal diffusive motion.

In conclusion, highly efficient guiding of MT transport propelled by immobilized kinesin motor molecules has been achieved in PEO coated polymer nanotracks on a glass substrate. This technique significantly improves both the resolution and the contrast of motor protein patterning and physical confinement for guided MT transport. With this technology, we can apply CYTOP nanotracks to a variety of device applications. For example, CYTOP nanotracks can be integrated to microscale fluidic channels to construct a hybrid micro-/nanoscale system with useful functionalities. The integration makes it possible to precisely locate and efficiently

utilize nanoscale motor proteins to achieve more complex functions, including conveyance of molecules between different chemical reservoirs, or sorting and separation of specific molecules from chemical flow streams. Based on the versatility of nanoimprinting, the configuration of CYTOP nanotracks can be custom-designed to guide single microtubule transport along complex paths. The technology may pave the way to novel nanosystems for single molecule manipulation or detection that are powered by biomolecular motors.

2.3.3 Experimental

For NIL fabrication, a large area grating made of Si with 700nm in period and 500nm in depth was used as a mold. The mold was treated with a surfactant, perfluorodecyltrichlorosilane (Lancaster Synthesis, Windham, NH) to provide a low energy surface to facilitate the demolding process. The substrate we used, Corning coverslip (Corning, NY), was cleaned by our "standard clean" process, involving a 10-minute dip in Piranha solution (H_2SO_4:H_2O_2=2:1), a 10-minute rinse in deionized water, a 20-second dip in dilute HF (HF:H_2O=1:20) and another 10-minute rinse in deionized water. After dehydration of the coverslip, the material to be imprinted, 370nm thick CYTOP, was spun onto a coverslip followed by a 10 minute of baking at 50 ^oC and 30 minutes of curing at 180^oC. The mold and substrate were then brought into physical contact at 150^oC, and a pressure of 35Kg/cm^2 was applied for 5 minutes followed by subsequent cooling. After mold separation, SF_6 reactive ion etching (RIE) (SF_6 gas flow = 20 sccm, pressure = 20 mTorr, power = 120W, self DC bias = 275V) was applied to remove the CYTOP residuals in the trench regions to expose the glass surface. The

CYTOP etching rate is about 130 nm/min. Finally, the whole CYTOP grating chip is dipped in ammonia hydrogen peroxide mixtures ($NH_4OH:H_2O_2$=1:1) for 5 minutes and then rinsed in deionized water for 10 minutes.

For our experiments we used a bacterially expressed kinesin motor, NKHK560cys. This motor consists of the head of *Neurospara crassa* kinesin (amino sequence to 433) and neck and stalk of *Homo sapiens* kinesin (amino sequence from 430 to560) and a reactive cysteine at C-terminal end (Funatsu et al., 1997; Kallipolitou et al., 2001; Lakämper et al., 2003). The NKHK560cys gene was ligated into the pT77 plasmid and transformed to Escherichia Coli BL21 cell. Cells were incubated in TPM medium with 50µM ampicllin at 37°C. Expression was induced by adding 0.1 mM IPTG at a cell density corresponding to an OD of 0.6-0.8 and continued over night at 22°C. Cells were centrifuged and re-suspended in lysis buffer containing protease injhibitors, DNAse and lysozyme followed by sonification. The supernatant of this was loaded on SPFF ion exchanger (SP Fast Flow, Amersham Biosciences, Piscataway, NJ, USA) and kinesin was eluted by a step gradient to protocol.

Tubulin and TMR-labelled tubulin were obtained by standard procedures (Hyman et al., 1991)). Briefly, tubulin was purified from cow brain by three cycles of microtubule polymerization and depolymerization followed by phosphocellulose ion exchange chromatography (P11, Whatman, UK) to eliminate microtubule associate protein. Tubulin was labeled with TMR (5-6carboxytetramethylrhodamine (Molecular probes, Eugene, OR, USA) by reacting polymerized microtubules with a 20 folds

excess of dye at room temperature for 30 minutes. Competent, labeled tubulin was purified from this mixture by repeated depolymeriztion and polymerization.

For experiments, microtubules were polymerized by incubating 2 mg/ml tubulin (app. equal ratios of TMR-labeled and unlabeled tubulin) 1mM GTP and 4 mM $MgCl_2$ in BRB80 buffer at 37°C for 20 minutes. Microtubules were stabilized by the addition of 10µM taxol (Paclitaxel, Calbiochem, USA)**.**

Flow chambers were constructed from microscope slides and microfabricated glasses with 75µm cover glasses (Menzel, Germany) as spacers. The chambers were pretreated with 100 µl of an 2mg/ml aqueous solution of Pluronic (Pluronic® F108 Prill, BASF, NJ, USA) and then washed with 200 µl de-ionized water followed by 100 µl BRB80 buffer. Protein loading procedure was identical to that for standard kinesin gliding assays: Chambers were loaded with kinesin (47µg/ml casein and 1.4 µM kinesin in BRB80 buffer) and incubated for 5 minutes. Subsequently, microtubules in a BRB80 buffer containing ATP and oxygen scavenger system (4 µg/ml microtubules, 2mM $MgCl_2$, 10mM glucose, 100 µg/ml glucose oxidase, 80 µg /ml catalase, 10 mM DTT, 1 mM ATP and 47 µg/ml casein) were loaded.

2.3.4 Appendix

In deriving the kinesin binding kinetics, we use the fact that surface density of kinesin is very high compared to MT concentration close to the surface, and therefore can be taken as a constant. The binding rate of a single MT to the kinesin coated surface, *Ms,* is given by:

$$\frac{d}{dt}Ms(t) = k_{on} \cdot M(0,t) - k_{off} \cdot Ms(t) \qquad \textbf{(1)}$$

where k_{on} and k_{off} are binding and dissociation rate constants, respectively, and M(0,t) the volume concentration of free MTs right next to the binding surface at time t. The binding surface is the kinesin-coated surface and defined as x=0 (see Figure 2-18). Considering the diffusion of MTs from the solution to the kinesin binding sites with a diffusivity D, we can apply two boundary conditions for Fick's diffusion equation, $\dot{M}(x,t) = D \cdot M''(x,t)$. First, the diffusion flux equals to the binding rate at the surface, i.e.

$$D\frac{\partial}{\partial x}M(x,t)\bigg|_{x=0} = \frac{d}{dt}Ms(t). \qquad \textbf{(2)}$$

Second, the concentration of microtubule outside the unstirred layer (a volume within a distance δ from the surface) equals to M_b, a constant microtubule concentration in buffer (Figure 2-18):

$$M(\delta,t) = M_b. \qquad \textbf{(3)}$$

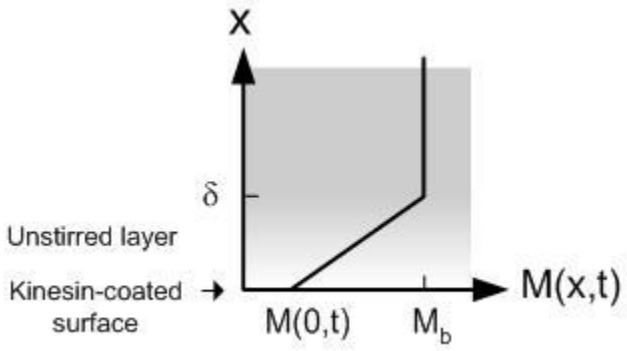

Figure 2-18: Schematic plot of MT concentration in a flow cell. The kinesin are immobilized on galss surface at x=0. Due to high concentration of MT in the bulk solution, MTs in the flow cell is assumed to be a constant, and no depletion of MTs occurs because of the binding of MTs to kinesins on the glass surface.

Since the amount of MTs in the buffer solution (with a concentration of $M_b \approx 1.5\times10^{11}$ cm^{-3} *) is much higher than the amount diffusing to and attached to the surface, we neglect the depletion of the microtubules in the buffer. To simplify the problem, we used an approximation that the microtubule concentration decreases linearly toward the surface across the unstirred layer (as shown in Figure 2-18). The boundary condition can then be recast as

$$\frac{d}{dt}Ms(t) = D\frac{\partial}{\partial x}M(x,t)\bigg|_{x=0} = D\frac{M_b - M(0,t)}{\delta} \qquad \textbf{(4)}$$

or

* Each microtubule is comprised of 13 linear protofilaments. Within each protofilament, the dimeric tubulin subunits repeat every 8 nm. Thus the concentration of microtubule (10μm long in average) polymerized from 4 μM (or 2.4×10^{15} cm^{-3}) tubulin is 1.5×10^{11} cm^{-3} [= 2.4×10^{15} cm^{-3}/(13×10μm/8nm)].

$$M(0,t) = M_b - \frac{\delta}{D} \cdot \frac{d}{dt} Ms(t) . \qquad \textbf{(5)}$$

Substituting equation 5 into equation 1, we can solve for *Ms*(t)

$$Ms(t) = \frac{k_{on}}{k_{off}} M_b (1 - e^{\frac{-1}{1+Da} k_{off} \cdot t}) \qquad (6)$$

where $Da = k_{on}\ \delta/D$, is a dimensionless parameter, known as the second Damkőhler number. It represents the ratio of surface reaction rate to the bulk diffusion rate. Prior to extracting k_{off} from the experimental data, it is appropriate to evaluate the Damkőhler number and find out which process is the rate-limiting one. Typically δ, in the same order of $\sqrt{D \cdot t}$, is about 10 μm. The diffusion coefficient D of MT is about 2×10^{-9} cm^2/s. k_{on} can be estimated from the slope of the binding curve at t = 0, i.e. $(1/k_{on} + \delta/D)^{-1} M_b$. The slope, about $467.7 cm^{-2} \cdot s^{-1}$ obtained from the fitted curve, gives k_{on} = 3.1×10^{-9} cm/s. Substituting these values into the Damkőhler number yields $Da=1.6\times10^{-3}$, *i.e.* $Da << 1$. This means that the microtubule binding rate is much smaller than the diffusion flux. In other word, the diffusion process can be neglected when considering the MT surface binding kinetics. Therefore, the binding kinetics can be reduced to a simple form:

$$Ms(t) = \frac{k_{on}}{k_{off}} M_b (1 - e^{-k_{off} \cdot t}) \textbf{ (7)}$$

This is the equation used in fitting the data presented in Figure 2-17(page 48) to obtain the MT dissociate rate.

2.4 Biomolecular motor-powered molecular sorter[3]

2.4.1 Abstract

We demonstrate a novel, stand-alone device for sorting and concentrating biomolecules by combining biomolecular motor and microtubule systems with micro-/nano-fluidic technologies. The device consists of a microfluidic channel network to produce an analyte stream and nanoimprinted nanotracks to guide functionalized microtubules to move across the analyte stream. The functionalized microtubules translocated by kinesin are capable of selectively capturing and transporting a few thousand target molecules per second from the analyte. Subsequently, the target molecule-bound-microtubules are concentrated at a designed collector, resulting in higher concentration of target molecules up to three orders of magnitude within an hour. The characterization of the device and optimized microfabrication techniques will be significantly useful to engineer biomolecular motor-driven applications.

2.4.2 Introduction

Recently, biomolecular motor (kinesin) and microtubule systems have shown a high potential to substitute traditional energy sources such as mechanical pressure and electrical voltage with biological energy sources for efficient, stand-alone, and self-contained micro-/nano-devices because kinesin motors are truly nanoscopic(Heuser et al., 1988), but generate significant forces about 4–7 pN(Gittes et al., 1994; Hunt et al.,

[3] Material in this section is published recently: Kim, T., L.-J. Cheng, M.-T. Kao, E.F. Hasselbrink, L. Guo, andE. Meyhofer. 2009. Biomolecular motor-driven molecular sorter. *Lab on a Chip* 9(9):1282-1285.

1994; Meyhofer and Howard, 1995; Svoboda et al., 1993) when translocating microtubules at the speed of about 1 μm/s via 8nm steps(Kojima et al., 1997; Svoboda et al., 1993). In addition, they not only have low total energy consumption compared to most externally-driven micro-/nano-systems, but also are significantly efficient up to 50% in converting chemical energy to mechanical work(Vale et al., 1985c) because one 8 nm step requires one hydrolyzed molecule of ATP but 67kJ/mol is released from ATP hydrolysis(Howard, 1996). The feasibility of biomolecular motor powered micro-/nano-devices has been promising due to the development of the directional control methods of microtubules on kinesin-immobilized surfaces using various types of mechanical structures(Clemmens et al., 2003a; Hiratsuka et al., 2001; Lin et al., 2006), nanoimprinting technology(Li-Jing Cheng 2005), and even external fields(Kim et al., 2007a; Kim et al., 2007b; van den Heuvel et al., 2006). These fundamental methods have inspired one to develop molecular sorting devices(Ramachandran et al., 2006; van den Heuvel et al., 2006) and nanotransport systems that make it possible to transport beads or biomolecules(Bachand et al., 2006; Jia et al., 2004; Yokokawa et al., 2004). Even though these approaches successfully made first steps towards functional devices/systems, some devices appear not to fully exploit the advantages of biomolecular motors and are not efficient because they still depend on external power sources such as electric fields(van den Heuvel et al., 2006). Furthermore, the nanotransport distance of those systems is largely limited to the length of immobilized microtubules up to a few tens μm and they seem to lack the ability to concentrate target molecules at a certain place(Ramachandran et al., 2006; Yokokawa et al., 2004).

Here we develop a state-of-an-art, efficient, and self-powered device that can selectively sort and highly concentrate target biomolecules by incorporating the advantages of nanotransport ability of kinesin and microtubule systems with micro-/nano-fluidic technologies. In addition, the device overcomes the limited travel distance of previous nanotransport systems and enables us to concentrate the transported target molecules at a designated spot. The working principles of the device are that kinesin adsorbed on the nanoimprinted nanotrack surfaces translocates functionalized microtubules along the nanotracks and across an analyte stream. While passing the analyte stream the functionalized microtubules can selectively bind to target molecules and carry them to a collector. The horseshoe-shaped collector (top side) bonded with the bottom side nanotracks concentrates the target molecule-bound-microtubules into the fringe which is likely to be generated between the top side microfluidic structure and the bottom side nanotracks. We implemented these principles into the device using newly developed, biocompatible micro-/nanofabrication techniques, so that we demonstrated that the device can selectively sort and transport a few thousand target molecules per second from the analyte and then even concentrate them up to three orders of magnitude within an hour. We also characterized the performance of the device by quantifying the experimental results.

2.4.3 Materials and methods

2.4.3.1 Nano-/micro-fabrication

Several nano-/micro-fabrication techniques were developed to build the device. The technique consists of creating nanotracks on glass substrates through direct nanoimprinting of a cyclized perfluoropolymer called CYTOP^{TM}, and a polymer inking method for bonding CYTOP^{TM} nanotracks with the microfluidic channels. In the microfluidic part, the standard microfabrication procedure was used to etch microchannels on glass substrate (the top side, including the collector) (Figure 2-19). In parallel, CYTOP^{TM} nanotracks on glass coverslips (the bottom side) were fabricated via nanoimprint lithography (NIL). The mold used for NIL has nanoscale grating structure with 700nm in period and 50% of duty cycle made by interference photolithography and dry etching. Such dimension allows us to create 350nm-wide track-arrays separated by 350 nm-wide CYTOP^{TM} barriers. Since CYTOP^{TM} (Asashi, Japan), a type of Teflon, has a good adhesion to glass substrates but low differential protein binding compared to glass. The imprinting temperature and pressure was 150 °C and 600 psi, respectively. After mold separation, SF_6 reactive ion etching (RIE) was applied to remove CYTOP^{TM} residuals in the nanoscale trenches and expose glass surface. The more detailed process of nanotracks and its guiding efficiency of microtubule are found in our previous study(Li-Jing Cheng 2005).

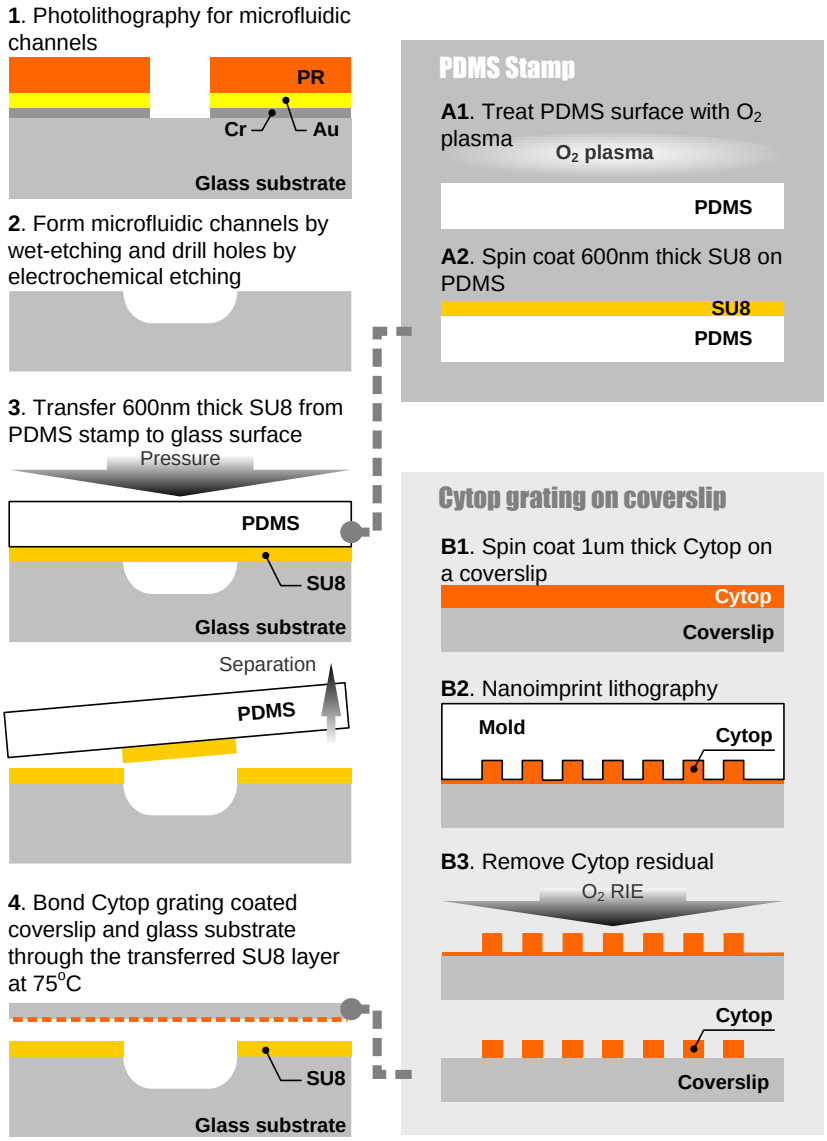

Figure 2-19: Step 1 and 2 show the procedure of the microchannel fabrication. Microfluidic channels are HF-etched and electrochemical drilled to form pores connecting to the microchannels. In step A1-A2 and 3, SU-8 thin film is selectively transferred to the top of microfluidic substrate and served as an adhesive bonding with glass coverslips. CYTOP™ nanotracks on a glass coverslip are made via nanoimprinting lithography (step B1–B3).

To integrate microfluidic channels with CYTOP^{TM} nanotracks, a polymer transfer bonding technique was used to bond these two parts. As illustrated in Figure 2-19, a 500nm thick SU8 layer was first spun on an oxygen-plasma treated PDMS (polydimethylsiloxane) stamp and, afterward, transferred on the microfluidic chip. Because the surface energy of PDMS stamp is relatively low and SU-8 layer is thin enough, it is possible to selectively transfer SU-8 on top of the microfluidic chip when these two pieces were put into physical contact. After baked at 80 ºC for 2 minutes, the SU-8 topped microfluidic chip was then bonded onto the CYTOP^{TM} grating chip at 75 ºC at 300 psi for 25 minutes. After cooling, the bonded chip was cured by flood UV exposure and hard-baked at 95 ºC for 5 minutes. Since the glass transition temperature (T_g) of CYTOP^{TM} (T_g=110 ºC) is higher than the T_g of SU-8 (T_g=75 ºC), this low temperature polymer transfer bonding is capable of sealing the microfluidic channels and nanotracks with no effect on CYTOP^{TM} nanotracks. The SEM cross section view in Figure 2-20C shows the SU-8 layer were selectively coated on top of microfluidic chip and acts as an adhesive (see also Figure 2-21). The results showed that the SU8 layer provides a strong bonding and therefore forms a well-sealed microfluidic channels with CYTOP^{TM} nanotracks. Finally, glass pipettes were connected on the chip by UV-glue and epoxy served as external reservoirs for loading or draining of analyte solutions and motor proteins. A similar microfabrication technique is also found elsewhere(Kim et al., 2007b).

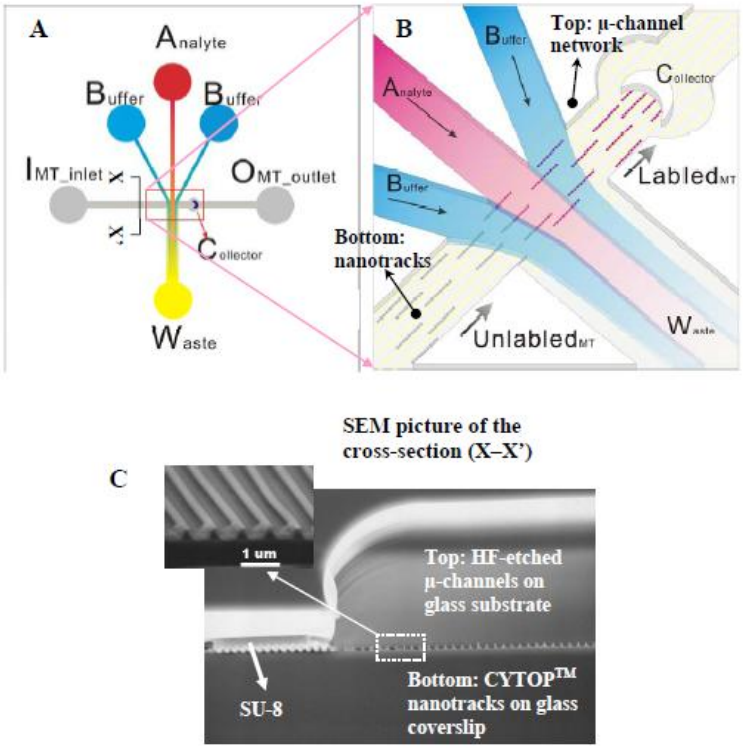

Figure 2-20: (A) A schematic view of a biomolecular motor-driven selective binding and concentrating device and (B) its detailed view of the intersection and the collector. An analyte containing fluorescently labeled target molecules flows towards waste and two buffer flows make the analyte flow hydrofocused to prevent other molecules from diffusing to the collector at the intersection. All flows are controlled by using hydrostatic pressure differentials among reservoirs to make the device stand-alone. Unlabeled microtubules at left are translocated by kinesins adsorbed on glass surfaces towards the collector at right. They are guided to move straight across the analyte channel by nanotracks on the bottom and bind the target molecules (streptavidins) from the analyte stream. The labeled microtubules are accumulated at the horseshoe-shaped collector. (C) The SEM image of the cross-section (X–X') shows wet-etched glass substrates for microfluidic channels and nanoimprinted nanotracks (see the inset) on a coverslip. SU-8 was selectively transferred only to the junctions between the glass substrate and the coverslip as a sealant due to the polymer transfer bonding technique.

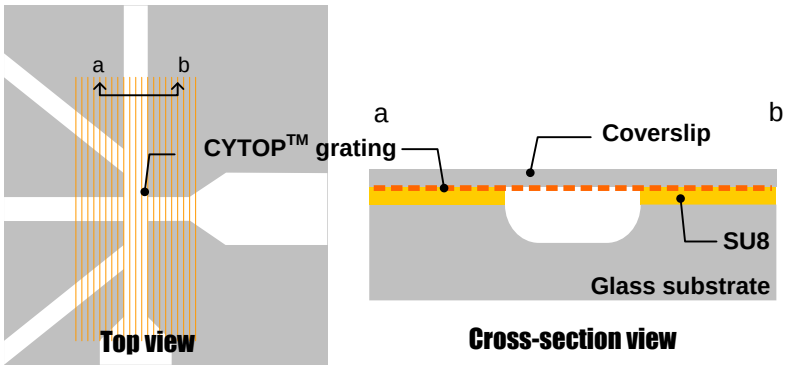

Figure 2-21: The top view and cross-section view of the resulting bonding.

2.4.3.2 Kinesin and microtubule preparation

For most experiments we used a bacterially expressed kinesin motor, NKHK560cys. This motor consists of the head and neck domain of *Neurospara crassa* kinesin (amino acids 1-433) and stalk of *Homo sapiens* kinesin (residues 430 to 560) and a reactive cysteine at C-terminal end. Kinesin was expressed and purified as described previously. Tubulin was purified from cow brain by three cycles of microtubule polymerization and depolymerization followed by phosphocellulose ion exchange chromatography, and fluorescently-labeled tubulin (TMR-tubulin) was prepared by reacting polymerized microtubules with a 20 folds excess of tetramethylrhodamine (Molecular Probes) at room temperature for 30 minutes. Labeled tubulin was purified from this mixture by repeated depolymeriztion and polymerization. For all experiments, microtubules were polymerized by incubating 2 mg/ml tubulin, 1mM GTP and 4 mM $MgCl_2$ in BRB80 buffer at 37 °C for 20 minutes. Microtubules were stabilized by the addition of 10 μM taxol. To make biotinylated microtubules, 1 μL of 10 mM of biotin was mixed with 200 μL of polymerized microtubules and then

this mixture was incubated about 30 min. To quench free biotin bindings, 2 μL of 1 M of glycine was added to the mixture, followed by additional 10 min incubation. Finally, biotinylated microtubules were purified by repeatedly running a high speed centrifuge process consisting of discarding the supernatant and resuspending the pellet. All motility assays were carried out in BRB80 buffer (80 mM of PIPES adjusted to pH 6.8 with potassium) at room temperature.

2.4.3.3 Experimental procedure

The device was tested as followings: initially, each 200 μL of BRB80 buffer was injected into all reservoirs except 'waste' reservoir and then vacuum pressure of ~50 kPa was applied to the 'waste' reservoir for 20 min using a hand vacuum pump with gauge (S94224, Fisher Scientific). To help kinesin adsorb better to channel surfaces and prevent nonspecific binding of target molecules, all channels were flushed with 200 μL of 0.14 mg/ml casein (Sigma-Aldrich) by repeating the previous injection step with the same pressure, followed by allowing it to incubate for 5 min. And then, to adsorb kinesin on the nanotracks at a higher density, 100 μL of 0.45 mg/ml of kinesin was injected into all reservoirs except the microtubule outlet reservoir and then vacuum pressure of ~25 kPa was applied to the outlet reservoir for 20 min, followed by 5 min incubation. Subsequently, 200 μL of an analyte solution was injected into the analyte reservoir in the absence of additional, external pressure.

The analyte required about 5 min to arrive at the intersection of the device because the hydrostatic pressure of the reservoir (~100 Pa) produces about 100 μm/s flow speed. The analyte was prepared by mixing an anti-bleach solution with 2 nM of

TMR-labeled streptavidin, 1 mM of ATP, and 0.45 mg/ml of kinesin. Addition of kinesin molecules into the analyte is believed to maintain the surface density of kinesin by reducing the gradient of kinesin concentrations between the bulk analyte solution and the surface.[16] The anti-bleach solution was made by mixing BRB80 buffer with 10 μM of Taxol, 0.047 mg/ml casein, 0.08 mg/ml catalase, 0.1 mg/ml glucose oxidase, 10 μM glucose, and 10 μM DTT to prevent the photo-bleaching of fluorescently-labeled molecules. Finally, functionalized, unlabeled microtubules were injected into the microtubule inlet reservoir and then observations were made using an inverted epifluorescence microscope (Axiovert 200, Carl Zeiss Microimaging, New York, USA) with a 40x oil immersion objective to obtain fluorescent imaging via a digital CCD camera (Orca ER II, Hamamatsu, Japan). After experiments, quantifications were conducted using Image J.

2.4.4 Results and discussion

To accomplish our goal we designed and fabricated a molecular sorter device using a typical microfluidic channel network, nanoimprinted nanotracks, and a polymer transfer bonding technique as illustrated in Figure 2-20(see also Figure 2-19 & Figure 2-21). First, a 20 μm deep and 50–100 μm wide microchannel network was fabricated as the top side of the device in which the horizontal channel was used to introduce kinesin and functionalized microtubules and the vertical channel was used to deliver target molecules to the functionalized microtubules as well as to provide ATP with surfaceimmobilized kinesin. Two buffer channels were used to achieve high selectivity by preventing other molecules dissolved in the analyte from diffusing towards the

collector. Second, to guide the functionalized microtubules to move towards the collector, nanoimprinted nanotracks were fabricated and then integrated as the bottom side of the device using a polymer transfer bonding technique (Figure 2-20C). This bonding technique enabled a horseshoe-shaped collector to concentrate the target molecules transported by the functionalized microtubules at a small spot of the device. Finally, to make the device operate without use of other external equipment such as a syringe pump, a dynamic range of flow rates of the analyte and buffer solutions was controlled by designing the microchannels to have proper hydrodynamic resistances and by adjusting hydrostatic pressure differentials among reservoirs (0–100 Pa).

To test the proposed device, we performed experiments using biotinylated microtubules and TMR labeled streptavidin containing analytes as shown in Figure 2-22. Biotinylated microtubules loaded at the bottom of the image (Figure 2-22A) are invisible because they are not labeled, but they are seen at the top of the image because they bind to fluorescently-labeled streptavidins while passing the analyte stream. This verifies that kinesin molecules adsorbed on the nanotracks surfaces successfully translocate the microtubules and the nanotracks guide them to move straight across the analyte stream towards the collector. In addition, the analyte flow is well hydrofocused by the buffer flows by controlling the hydrostatic pressure of reservoirs. Here, the volume of the analyte in the reservoir is about 200 μL, each volume of the buffer is about 100 μL, each volume of the microtubule containing solution in inlet and outlet reservoir is about 50 μL, and the waste reservoir is almost empty.

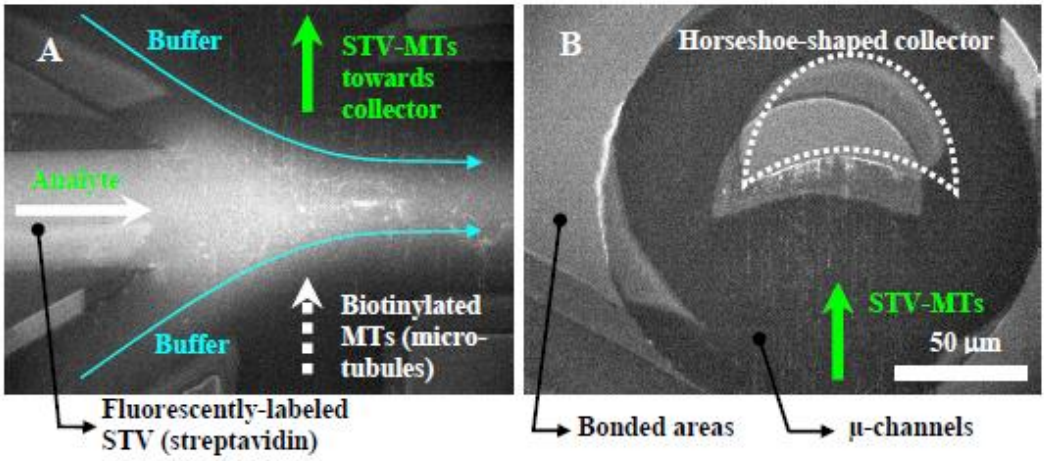

Figure 2-22: (A) shows the intersection of the device. A fluorescently labeled analyte stream flows from the left to the right and is well hydrofocused by two buffer flows. Biotinylated microtubules are heading upwards across the analyte. Prior to passing the analyte (at the bottom of the image) microtubules are invisible. However, after passing the analyte they are visible (at the top of the image). This is because the microtubules capture the fluorescently labeled target molecules (streptavidins) during passing the analyte stream. (B) Microtubules approaching the horseshoe-shaped collector are trapped at the deadlock of the collector and then chemically cross-linked, implying that the collector increases the concentration of target molecules

The horseshoe-shaped collector concentrated the target molecule-bound-microtubules as demonstrated in Figure 2-22B. After the microtubules have passed the analyte stream, the streptavidin-boundmicrotubules are continuously translocated by kinesin until they approached the collector (the white spots indicate the movement of microtubules). We can see most of the labeled microtubules accumulate at the deadlock of the collector and we believe that the collection of the microtubules proceeds via the following mechanisms: first, the leading ends of the microtubules are trapped into the gap which is likely to be generated at the fringe of the collector (between the top glass

substrate and the bottom nanotracks during the polymer transfer bonding process). Second, microtubules trapped in the collector decrease the number of locally available, active kinesins, thereby reducing the transport efficiency. Furthermore, microtubules are linked together since each streptavidin molecule can bind four biotins. These concentration mechanisms lasted more than an hour and increased gradually the target molecules at the collector as demonstrated in Figure 2-23.

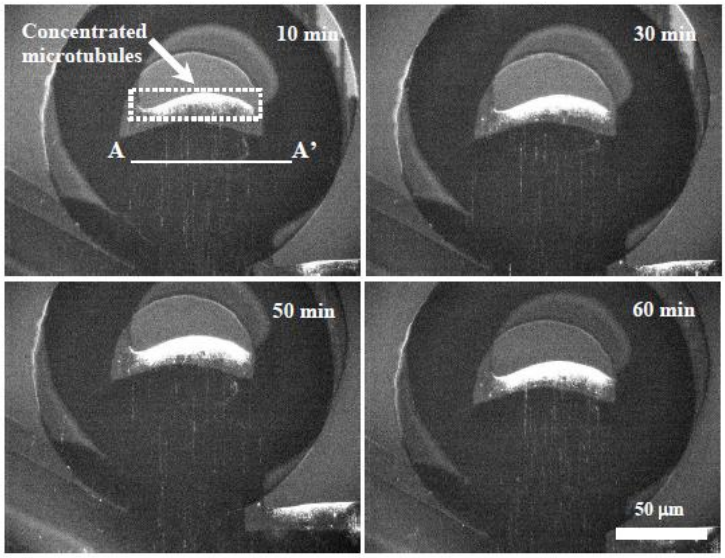

Figure 2-23: Image sequences of the horseshoe-shaped collector with time. The white spots within the rectangle (*t*=10 min) indicate the concentrated microtubules. The number of the microtubules approaching the collector and subsequently being cross-linked continues to increase more than an hour, resulting in higher concentrations of target molecules. The line of A–A' is used to estimate the sorting rates of target molecules in Figure 2-24A and the rectangle which is 25 µm by 70 µm is used to estimate the total number of concentrated target molecules from fluorescent signal enhancement in Fig. 4B.

As the functionalized microtubules carry the streptavidin molecules, we can estimate the sorting rate from the fluorescent intensity and the translocation speed of the microtubules (about 1.7 μm/s). Figure 2-24A shows the pixel intensities along the line of A-A' in Figure 2-23, *t*=10 min. The background signal is somewhat lower than the signal of the TMR-labeled microtubules heading towards collector. The integrated fluorescent intensity along the pixel line (220 pixels correspond to ~70 μm since a pixel resolution is 0.322 μm) is about 1000 AU (arbitrary unit) and 1AU corresponds to 3.1 streptavidin molecules/μm which was estimated by calibrating the microscope and camera setting(Kural et al., 2005). Therefore, the sorting rate of streptavidin molecules is calculated to be *Rate* = 1000 AUpixel × 3.1 molecules/μm2/AU⍰~0.322μm/pixel ×1.7 μm/s, which results in approximately 1700 molecules/s. This rate remained almost constant at different timeframes.

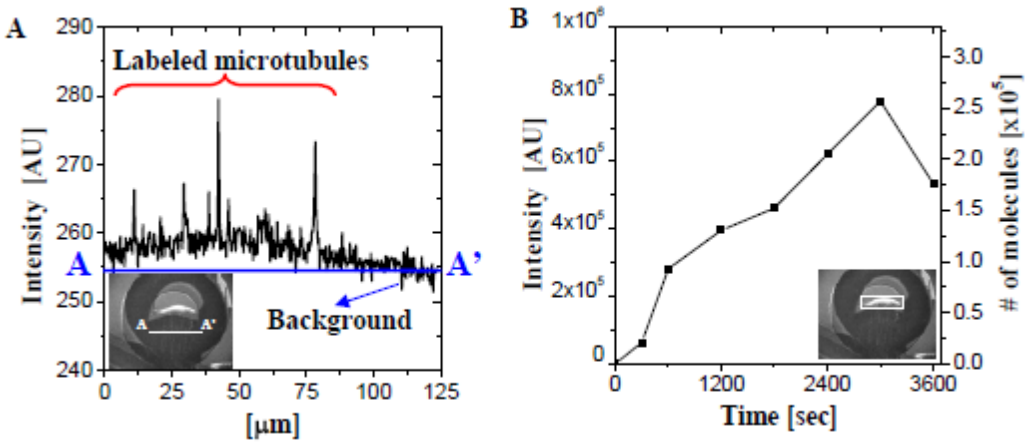

Figure 2-24: (A) shows the fluorescent intensities along the pixel line of A–A' in Figure 2-23, *t*=10 min (see also the inset) to estimate molecular sorting rates. From the microscope and camera calibration data and stoichiometry between biotinylated microtubules and streptavidins, it is estimated that ~10$_3$ molecules/s are removed

from the analyte stream and transported towards the collector. This is entirely due to the microtubule transport by kinesin. (B) The concentrated microtubules increase the fluorescent intensity, which was measured by summing up the intensities of every pixel in the dotted rectangle of Figure 2-23 with time (see also the inset). These intensity signals were also converted to the number of molecules. For example, $8\times10_5$ AU (arbitrary unit) (t=50 min) corresponds to ~$2.5\times10_5$ molecules in the collector (25 μm by 70 μm).

Another quantification of the device is to analyze the signal enhancement factor of the collected molecules. We determined a rectangle around the collector which is about 25 μm by 70 μm (see Fig. 3, t=10 min) and then summed up all intensities within the rectangle. Figure 2-24B shows the fluorescent intensity enhancement as well as the resulting number of streptavidin molecules concentrated at the collector with time. Since microtubules are translocated by kinesin in general gliding assay about 25–50 nm above the bottom substrate, the volume of the concentrated microtubules can be approximated to be V_{col}=50nm×~25μm× ~70μm. Hence, the molar concentration can be estimated to be ~5 μM ($2.6\times10_5$molecules/V_{col}) which is about 2×10^3 folds higher than the initial concentration of the analyte (2 nM). This result is quite comparable compared to other traditional methods(Quirino and Terabe, 1998) but overall the device is significantly efficient(Ramachandran et al., 2006; van den Heuvel et al., 2006).

The nanotracks played an important role in governing the performance of the device because the sorting rate of target molecules from the analyte stream to the collector is directly proportional to the number of microtubules guided by nanotracks. The width of the horizontal microtubule channel is about 100 μm but the width of collector is about 70 μm (see also Figure 2-23, t=10 min and Figure 2-24A). Since the

width of a repeatable pattern of the nanotracks is about 700 nm (350 nm valley and 350 nm bank), approximately 100 nanotracks (=70μm/700nm) can contribute to the sorting rate. Assuming that every nanotrack guides at least a microtubule and all biotin molecules bind to streptavidin molecules, the resulting sorting rate can be estimated to be $1.7\mu m/s \times 100 \times 160 biotins/\mu m = 2.7 \times 10^4$ molecules/second, which seems to be overestimated compared to the experimentally measured sorting rate by a factor of ten. However, if we take into account the binding affinity between biotin and streptavidin, the difference can be explained. Moreover, our previous study on the efficiency of the nanotracks supports that every nanotrack is unlikely to guide a microtubule at the same time.

To increase the binding affinity between target molecules (streptavidins) and functionalized (biotinylated) microtubules which is directly related to the performance of the device, the diffusion and/or saturation time of the target molecules to the functionalized microtubules needs to be optimized. From the analyte flow speed of 100 μm/s and the overlapping distance of the analyte channel with the horizontal channel (100 μm), the streptavidin molecules should diffuse to the bottom where the microtubules are translocated (25–50 nm above the bottom substrate[8]) within a second (t=100μm/100μm/s). From the diffusion equation of $\delta = Dt$ (where δ is the diffusion distance, $D=(10^{-10}–10^{-9})m^2/s$ is the diffusivity of streptavidin, and t =1 is diffusion time), the streptavidin molecules can travel as far as 10–30 μm in a second, which is longer than half of the channel depth (10 μm). Therefore, we expect that most of the streptavidin molecules can be bound to the biotinylated microtubules. Of course, for a

slow flow velocity, since the diffusion time increases, more target molecules can be bound to the functionalized microtubules. However, this can deteriorate the performance of the device because the target molecules can saturates the binding sites of the functionalized microtubules. On the other hand, for a fast flow velocity, shorter diffusion time cannot allow the target molecules to bind to the functionalized microtubules and the drag force caused by strong hydrodynamic shear may cause the microtubules to be lifted off. Therefore, the diffusion and saturation limit of the target molecules to the functionalized microtubules were carefully determined when the microchannels was designed and fabricated.

Finally, the performance of the device may depend on the conditions of the motility of kinesin and microtubule. Therefore, it is worth confirming that the device can provide enough ATP with kinesin at the intersection and the reservoirs contain a sufficient amount of analyte and buffer solutions during the experiments. Since the fastest analyte flow speed is about 100 μm/s and the channel is 20 μm deep and 50 μm wide, the required analyte volume over an hour is calculated to be 100 μm/s×20 μm×50 μm×1hr =0.36 μL, which is far smaller compared to the analyte volume in the reservoir (~200 μL). Similar calculations can be applied to the buffer and the flow of microtubule containing solutions, but the buffer and other reservoirs contain a sufficient amount of solutions to last much longer than an hour. In addition, the continuous flow rates ranging from 10 μm to 100 μm are believed to prevent local pH change and ADT accumulation via ATP hydrolysis by flushing all channels with fresh solutions.

In conclusion, we successfully demonstrated a state-of-the-art and self-powered micro-/nano-fluidic device for selective molecular sorting and higher concentration by employing the nanotransport ability of kinesin and microtubule as operating energy sources. We used microfluidic channels so that target molecules, buffer solutions, and ATP were properly delivered to the intersection where functionalized microtubule are translocated by kinesin and the flow rates within the microchannels were well controlled by adjusting the volumes of analyte, buffer, and other solutions in the reservoirs. We also used nanoimprinted nanotracks so that the functionalized microtubules were guided to move across the intersection. While the functionalized microtubules passed the intersection, they were able to bind to target molecules and transport them away from the analyte stream. Subsequently, we concentrated the target molecule-bound-microtubules at a fixed spot on the device for sensitive detection with a high NA objective by integrating the horseshoe-shaped collector with nanotracks via the polymer transfer bonding technique. The designed collector physically trapped the leading ends of target molecule-bound microtubules into the gap between the nanotracks and the horseshoe-shaped microstructure, followed by chemical cross-linking. We used biocompatible materials to obtain better motility of kinesin and microtubule in the device, so that it was possible to selectively remove a few thousand biomolecules from the analyte stream and achieve as high as 10^3 folds pre-concentration within an hour. Finally, we note that this approach can be useful to build portable, selective, and sensitive biosensors and promises integration of other microanalysis steps for complete, stand-alone, and lab-on-a-chip applications.

CHAPTER 3

STRUCTURAL DETERMINANT OF KINESIN'S DIRECTIONALITY

3.1 Introduction

Molecular motors move along cytoskeletal filaments by generating mechanical forces from the energy made available by ATP hydrolysis and are responsible for various tasks in different cell types. For example, an actin-based molecular motor, myosin II, can sliding along a actin filament and is responsible for muscle contraction; another actin-based motor, myosin V and the microtubule-based motors cytoplasmic dynein and kinesin-1 function as carriers and transport organelles by moving along their respective filaments; one member of kinesin-14 family, Ncd, can produce force on microtubules to help maintain and elongate the length of mitotic spindles(Hirokawa et al., 1998; Johnston et al., 1991; Sharp et al., 1999).

The detail mechanism by which molecular motors convert the chemical energy from ATP to generate mechanical force remains fundamentally unclear and significant efforts from a number of group are directed towards closing these gaps in our understanding. One very important unresolved question is how different motors from the same motor superfamily with virtually identical structure in the head domain can

generate the forces and movements in different directions along cytoskeletal filaments. These different directionalities within the same kind of motors can be found either in the myosin or in the kinesin superfamily. For example, in the kinesin superfamily, most members are microtubule plus-end-directed motors, whereas the members in kinesin-14 family are minus-end directed motors. As pointed out above, the interesting (surprising) observation is that the crystal structures (Kozielski et al., 1999; Kozielski et al., 1997; Sack et al., 1997)of these motors are so similar that we expect that the fundamental mechanisms of ATP energy transduction and motility to be very similar, yet they can produce movements in the opposite direction along filaments. Therefore, studying motor's directionality can not only tell us how motors control their directionality, but also give us more information on how motors regulate their motions. The goal for my work was to determine which domain of kinesin motors controls their directionality. For this work I used a mutagenesis-based approach to create kinesin mutants in which domain hypothesized to be determinants of kinesin's directionality were altered and the functional consequence of the changes where experimentally tested by multiple motor in vitro motility assays.

3.1.1 Kinesin's directionality

As described above, one of the motor superfamily that is comprised of motors with different directionalities is the kinesin superfamily. The kinesin superfamily contains fourteen different families(Lawrence et al., 2004). A key feature of kinesins is that they move in a predetermined direction along the microtubule that they interact

with. All families of kinesin superfamily, except kinesin-14, are plus end-directed motors which means that they move toward the microtubule's plus-end or fast growing end(Vale et al., 1985b; Walker et al., 1990). Kinesins contain a motor domain (also called the head domain or catalytic core domain), a neck, coiled-coil part and a tail domain. Most kinesins are N-terminal motors in which the head domain is at the amino-terminal end of the protein whereas some kinesins are C-terminal motors in which the head domain is located at the carboxyl terminus of the protein. Interestingly, all plus end-directed kinesins are N-terminal motors, whereas minus end-directed motors are C-terminal motors(Endow, 1999). The exact mechanism by which kinesins can be directed to the minus-end or plus-end of microtubules is still unknown.

Kinesin-1 (also referred to as conventional kinesin or kinesin) was the first discovered (Brady, 1985; Funatsu et al., 1997) and remains best studied. Ncd (Non-claret disjunction), which belongs to the kinesin-14 family, has been discovered early on the 90' and it became soon thereafter apparent that Ncd moves in the opposite direction as kinesin(McDonald and Goldstein, 1990; Walker et al., 1990). Therefore, kinesin, along with Ncd, are used as kinesin directionality model. Interestingly, although the amino acid sequences of kinesin and Ncd are only 40% homologous in their catalytic cores(Endow et al., 1990; Sablin et al., 1998) the crystal structures of kinesin and Ncd show that the head domains are nearly identical(Kozielski et al., 1999; Kozielski et al., 1997; Kull et al., 1996; Sablin et al., 1996).

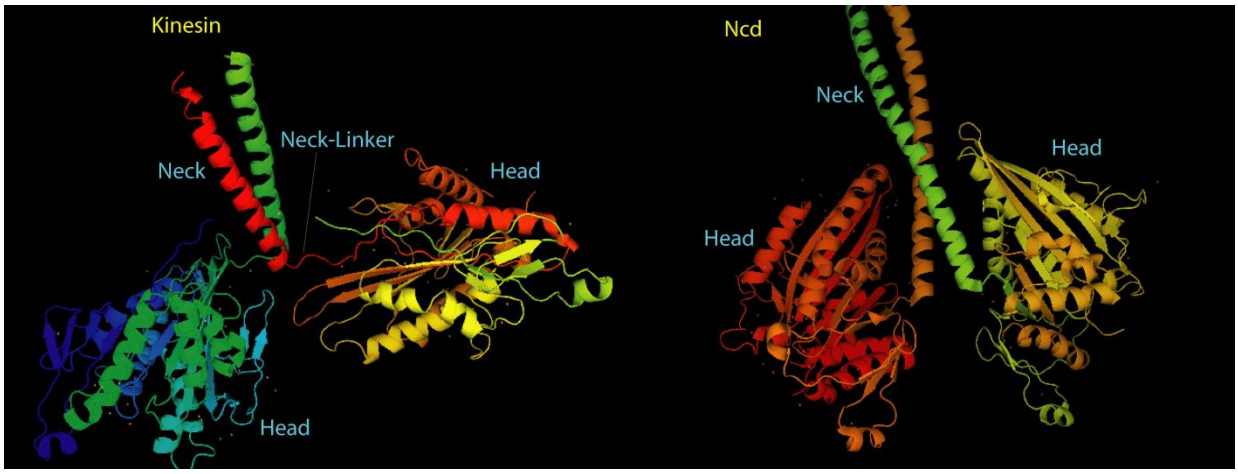

Figure 3-1: The crystal structure for kinesin (dimer crystal structure; PDB # 3KIN (Kozielski et al., 1997)) and Ncd (dimer crystal structure; PDB #1C7Z (Sablin et al., 1996)). Pictures were generated by Pymol, DeLano Scientific LLC.

The crystal structure of the N-terminal region of kinesin is shown on the left of Figure 3-1. The head domain which has amino acid residues 1-338, contains a flexible, about 15 a.a. neck-linker in the C-terminus of head domain followed by a ~30 a.a. long coiled coil commonly referred to as the neck domain. The head domain includes the microtubule binding and ATP hydrolysis sites. Associating with the binding of ATP, the head domain has a large structural reorganization that is believed to directs kinesin motor toward the plus end of microtubules(Rice et al., 1999; Tomishige and Vale, 2000) and plays an important role in the processivity of kinesin(Rosenfeld et al., 2003). The neck domain is responsible for dimerization of kinesin and is also implicated in influencing to the processivity of kinesin(Thorn et al., 2000). As shown on the right side of Figure 3-1, a crystal structure of Ncd indicates that the head domain of Ncd is located at the C-terminus, and with the neck domain extended N-terminally from the head domain. The head domain of Ncd, similar to that of kinesin, contains the sites for

ATP-hydrolysis and microtubule-binding, while the neck domain dimerizes Ncd and is postulated to direct the motor to the minus direction(Sablin et al., 1998). Structurally, the similarities of kinesin and Ncd are: (1) The head domains of kinesin and Ncd are virtually identical even they are only 40% identity in their amino-acid sequences. (2) The functions for both heads are the same. They both bind microtubule and hydrolyze ATP. (3) The dimerization function for both necks is the same. The most striking structural differences between the two kinesins is that Ncd does not have neck-linker between neck and head domains.

3.2 Result and discussion

3.2.1 Does the neck domain of kinesin determinant motor's directionality?

In an early study, Kinesin and Ncd were truncated leaving different lengths of coiled-coil domains at their C-terminus and N-terminus, respectively (Stewart et al., 1993). These truncated kinesin and Ncd mutants did not change their direction of movement along the microtubules. This result suggested that some parts close to the motor domains of kinesins dominate their directionality (Figure 3-2). In addition to this truncation study, two reports coincidentally constructed kinesin chimeras in which kinesin-1's catalytic core domain was replaced with Ncd's head domain(Case et al., 1997; Henningsen and Schliwa, 1997). Although these kinesin chimeras have the head domain of wildtype Ncd which supports minus-end directioned movement, these chimeras are plus-end directed motors (Figure 3-2). Both experiments indicated that the head domains do not determine kinesin's directionality.

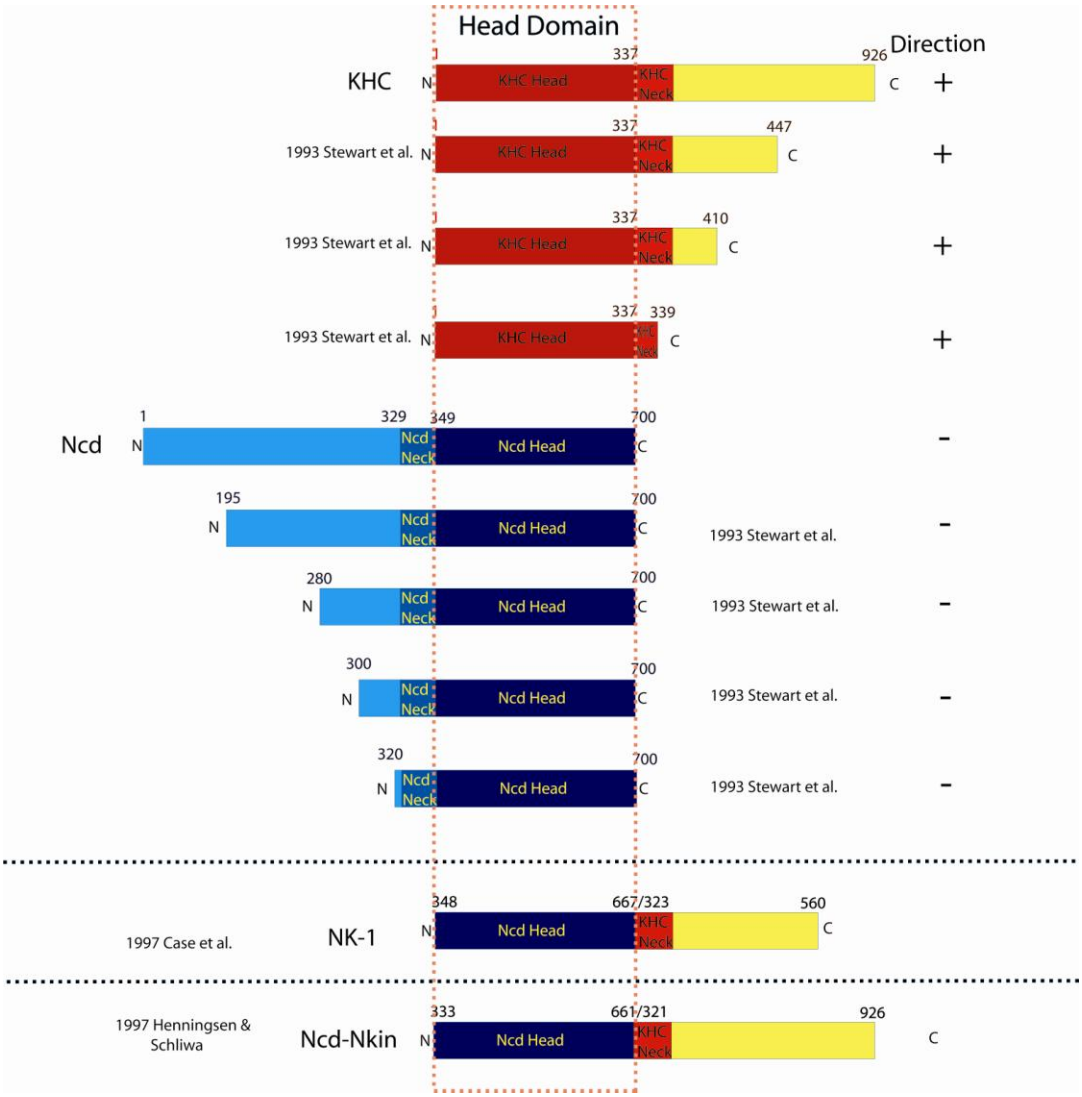

Figure 3-2: Kinesin directionality studies. Early work regarding kinesin's directionality was based on truncation on kinesin's stalk domains or replacing kinesin's head domain with Ncd's head domain(Case et al., 1997; Henningsen and Schliwa, 1997; Stewart et al., 1993).

3.2.1.1 The neck domain

Truncation studies and the kinesin chimera studies, together, suggested that domains close to but outside of the head domain may control kinesin's directionality.

This domain, in both plus-end and minus-end directional motors, is identified as the neck domain from the amino acid sequences.

The neck domain, in both conventional kinesin and Ncd, is a rigid coiled-coil structure formed by two identical α helixes with heptad repeats arrangement. This heptad repeat, which is a sequence of amino acids with every seven residues as a section and in each section the first and the fourth amino acids are hydrophobic residues, has been recognized as an important identification for the coiled-coil structure(Kozielski et al., 1997). This coiled-coil neck domain is rigid; thus, the neck domain is ordered in crystal and demonstrated in most x-ray scattering structures of kinesin(Kozielski et al., 1999; Kozielski et al., 1997; Kull et al., 1996; Sablin et al., 1996). This coiled-coil property of the neck domain is responsible for several functions of kinesin. First, the rigid neck domain accompanied by another coiled-coil domain, the stalk domain, is believed to be sufficiently rigid such that this coiled-coil part acts as a rigid rod (lever arm) to provide a power stroke for the forward motion of the Ncd motor(Endres et al., 2006). In addition, this lever-arm power stroke mechanism is further confirmed by an early crystal structure study of Ncd which shows that the neck domain is able to rotate about 75 degrees relative to its head domain with a pivot point in the junction of the neck and head(Yun et al., 2003). Also, the coiled-coil structure of the neck domain is responsible for kinesin's dimerization in which two kinesin monomers form a functional dimer in their neck and stalk domains. Another function of the neck domain is to support kinesin's processive movement. This processive movement of kinesin is aided by highly positive-charged residues in the neck domain

that interact with the negative-charged C-terminal region of β tubulin (E-hook). This electric static interaction helps kinesin stay on and processively move along microtubules and thus, increases kinesin's processivity(Thorn et al., 2000).

3.2.1.2 The sequence and crystal structure of kinesins suggest neck domain has interaction with head domain

The amino acid sequences and crystal structures comparisons show that this neck domain is directly jointed to the head domain in both conventional kinesin and Ncd but with different joint positions (Figure 3-3 and Figure 3-4). The C-terminus of the coiled-coil neck domain is joined to the N-terminus of Ncd's head domain; while in conventional kinesin, the neck domain extends from the C-terminus of kinesin's head domain. Although no direct evidence indicates that the neck domain interacts with the head domain, the proximity between kinesin's head and neck domains makes it likely that the neck domain has interactions with the head domain. These head-neck interactions may, therefore, control kinesin's directionality.

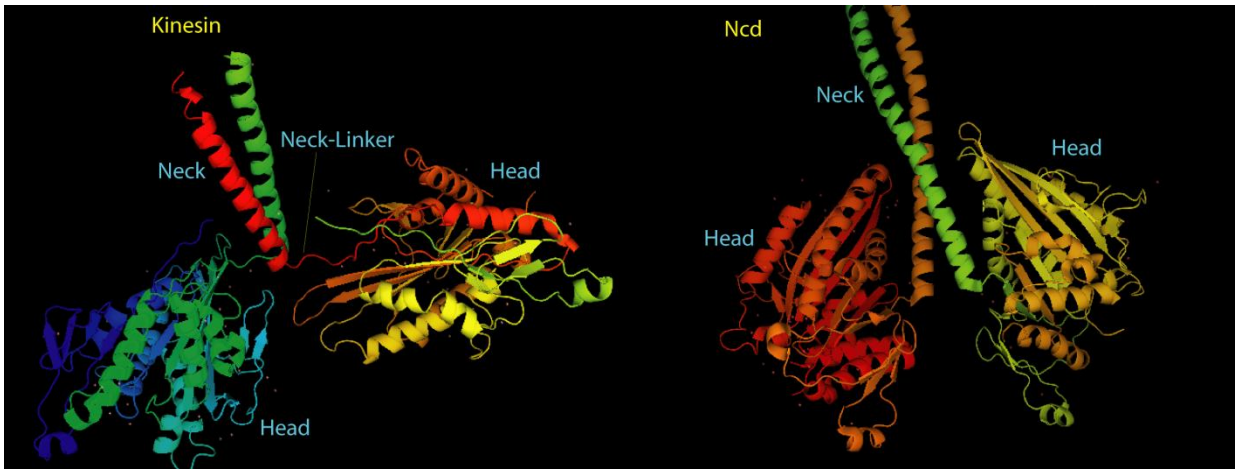

Figure 3-3: The crystal structure for kinesin (dimer crystal structure; PDB # 3KIN (Kozielski et al., 1997)) and Ncd (dimer crystal structure; PDB #1C7Z (Sablin et al., 1996)). Pictures were generated by Pymol, DeLano Scientific LLC.

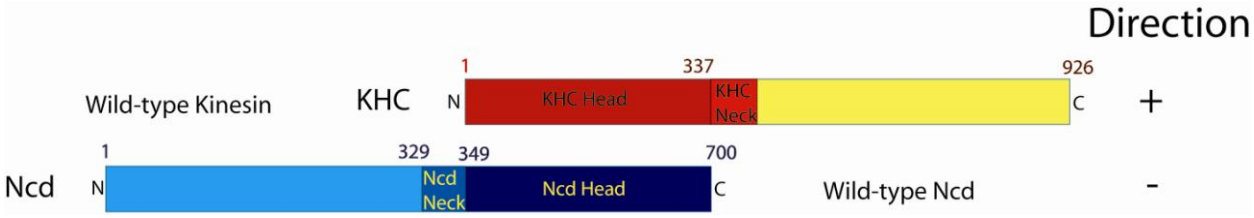

Figure 3-4: Amino acid sequences (primary structures) for kinesin-1 (KHC) and Ncd and their moving direction on the microtubules

If the kinesins' directionality is controlled by interactions between the neck domain and the head domain, the steric position (or proximity) between these two domains becomes essential. In other words, if there is any change in the relative orientation on these domains, the interaction between the neck and head domains will be disrupted. This proximity is confined by the connection between the neck and head domains. In minus-end directed kinesin, Ncd, it is the C-terminus of the neck domain that is connected to the head domain; thus the C-terminus of Ncd's neck domain is

closer to the head domain than its N-terminus. On the contrary, in conventional kinesin, the N-terminus of the neck is directly connected to the head domain; therefore, the head domain's proximal neck is the N-terminus of neck domain. Consequently, Ncd's C-terminal neck is more likely to interact with its head while it is kinesin's N-terminal neck that may interact with its head domain. It is possible that the neck controlling kinesin's direction is through this proximal interaction between the head and neck. Therefore, if a kinesin has its neck replaced by a neck from a different directional kinesin, the new neck domain may interact with the head domain reversely and move to different direction. As a consequence, this neck-replaced kinesin will change its moving direction.

3.2.1.3 Mutation experiments for testing if the neck domain controls kinesin's directionality

To test if the neck domain controls kinesin's directionality, PCR techniques were used to engineer the mutants, HKNcd and NcdHK. HKNcd is constructed based on a truncated human kinesin (kinesin-1) containing residues from 1 to 560, and its neck is replaced with reversed Ncd's neck to mimic the potential proximal interactions between Ncd's neck and head domains. NcdHK was engineered from a wild-type Ncd with its neck domain being replaced with reversed kinesin-1's neck domain to mimic the potential interactions between the conventional kinesin's neck and head domains(Figure 3-5).

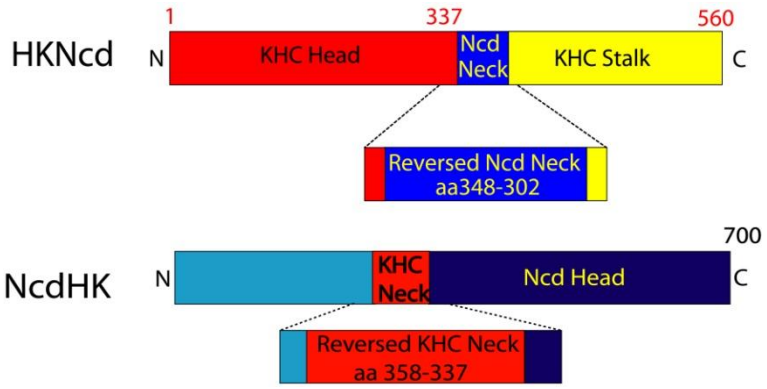

Figure 3-5: Amino acid sequences of HKNcd and NcdHK

Kinesin mutants are tested in multiple motor gliding assays (Figure 3-6) with polarity-marked microtubules which have both ends brighter than the center part and a longer plus end than the minus end(Howard and Hyman, 1993) (Figure 3-7). The fidelity of end labeling of polarity marked microtubules are tested by wild-type human kinesin which is known a plus-end directed kinesin. The result showed that more than 98% of microtubules are labeled correctly (N>300).

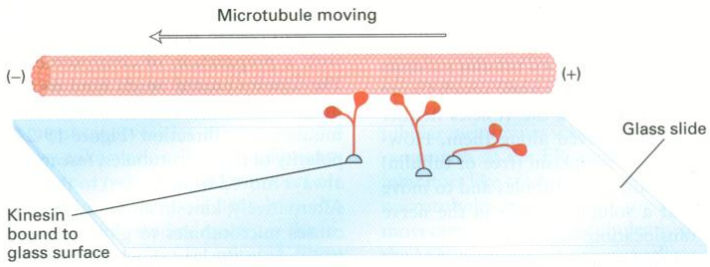

Figure 3-6: Arrangement of kinesin motors and microtubules in multiple motor gliding assays and polarity-marked microtubule gliding assays. This figure depicts plus-end directed kinesins. Figure is taken from Molecular Cell Biology 5E, Lodish et al(H. Lodish, 2003).

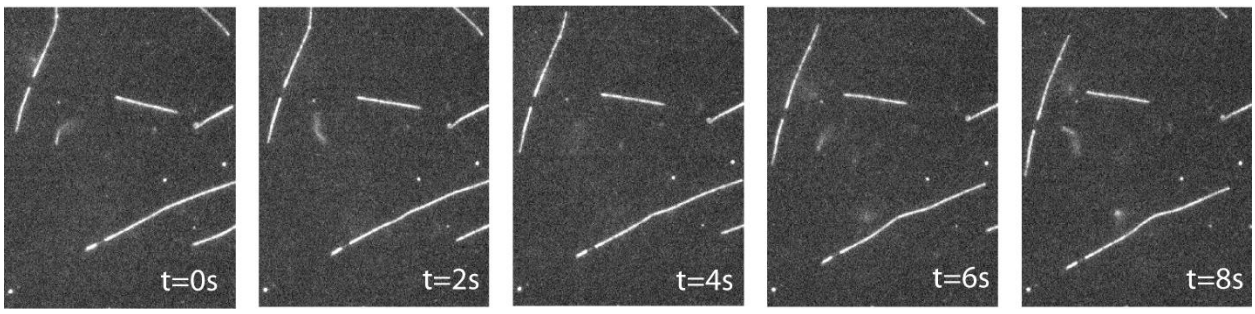

Figure 3-7: Multiple motor gliding assay with polarity-marked microtubules. The slow-growing minus-ends are marked by short bright segments and, conversely, the fast growing, plus-ends are marked by long bright segments. In this sequence of video images two polarity-marked microtubules are seen to move with the short, bright ends leading which indicates that HKNcd is a plus-end directed motor.

3.2.1.4 The neck domain does not control the directionality of conventional kinesin

The results of motility properties of the chimera HKNcd and NcdHK are summarized in Figure 3-8. The gliding velocity of HKNcd is similar to wild-type conventional kinesin, and the directionality of HKNcd is the same as kinesin. This indicates that Ncd's neck does not alter the directionality or the speed of conventional kinesin. This result also indicates that the neck domain is not the sole determinant of directionality for conventional kinesin. The gliding assays show that NcdHK does not support motility in gliding assays. This suggests that Ncd's neck plays a specific and essential role in the force generating mechanism of Ncd motor. Certainly, the neck domain of Ncd does alter or revert the directional properties of the kinesin-1 motor domain.

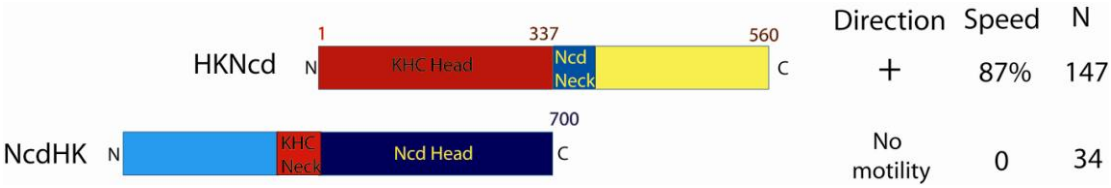

Figure 3-8: Amino acid sequences of HKNcd and NcdHK with directionalities and speed measured in the multiple motor gliding assays with the polarity-marked microtubules.

The mutant of convention kinesin, HKNcd, has the same directionality as wild-type conventional kinesin regardless of its neck being replaced with a comparable part of the reverse directional motor. This result implies that the neck domain does not dominate kinesin's directionality. This conclusion, in combination with the results from the kinesin truncation experiments by Stewart et al., which suggested that parts close to the head domain control the directionality, indicates that some parts much closer to the head domain than the neck domain control kinesin's directionality (Figure 3-9). It has been proposed on the basis of the crystal structure of conventional kinesin that the neck-linker, which is located between the head and neck domains, is much closer to the head domain than the neck domain and may be responsible for conventional kinesin's directionality.

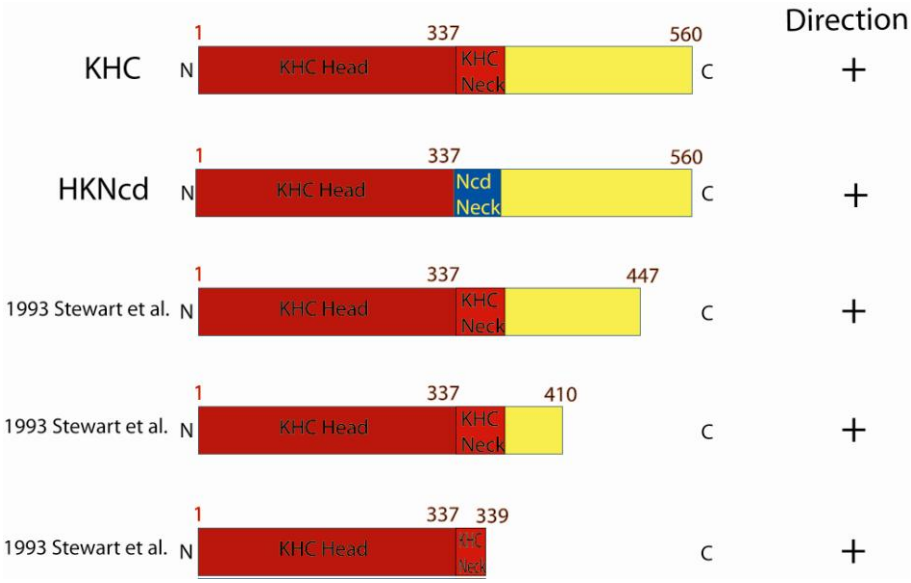

Figure 3-9: Mutations of kinesin-1. KHC: wild type kinesin, HKNcd: kinesin has neck region replaced with Ncd's neck and coiled-coil domain truncated kinesins from Stewart et al., 1993.

3.2.2 Does the neck-linker determinant motor's directionality?

3.2.2.1 The neck-linker

The crystal structure of kinesin has showed that the neck-linker is a flexible linker between the globular head domain and the coiled-coil neck domain(Kozielski et al., 1997; Sindelar et al., 2002). Mutation of this neck-linker area disables kinesin's motility suggesting that the neck-linker is essential for kinesin's motility(Case et al., 2000). Cross-linking one residue from this linker at its C-terminus to the globule head domain dramatically reduces kinesin's velocity and processivity(Tomishige and Vale, 2000). This reduction in velocity and processivity suggests that the neck-linker detaches and reattaches to the head domain and has a conformational change linked to ATP hydrolysis. In addition to these kinesin mutant experiments, Cyro-EM images and

electron paramagnetic resonance (EPR) showed that kinesin's neck-linker changes its position coupled to changes in nucleotide state(Asenjo et al., 2006; Rice et al., 1999). Taken together, these studies indicated that the neck-linker is flexible at nucleotide-free and ADP states but becomes ordered when the motor domain is in the ATP state, and the neck-linker has its C-terminus pointing toward to the plus end of the microtubule. Although these experimental observations are from a number of separate experiments, together, they suggested that the transition of the neck-linker form a flexible to an ordered state that interacts with the globular head domain in a directed, ordered manner suggests that the neck-linker may play a key role in kinesin's plus-end directionality.

As highlighted above, previous studies of kinesin's directionality revealed that Ncd's head domain combined with some parts of kinesin-1 can result in plus-end directed motors, regardless the head domain is from a minus-end directional motor. These results indicated that parts beside the head domain control kinesin's directionality(Case et al., 1997; Henningsen and Schliwa, 1997). In these studies, three parts from plus-end directional kinesin were combined with Ncd's head domain: neck-linker, coiled-coil neck and stalk domains. As these studies suggested that the head domain does not control the directionality, which of these three kinesin-1 domains contributes to kinesin's directionality is unclear. That the neck and stalk domains control kinesin's directionality is ruled out because kinesins with necks from motors that support movement in different directions (this current study, HKncd) and kinesins without stalk(Stewart et al., 1993) do not change their direction. Based on these conclusions the neck-linker is the only structural domain left that may determine the

direction of movement. Indeed, the neck-linker appear a likely domain to control kinesin's directionality because first, as suggested from the study of HKncd, it is closer to the head domain than the neck domain. Second, it is randomly oriented in the nucleotide states other than ATP state and third, it is pointing towards the plus-end of the microtubule in the ATP-bound state. If the neck-linker determines kinesin's directionality, a conventional kinesin with its coiled-coil neck and stalk domains deleted will have the same directionality as wild-type kinesin-1. The results of this extremely truncated kinesin chimera, the early kinesin chimera experiments(Case et al., 1997; Henningsen and Schliwa, 1997) and the observations from previous truncated kinesin experiments(Stewart et al., 1993), together, will provide us with more information on which parts control kinesin's directionality.

3.2.2.2 Evidence that the neck-linker is an important determinant of kinesin's directionality

To test the hypothesis that the neck-linker determines kinesin's directionality, a kinesin mutant, HKnl, was cloned. HKnl has the head domain of conventional kinesin and the complete neck-linker but all coiled-coil neck and stalk domains were eliminated (Figure 3-10).

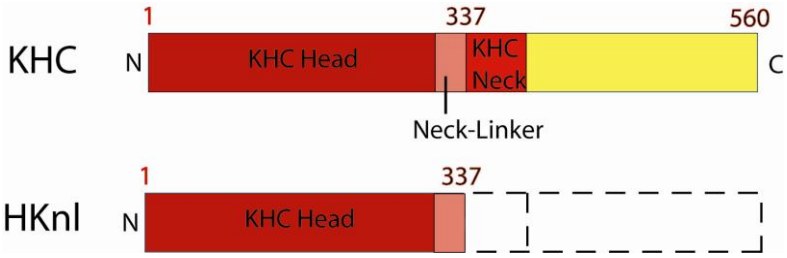

Figure 3-10: Domain organization of HKnl and conventional kinesin. HKnl laches the coiled-coil neck domain and stalk domain.

HKnl's directionality is measured in the gliding assays with polarity-marked microtubules. The gliding assays show that the microtubules moving with their short bright ends as the leading ends. This indicates that HKnl is a plus-end directional motor (Figure 3-11). This result suggests that the coiled-coil neck domain and the stalk domain are not necessary for kinesin's directionality.

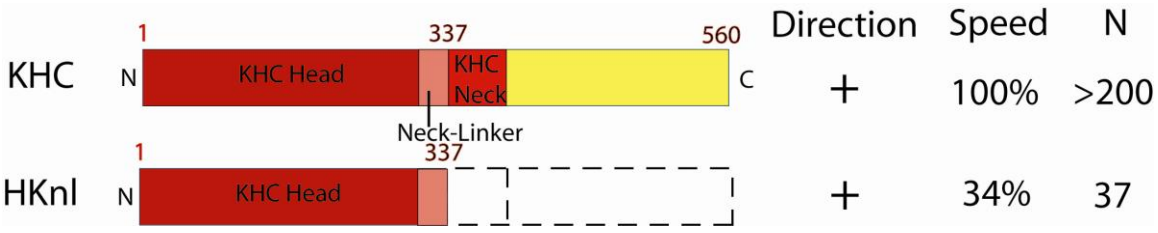

Figure 3-11: The result of HKnl shows that HKnl is a plus-end directed motor.

As discussed previously, two early kinesin studies in which kinesins' head domains are replaced with Ncd's head domain suggested that the head domain is not the determinant for kinesin's directionality(Case et al., 1997; Henningsen and Schliwa, 1997). In these studies, researchers eliminated the possibility that the head domain controls kinesin's directionality. However, they did not identify which part other than head domain determines the directionality. In this current study, a kinesin mutant,

HKnl, was engineered in which the neck domain and the stalk domain were deleted and only the neck-linker remains intact. This kinesin mutant, HKnl, does not change its directionality regardless that the neck and stalk domains are eliminated (Figure 3-12). This result accompanied by the results from Henningsen and Schliwa and that from Case et al. demonstrates that no matter how the kinesin's head domain is replaced or the coiled-coil parts are truncated, as long as there is a neck-linker, this motor is plus-end directed motor. Therefore, these results indicate that the neck-linker determines kinesin's directionality. In addition, two previous studies about mutations in the neck-linker indicated that the neck-linker also plays an important role in ATP hydrolysis function(Case et al., 2000; Tomishige and Vale, 2000). These neck-linker studies and current work, together, suggest that the neck-linker not only controls kinesin's directionality but also controls kinesin's ATP energy transduction.

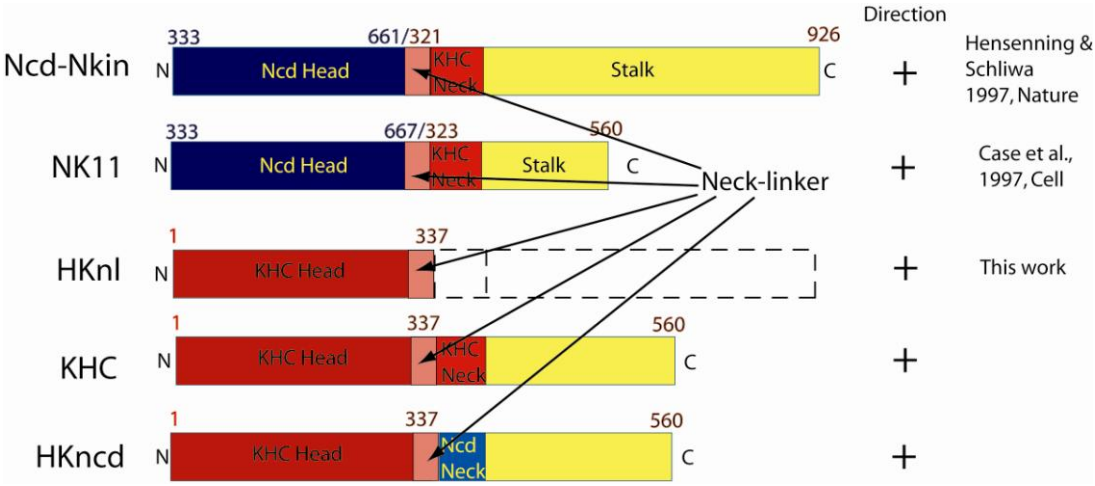

Figure 3-12: The neck-linker's role in directional motility. Regardless kinesin's head domain is replaced or the stalk domain is truncated, as long as the neck-linker is intact, the kinesins are the plus-end directed kinesins.

3.2.3 The neck-head joint does not determine the directionality of Ncd

In the above section I presented evidence that kinesin's directionality is controlled by the neck-linker. Since Ncd is an analogue to the conventional kinesin, I hypothesized that Ncd might use a domain similar to the neck-linker to control its directionality. However, from the sequence alignment of Ncd and kinesin, there is no part comparable to the neck-linker in Ncd. In addition to this sequence alignment, the crystal structure of Ncd shows that there is no residue between the neck domain and the head domain which is the place that the neck-linker presented in the conventional kinesin(Sablin et al., 1996). Therefore, Ncd does not appear to use an analogue of the neck-linker to control its directionality. However, Ncd may employ a mechanism similar to that used by the neck-linker to control its movement toward the minus end of microtubules. One of the necessary requirements for the neck-linker to direct kinesin is that the directional determinant must be very close to the head domain. In addition, the work of Steward et al. (1993) also showed that the part control Ncd's directionality must be sufficient close to the head domain(Stewart et al., 1993). Thus, this head-proximal part is reasonable candidates for the directional determinant in Ncd.

A head-proximal part that might control Ncd's directionality is the joint area of the neck and head domains. This joint has been reported in a previous study of kinesin's directionality by Endow and Waligora. In this study chimeric motors consisting of kinesins with Ncd's neck at the N terminus and kinesin motor domains in C terminus move either toward the plus or the minus end of the microtubule. This

reversal of direction seems to be based on mutating two residues in the junction of the neck domain and the motor domain (Endow and Waligora, 1998). Replacing two residues from Ncd's neck domain (glycine and asparagines, or GN) with two residues from kinesin's head domain (aspartate and serine, or DS) changes a minus-end directional kinesin to a plus-end directional motor (Figure 3-13). Although these kinesin chimeras have only two to nine percent of the speed of wild-type Ncd, this minor residue changes leads to a kinesin with reversed direction indicates that this joint of neck and head domains may play a leading role in Ncd's directionality.

In Endow and Waligora's study, however, the kinesins contain elements of both Ncd's neck domain and kinesin's head domain. Therefore, the conclusion that the neck-head joint controls wild-type Ncd's directionality remains uncertain. If this inter-domain joint determines Ncd's directionality, wild-type Ncd with neck-head joint mutated to the same change (G and N are replaced with D and S) may reverse the direction of wild-type Ncd and move toward the plus end of the microtubules.

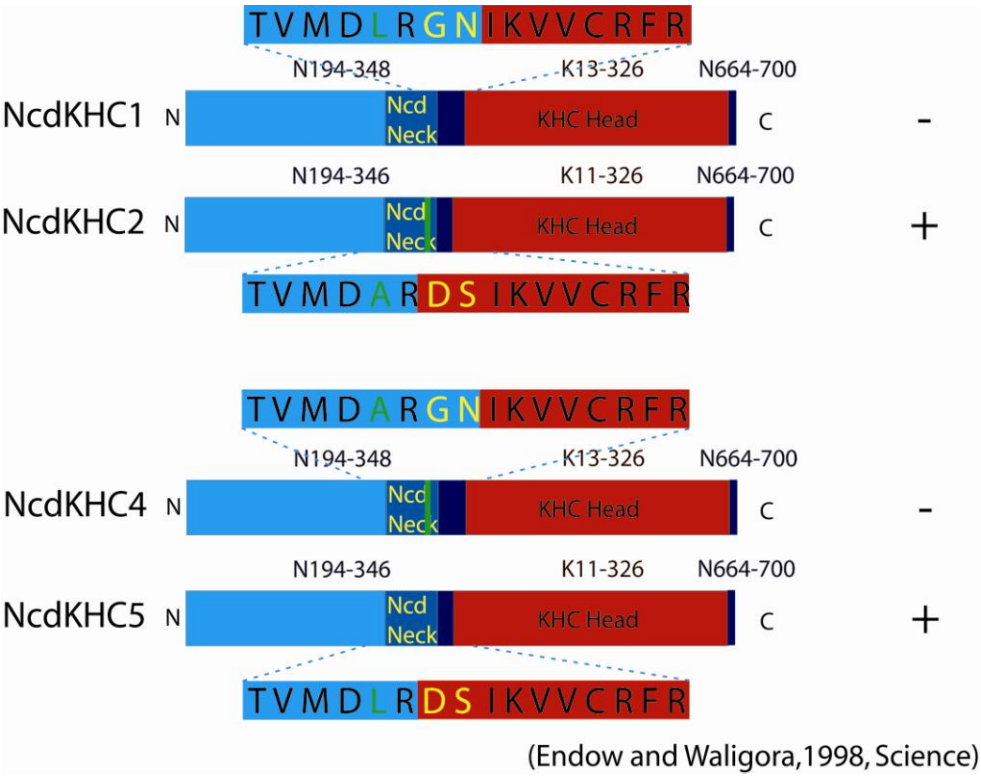

Figure 3-13: Kinesin chimeras with altered directionality. Kinesin mutation which has Ncd's neck domain and kinesin-1's head domain is either a plus-end or minus-end directed motor. The characters beside mutant's primary structure are detail amino acid sequences in the neck-head junction.

3.2.3.1 Experiments probing the role of the neck-head joint in Ncd's directionality

To test if the neck-head joint determines Ncd's direction, I constructed several Ncd mutants where residues in the joint area were replaced with different amino acids. The first Ncd mutant, NcdG347DN348S, has the residues in the joint area, G and N, replaced by residues D and S (Figure 3-14) as previously described by Endow and Waligora (1998). These authors reported that kinesin-Ncd chimeras with this DS replacement reverse their direction to the plus-end of the microtubules. I tested the directionality of NcdG347DN348S in the gliding assays with the polarity-marked

microtubules and found that the microtubules are bound to the motor coated surface only and do not have motility. This result indicates that NcdG347DN348S is not a functional motor and implies that the neck-head joint does not control Ncd's directionality.

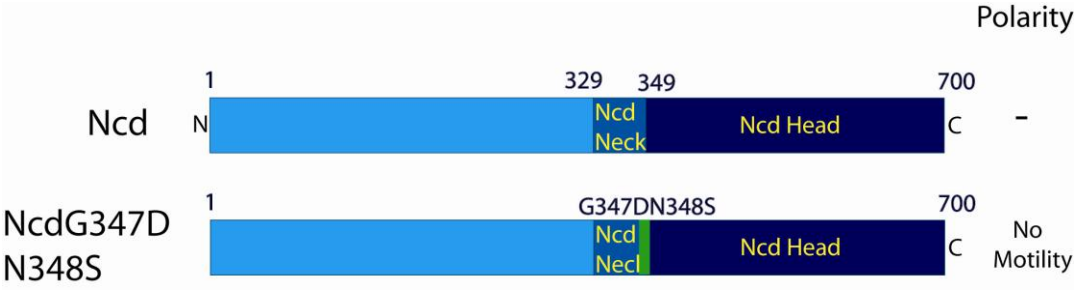

Figure 3-14: Ncd mutant NcdG347DN328S is an Ncd motor with neck mutations. Residues 347 and 348 are located in the neck-head joint.

Two reasons may be able to explain why this minor mutation in the joint area disables kinesin's motility. First, the ATPase activities of NcdG347DN348S are disabled by the replacement residues; therefore, NcdG347DN348S cannot support the multiple motor gliding assays. However, it is very unlikely that only two residues changes can destroy the entire ATPase activities of the motor. The ATPase activities should be reduced slightly with only two residues being mutated because in most of the mutant studies, the ATPase activities of motors will be gradually reduced by progressively mutating residues. Furthermore, these two residues are on the surface area of the motor domain which is not close to nucleotide binding pocket for intake the ATP molecules or in the energy transduction pathway of ATPase for transmitting energy of hydrolyzing ATP to provide motor's motion. Consequently, the mutation in this joint area will not interrupt the hydrolysis of ATP and should not fully block Ncd's

ATPase activities. On the contrary, if the ATPase activities are not entirely blocked by the replacement residues, NcdG347DN348S should support microtubules' movement in the multiple motor gliding assays. However, this mutated Ncd cannot facilitate microtubules' movement; as a result, the reason that the ATPase activities are disrupted by the replaced residues is ruled out.

The second reason is that the replacement residues disrupt the power-stroke mechanism of Ncd; and thus, mutated motors cannot support the gliding assays when their power-stroke mechanism is disrupted. An alternative, but similar reason may be that the power-stroke mechanism of the neck domain also facilitates ATP hydrolysis by the head domain and Ncd with disrupted power-stroke mechanism could neither facilitate microtubule movement nor undergo the ATPase activities. Therefore, the mutated motors could not support the multiple motor gliding assays. This disruption of Ncd's power-stroke mechanism by the replacement of only two residues may be based on these neck-head joint residues act as a pivot point of the coiled-coil lever-arm which swings relative to the head domain to provide a power-stroke. This coiled-coil neck and stalk domains provide the power-stroke in Ncd is supported by Ncd mutation studies (Endres et al., 2006) and a crystal structure study of Ncd which showed that the neck coiled-coil can rotate to provide power-stroke with this neck-head joint as a pivot point(Yun et al., 2003). In addition to this power-stroke study for microtubule-based motor, Ncd, another report suggested that an actin-based molecular motor, myosin II, which also uses lever-arm to provide a power-stroke for motor movement, uses a glycine residue as its pivot point to undergo power-stroke(Higuchi and Endow, 2002;

Ruff et al., 2001), and this glycine residue is the same as one of residues mutated in this current work. Therefore, this glycine, G347, in Ncd may act as a pivot point for Ncd's motion.

To further test that the G347 is a pivot point and confirm that the neck-head joint does not control Ncd's directionality, two more Ncd mutants, NcdN348K and ncdN348A, were constructed. These two mutants have the pivot-point residue G347 intact whereas in NcdN348K, the uncharged residue N348 is replaced with a highly charged residue lysine (K) and in NcdN348A, the large residue N348 is replaced with a small residue alanine (A). The multiple motor gliding assays with polarity-marked microtubules show that both NcdN348K and NcdN348A have the same directionality as wild-type Ncd (Figure 3-15 and Figure 3-16). This indicates that these replacement residues do not alter the function of Ncd, regardless of their charge or smaller size. In addition, these biophysical similarities between wild-type Ncd and the mutants NcdN348K and NcdN348A and the immotile property of NcdG347DN348S suggest that the residue N348 is not essential for Ncd's directionality whereas the residue G347 is crucial for supporting motility of Ncd. Besides, the residue G347 is in the neck-head joint, which is a point acts as a center for coiled-coil neck rotation(Yun et al., 2003), and it is exactly same amino acid residue glycine as the pivot point for myosin II(Ruff et al., 2001). Therefore, I propose that the residue G347 probably has the function as the pivot point for lever-arm of Ncd(Higuchi and Endow, 2002). In summary, G347 acts as a pivot point and N348 is not essential for Ncd's motility; these results suggest that these two residues in the neck-head joint do not control Ncd's directionality.

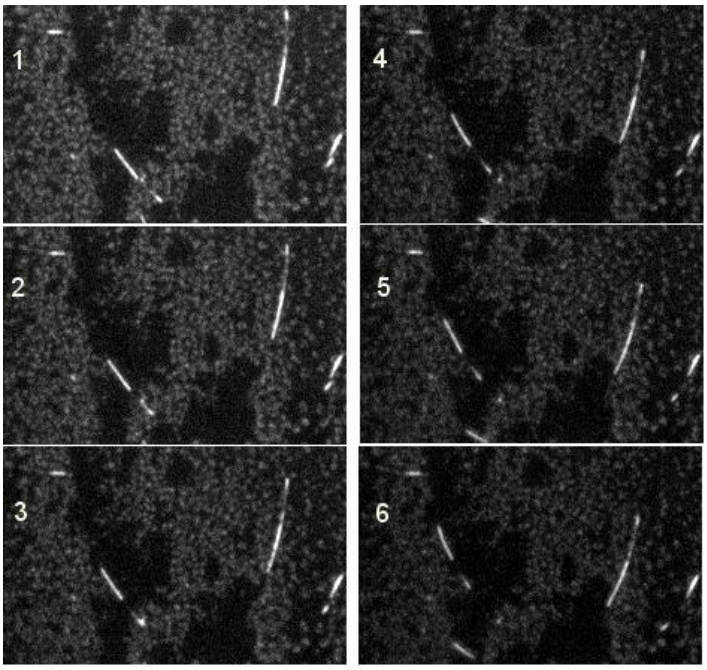

Figure 3-15: Image sequence of NcdGN348A. From 1 to 6, microtubule move with longer bright end (plus-end of microtubule) as a leading end indicating that NcdGN348A is a minus-end directed motor.

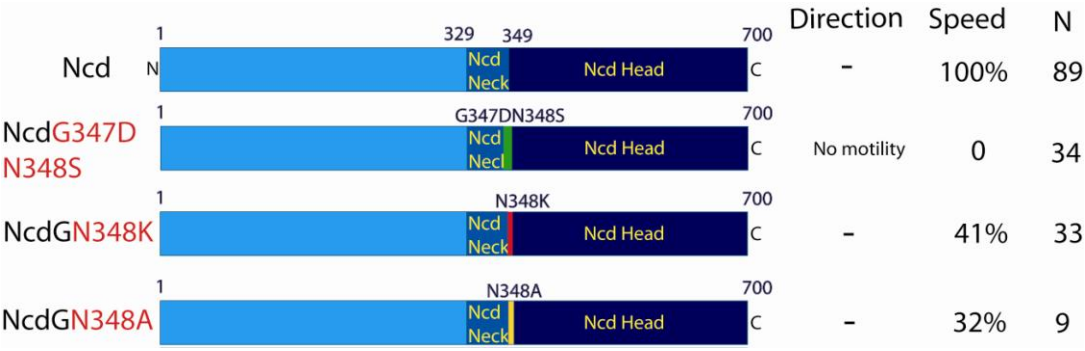

Figure 3-16: Ncd mutants to determine if the neck-head joint controls Ncd's directionality. Mutations in the residue number 348 to different amino acid (NcdN348A and NcdN348K) do not have large effect in both directionality and gliding speed, whereas mutations in residues 347 and 348 result in a non-functional motor.

3.2.4 The C-terminus of neck domain determines the directionality of Ncd.

As shown in amino acid sequence and crystal structure (Figure 3-1 at page 79 and Figure 3-16), Ncd can be divided into three major domains: the head, the neck and the stalk domains. According to one of previous directionality study of kinesin by Stewart et al., the stalk domain does not control Ncd's directionality(Stewart et al., 1993). Thus, the stalk domain is ruled out as determinant of Ncd's directionality. In addition, two studies on kinesin's directionality implied that head domain does not control kinesin motors' directionality(Case et al., 1997; Henningsen and Schliwa, 1997), and my work on NcdG347DN348S indicates that the neck-head joint is not responsible for Ncd's directionality. Therefore, only one of the components in Ncd is likely to control Ncd's directionality: the coiled-coil neck domain.

The neck domain is not the determinant of conventional kinesin's directionality (see the study of HKncd), however, it remains uncertain if the neck domain controls Ncd's direction. This neck domain was the focus of two previous studies for Ncd's directionality, and they reported that the direction of Ncd can be engineered successfully by modifying residues in this neck domain(Endow and Higuchi, 2000; Sablin et al., 1998). These results implied that the neck domain may be the determinant of Ncd's directionality. Sablin et al. replaced 12 amino acids of wild-type Ncd from the C-terminus of the neck domain with 12 random amino acids and showed that although the velocity is only about 2 percent of the velocity of wild-type Ncd, this Ncd mutant, Ncdr12, is a plus-end directed motor which is the reverse direction of wild-type Ncd(Sablin et al., 1998). The other group reported that Ncd can change it directionality

by modifying a single amino acid in the neck domain(Endow and Higuchi, 2000). In this study, the residue N340 was replaced with lysine, and this construct, NK11 (or NcdN340K), can move microtubules in one direction and switch to the reverse direction in the multiple motor gliding assays. This work suggests that NcdN340K is a bi-directional motor and implied that this residue N340 in the neck domain may be important for Ncd's directionality.

These two previous studies indicated that the neck domain may control Ncd's directionality. However, in this current study, these experimental could not be confirmed as reported previously. The Ncdr12 cannot facilitate microtubule's movement in the multiple motor gliding assays. This indicates that this mutant is a non-functional motor. This disabled Ncd mutant is largely expect, because a 12 random amino acid replacements that cannot form the coiled-coil structure in the neck domain results in a disrupted lever-arm power stroke mechanism that is required for Ncd's normal forward movement (Endres et al., 2006). Therefore, Ncdr12 cannot support microtubule movement. On the other hand, another neck domain mutant, NcdN340K, was reported to move the microtubules to forward and backward directions; however, in this current work the same Ncd mutant (NcdN340K) was tested and shown to be a minus-end directed motor which is the same as wild-type Ncd. While this contradicts the previous observations, I am confine that the number of polarity-marked microtubules (N=119) used in my experiment established the correct directionality for NcdN340K (Figure 3-17).

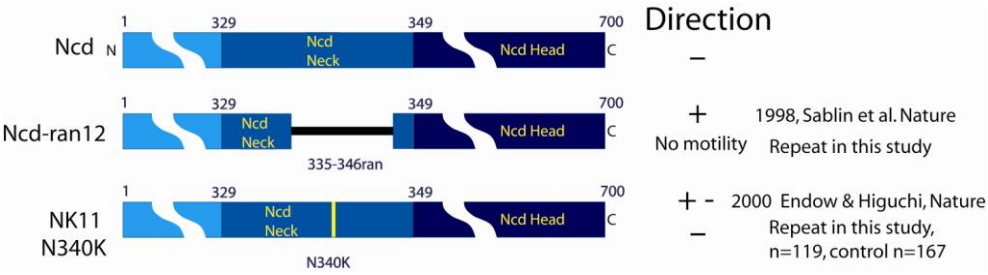

Figure 3-17: Mutated Ncd motors with reversed directionality. Ncd motors with their neck domain mutated (Ncd-r12 and NK11) are reported that they can move to reverse direction.

As discussed in the previous sections, the neck domain is the only part not being ruled out for controlling Ncd's directionality. To prove that the neck domain is the determinant and find out which part in the neck domain control Ncd's directionality, several experiments with truncated Ncd motors in it neck domain are necessary. Therefore, I engineered three Ncd mutants: Ncdhn1, Ncdhn2 and Ncd314. The Ncdhn1 is a mutated Ncd which has 7 amino acids from 331 to 337 in the neck domain eliminated to keep its coiled-coil structure intact and prevent disruption of the lever-arm power stroke mechanism. The Ncdhn2 is similar to Ncdhn1, but the eliminated neck part, which is from amino acid 334 to 340, is 3 more amino acids closer to the head domain. Another truncated Ncd is Ncd341 which is a Ncd having all stalk domain and the C-terminal part of the neck domain eliminated; that is, Ncd341 has the same head domain and neck domain as Ncdhn2 but all other coiled-coil parts are deleted.

The multiple motor gliding assays show that Ncdhn1 is a minus-end directed motor with 0.55 percent of velocity of wind-type Ncd(Figure 3-18) whereas Ncdhn2

and Ncd341 are non-functional motors and do not support microtubule movement (Figure 3-19).

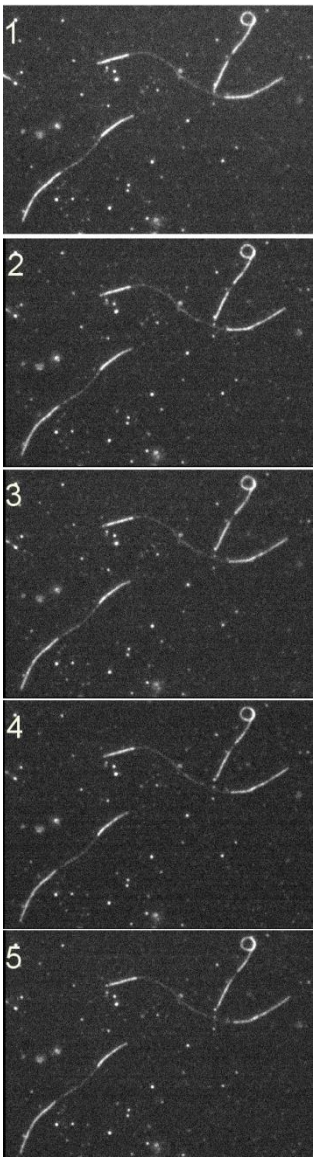

Figure 3-18: Image sequence for Ncdhn1 shows that Ncdhn1 is a minus-end directed motor.

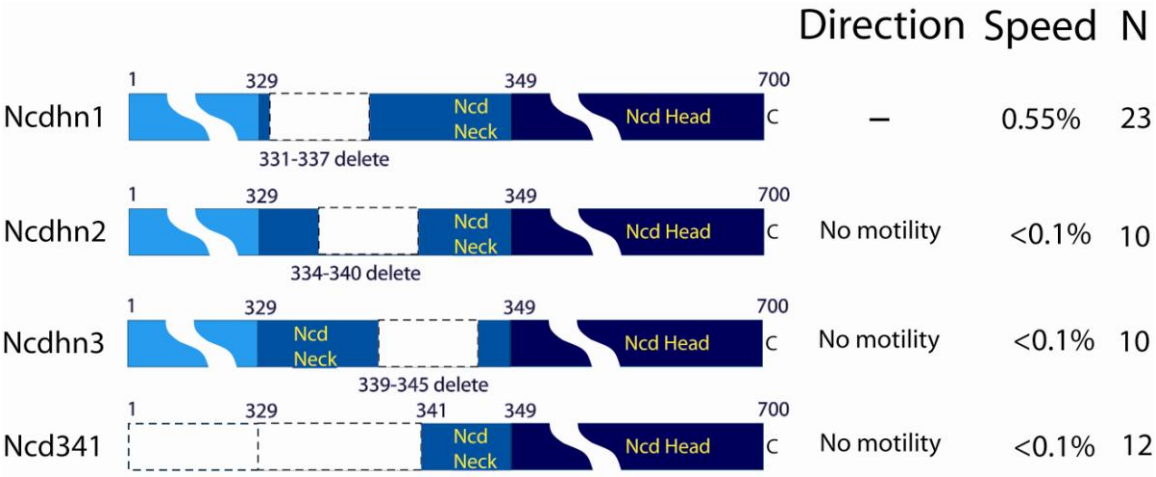

Figure 3-19: Ncd derivative mutants for study its directionality. Only Ncdhn1 is a function motor. Others are non functional motors.

The primary structure and the directionality of these Ncd mutants, wild-type Ncd and two of Ncd chimeras from previous study are shown in Figure 3-20. As can be seen the comparison of motors derivative from Ncd, no matter on whether head domain is replaced or the stalk domain is eliminated, as long as the C-terminus of the neck domain is intact, the Ncd mutants can support motility in gliding assay and move toward the minus-end of the microtubules. This suggests that the C-terminal segment of the neck domain may control Ncd's directionality.

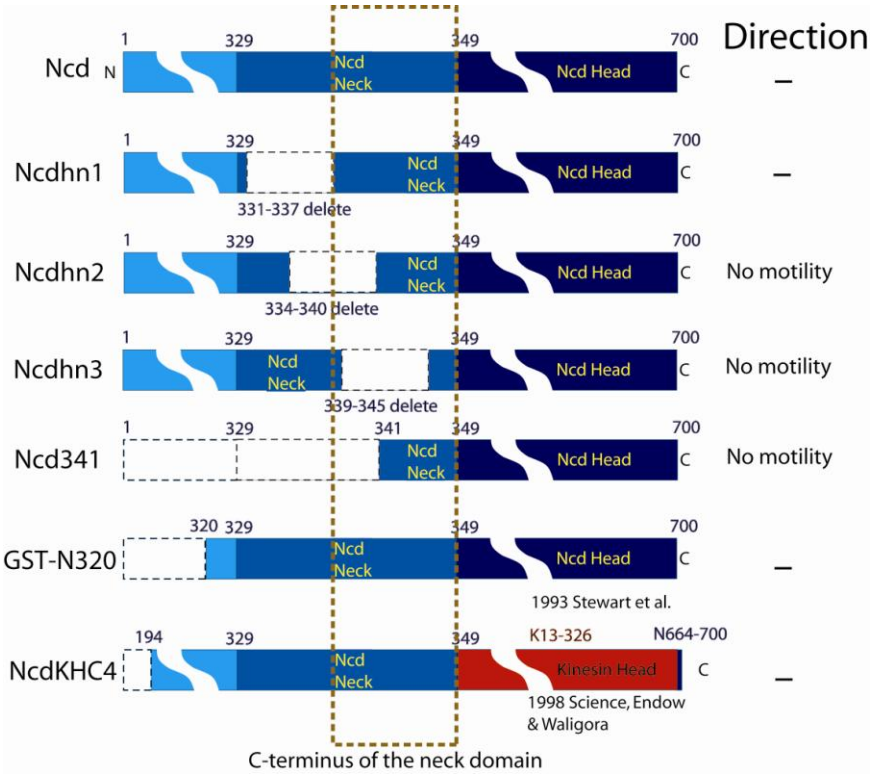

Figure 3-20: Ncd derivative mutants. Regardless the head domain is replaced (NcdKHC4) or the stalk domain is truncated (Ncdhn1 and GST-N320), as long as the C-terminus of the neck domain is intact (red dashed box), the motors are minus-end directed motors.

3.3 Conclusion

From the studies of kinesin mutants in the current work, I found that that the directionality determinant of the plus-end directioned kinesin, kinesin-1, may be the neck-linker and the determinant of the minus-end directioned kinesin, Ncd, may be the C-terminus of the neck domain. The similarity between the neck-linker of kinesin-1 and the C-terminal neck domain of Ncd motor is that they are right on the immediate

extension of the head domain. This coincident similarity indicates that different directional motors may use similar mechanisms to control their directions. One of the well known mechanisms that Ncd uses to provide its motion is the lever-arm-power-stroke mechanism. Kinesin-1 may use a mechanism similar to Ncd's mechanism by providing power-stroke via zipping and unzipping of neck-linker to the motor domain. The zipping and unzipping of neck-linker to the head domain is a crucial step to help ATP hydrolysis; thus, one might speculate the Ncd's rotation of the neck domain relative to its head domain may have similar function/control on the motor's ATPase activity. These similarities provide some insight into the conformation changes of kinesins during ATP turnover, however, strong, direct support to prove this hypothesis is lacking both in previous studies and this current work. Therefore, more detailed investigations of these mechanisms are necessary.

CHAPTER 4

INTRA-MOLECULAR COMMUNICATION BETWEEN KINESIN'S HEADS

4.1 Introduction

The molecular motor kinesin is responsible for several mechanical tasks inside cells. One of the roles for one of the kinesins, conventional kinesin, is long distance transport along microtubules. To accomplish this task, conventional kinesin need to continuously move along a single microtubule without detachment, known as processive movement. This processive movement is achieved by having the two motor domains (or head domains) of kinesin stepping forward alternately in a hand-over-hand fashion (Yildiz et al., 2004). Each step displaces the motor's neck domain (joint point of the two head domains) 8 nm forward along the microtubule (Schnitzer and Block, 1997). This continuous movement is so high, sometimes it can reach more than 100 steps for each time it encounters a microtubule(Thorn et al., 2000). Consequently, most researchers in the field believed that there must be a coordinating mechanism between the two heads to always keep at least one head attached and a tethered head moving forward the direction it is headed. Therefore, this coordination has been modeled by several theories which can be divided into two categories: strain gating models and non-strain gating models. The non-strain gating models state that the coordination

between two heads is a mechanism of steric inhibition in which a microtubule bound head masks the binding site on the microtubule to prevent the tethered head from moving forward(Alonso et al., 2007). The strain gating models, on the other hand, appear to have more general support than non-strain models because there is long-standing theoretical support (Hancock and Howard, 1999; Purcell et al., 2005; Shima et al., 2006)for this concept and most researchers believe (intuitively) that mechanical signals are the logical choice in coordinating the alternate mechanical stepping of kinesin's two heads. Most frequently it is proposed that mechanical (strain) signals between the heads accelerate or inhibit microtubule binding or unbinding events and thereby modulate the ATPase activity within specific nucleotide states of each(Block, 1998; Guydosh and Block, 2006; Hancock and Howard, 1999; Rosenfeld et al., 2003; Spudich, 2006; Tomishige and Vale, 2000; Uemura et al., 2002). Most studies which support strain gating models, assumed that during the two-head bound state strain is present between two motor domains, however, a direct validation of such internal strains and their consequences on the processive motion of kinesin remain elusive.

Recently, first direct evidence for the strain gating model, using single kinesin TIRFM and optical trapping experiments, was presented (Yildiz et al., 2008). In this study, kinesin's neck-linker was extended by different length of polyproline inserts. The biophysical properties of the polyproline insert mutants suggest that intramolecular strain facilitates kinesins forward movement. Concurrently, I used a similar strategy to test the idea that a mechanical strain coordinates kinesin's motion by inserting a set of flexible amino acids between the neck-linker and neck of kinesin. I expect these inserts

to disrupt the mechanical (strain) signal by which kinesin's heads communicate. Consequently, I expect kinesin's gliding velocity/motility to decline in the presence of these inserts. Surprisingly, my study shows that kinesin's velocity is not influenced by inserts, and the decline in processivity observed for the shortest insert (~30%) is somewhat recovered with increasing insert length. These results are in disagreement with strain-gating models and suggest that mechanical signal may not be essential for kinesin.

4.2 Result

The crystal structure of kinesin reveals that two heads are extended by neck-linker and jointed at the junction of the neck-linker and neck domain (Figure 4-1a) (Kozielski et al., 1997). If a mechanical signal is transmitted from one head to the other, mechanical stresses are transmitted along a pathway starting from the first head, passing through the first and second neck-linker to the second head. An additional flexible structure inserted in this pathway would disrupt or modulate the mechanical signal transduction. And therefore, by inserting flexible linker of variable length in this pathway one can test if the mechanical signal plays a major role in the coordination of the two heads. To test this hypothesis, truncated human kinesin, HK560 (referred to as wild-type kinesin in this study), was mutated by inserting a set of flexible amino acid residues into the junction of the neck-linker and the neck domains (Figure 4-1). All wild type kinesin and mutants, HKI1, HKI6 and HKI12, were C-terminally tagged with 6xHis sequence and a reactive cys-tag to facilitate protein for purification and dye labeling(Funatsu et al., 1997; Vale et al., 1996), respectively.

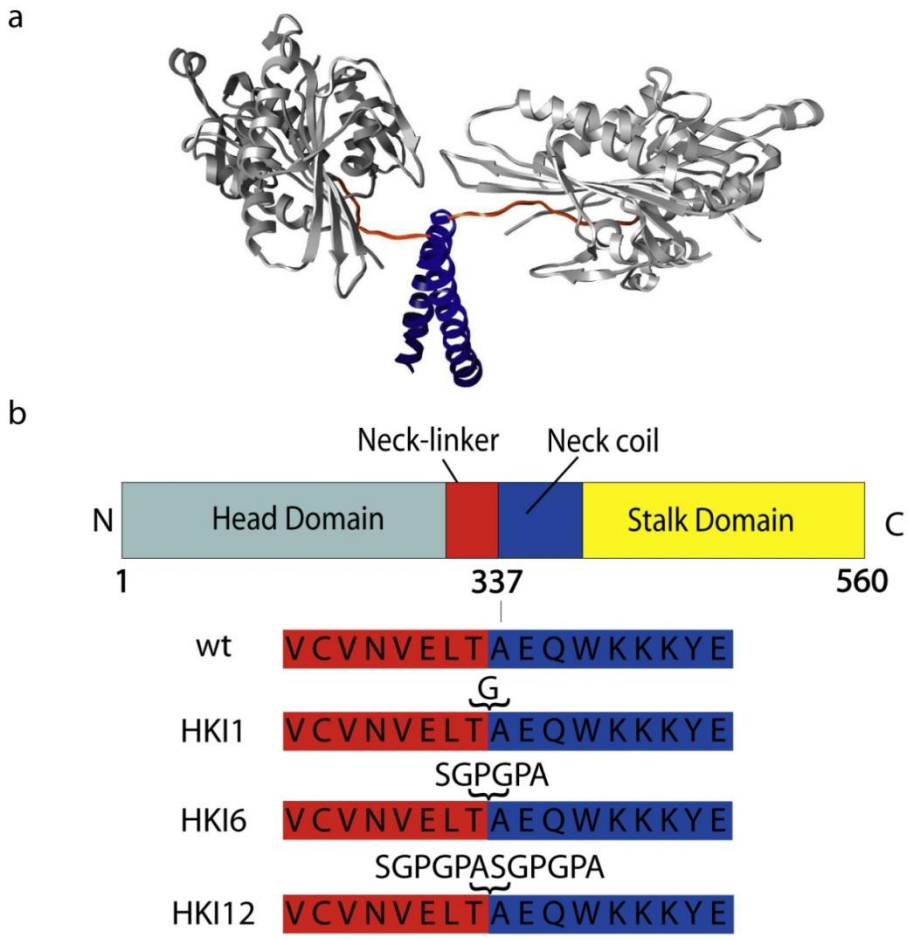

Figure 4-1: Wild-type kinesin and kinesin mutants. (a) Crystal structure wild type kinesin (PDB #3KIN(Kozielski et al., 1997)). The head domain, neck-linker and neck domain are shown in gray, red and blue, respectively. (b) Wild type human kinesin and mutants, HKI1, HKI6 and HKI12. The insertions are added between the end of neck linker Thr336 and the beginning of the neck coiled-coil Ala337, Ala339 in rat kinesin and Ala345 of Drosophila kinesin.

The motility of the single dye labeled motor was observed in a total internal reflection fluorescent microscope (TIRFM) and digitally recorded for further analysis. The analyzed average velocities of kinesin and mutants are provided in Figure 4-2. As can be seen, the velocities of mutants are slightly lower than that of wild type kinesin

(about 11%). The velocities for inserted mutants, however, are surprisingly similar regardless of the different length of insertions. We further confirmed, by ANOVA, that the average velocities of all mutants are statistically not significant different. (Adapting on 5% of error, the probability that the mean velocities of HKI1, HKI6 and HKI12 are equal is 94.8%.) The similarity in the velocity of the different kinesin constructs is consistent with a previous ATPase study for kinesins using the same insertions (Hackney el al., 2003) This work showed that the maximum ATP hydrolysis rate, K_{cat}, for insert mutants is slightly lower than that of wild type kinesin and has similar values for all mutants(Hackney et al., 2003). The consistent velocities of wild-type motor and insert mutants indicate that the flexible inserts do not delay or interrupt the intra-molecule signal transduction between two heads.

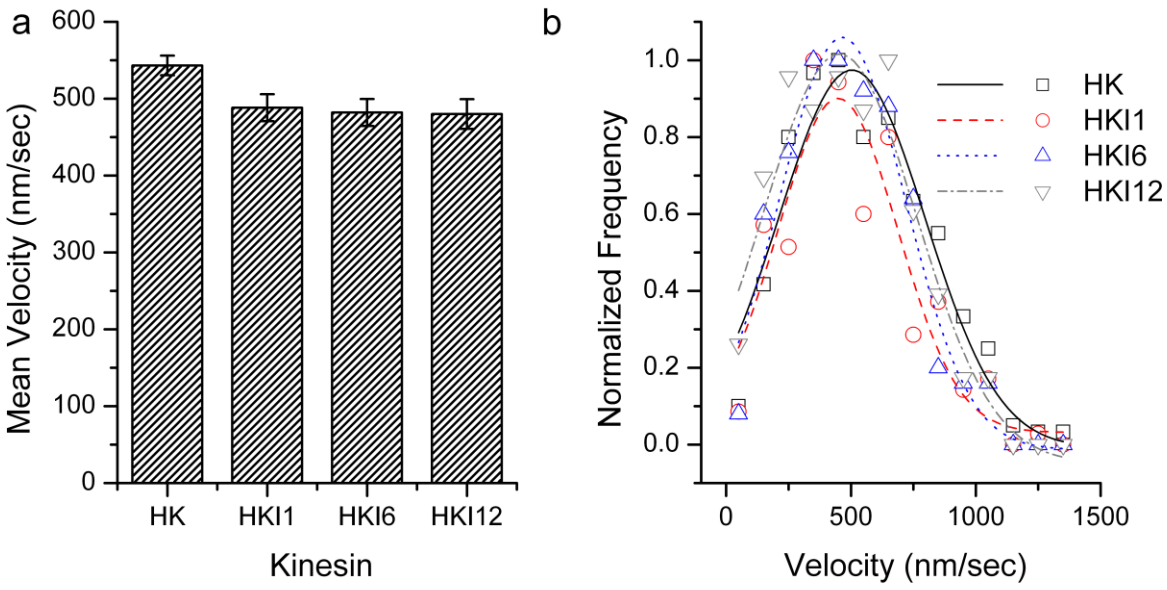

Figure 4-2: Velocities of wild-type kinesin and mutants. (a) Mean velocity of kinesins. (b) The velocity distribution for each kinesin for bin size 200 nm/sec. Lines indicate the fit of a Gaussian distribution to the velocity data of each kinesin.

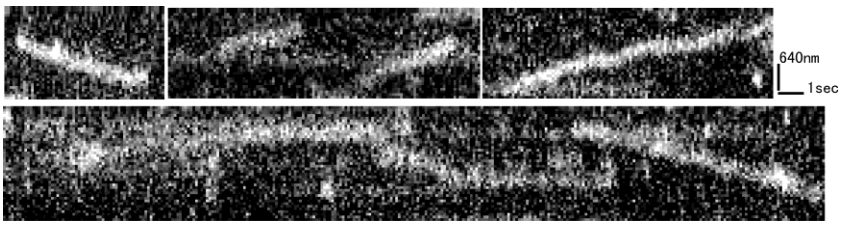

Figure 4-3: Kymographs showing the processive movement of several Cy3 labeled kinesin motors.

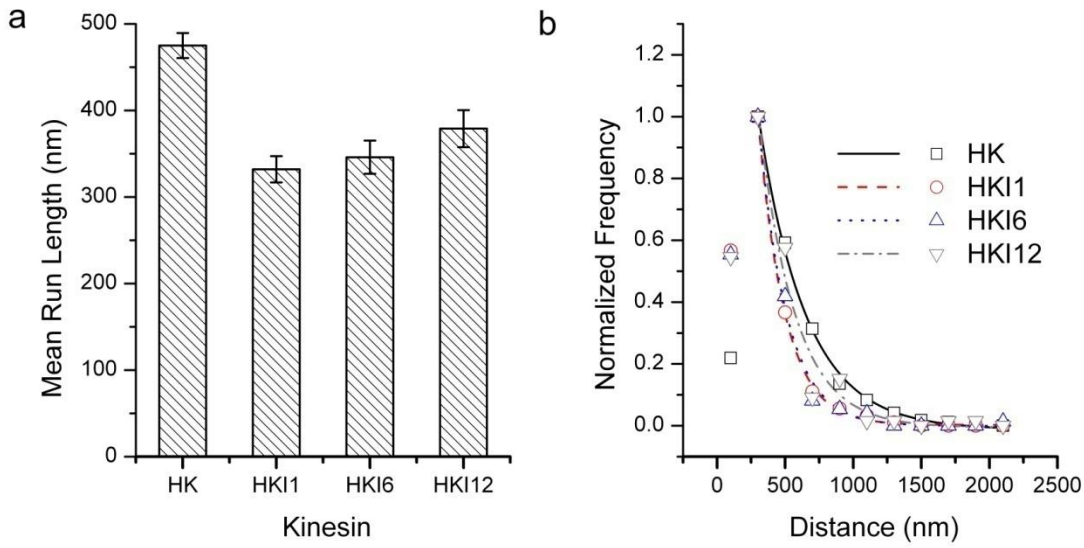

Figure 4-4: The processivities (run distance) for kinesin and mutants. (a) Mean run length for different kinesin. (b) The processivity distribution for kinesins using bin size of 200nm. The lines represent fits of the data for run length distance larger than 200nm with single exponential decay functions.

The average processivity (run length) for individual kinesins is shown in Figure 4-4. First of all, all kinesin mutant motors tested here are processive. However, insert kinesins have considerably impaired processivities. This significant reduction in processivity is, again, consistent with the biochemical processivity measurements ($K_{bi(ratio)}$) which declined as inserts were added into kinesin(Hackney et al., 2003). This drop indicates that the inserts alter the processivity mechanism in kinesin which may also be due to charge interaction between kinesin and tubulin. In addition, a surprising result was found in kinesin mutants. Inserted kinesin shows that the processivity gradually recovers as the insert becomes longer. This recovery in processivity by kinesins with longer inserts has not been shown before. However, one earlier study reports an increasing processivity associated with inserting/introducing more positive-charged residues in the neck region(Thorn et al., 2000). Notice that in work of Thorn et al.,(Thorn et al., 2000) the neck-neck linker region was extended by introducing positively charged residues into the neck. Therefore, this increase in run length for kinesin could be contributed to both charge interaction and neck extension effects.

4.3 Discussion

To determine whether mechanical signals coordinate the kinesin's two heads, I modified kinesin-1 by inserting a set of amino acids with different lengths. As presented above, mutated kinesinsHKI1, HKI6 and HKI12 do not show significant reductions in velocity. A similar phenomenon of comparable velocities has also been shown in previous reports in which identical amino acid residues are inserted into this

region(Hackney et al., 2003). These equivalent values of velocity of inserted kinesins indicate that the mechanical signal or "strain" between two heads for coordination are not disrupted by flexible inserts and, therefore, support the interpolation that the mechanical signal communication is not present in the rate limiting step of kinesin in its processive movement.

The finding in this work, however, is contradictory to the recent report by Yildiz et al. in which kinesins with extended neck-linkers significantly reduced the velocity while the processivity of kinesin mutants largely remain unchanged(Yildiz et al., 2008). The only difference between this previous report and my work is that two distinct sets of amino acid insertions are used. The work of Yildiz is used polyproline as insert. The structure of polyproline has been studied extensively (Schimmel and Flory, 1967; Schuler et al., 2005). The polyproline is rigid with a persistence length of 22 nm (Schimmel and Flory, 1967). Recent FRET work showed that polyproline is perhaps not as rigid as previously estimated and the persistence length may be as short as 4.4 nm (Schuler et al., 2005). However, in any case, the persistence length of polyproline is comparable to the dimension of kinesin's head domain (about 4 nm x 4 nm x 5 nm) and is much larger than the persistence length of the neck-linker (1.4nm) (Watanabe et al., 2002). This comparison suggests that the polyproline is considerably rigid for mechanical signal transmission. On the other hand, the inserts used in current work, (SGPGPA)n, contain multiple glycine residues, which are known to be highly flexible, and thus, these inserts will not be rigid. Besides, the rigidity of two different inserts was

further estimated by protein secondary structure prediction (Rost et al., 2004). The structure prediction shows that polyproline is less flexible than (SGPGPA)n insert.

The different rigidity of inserts is expected to contribute to different mechanical signal delaying and produce kinesin with different velocities. In mechanical dynamics, a mechanical signal transmitted through a rigid component, such as polyproline, will have little time delay. Therefore, kinesins with polyproline inserts should not decrease their velocity. On the contrary, a flexible component (this study) in the mechanical signal pathway will delay signal transmission to a certain degree and thus, kinesin mutants' velocity should decrease. However, this estimate of kinesin's velocity by simple mechanical dynamics is different from the kinesin's velocity provided in the recent study by Yildiz et al. and current work. This contradiction directly indicates either that the signal is not transmitted through the pathway or the polyproline is less rigid than (SGPGPA)n inserts. However, as we discussed in previous sections about the structure of kinesin and the rigidity studies for inserts, these explanations for the disagreement are not logical.

An alternative explanation for our finding is that the mechanical signal is not essential. The measurement presented in current work and the report from Yildiz et al. indicate that the signal does not delay in a more flexible pathway. Therefore, the assumption that a mechanical signal transmitted through this pathway is wrong, that is, the mechanical signal is not transmitted through this pathway. Thus, I conclude that the mechanical signal between two heads may be not essential for two heads' communication during kinesin's mechanochamical cycle.

In this study, kinesins with insert have severely reduced processivity, particularly in mutants with short inserts.. The decrease is probably due to the electric charge interaction while the recovery may be explained by the releasing of steric inhibition. The electric charge interaction between kinesin's neck coil and the C-terminal region of tubulin (E-hook) has been previously shown to contribute to the processivity of kinesin(Lakamper and Meyhofer, 2005; Thorn et al., 2000; Wang and Sheetz, 2000). Because the charge of the inserted residues used in our work is nearly neutral and these residues may replace interactions of the native neck domain, weak interactions between the neck coil and E-hook could be reduced. Therefore, the processivity of mutants significantly decreases.

In addition, it has been suggested that the binding of the freely diffusing head (tethered head) of kinesin could be inhibited to binding to microtubule by s steric mechanism(Alonso et al., 2007). On the other hand, the other study indicates the inhibited head can be released and bind to next binding site by increasing the length of inserts(Hackney et al., 2003). This release allows both heads to simultaneously bind to the microtubule surface and thus reduces the chance of kinesin detaching from microtubule. As long as the detaching rate is reduced, kinesin tends to stay more stably on microtubule, thus, increase the processivity. Therefore, I suggest that the recovery of processivity by longer inserts may be due to the extended neck-linker releasing the steric inhibition.

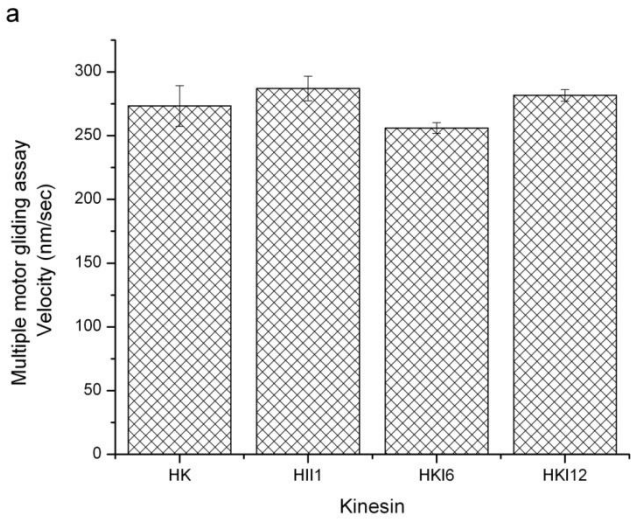

Figure 4-5: Average velocity of kinesin and inserted mutants from multiple motor gliding assays.

	Single motor					Multiple motor	
	Velocity		Processivity			Velocity	
Kinesin	*nm/sec*	*nm/sec*[a]	*nm*	*nm*[b]	*n*	*nm/sec*	*n*
HK	543±12.8	503±20.8	475±14.5	348.44±17.4	410	273±16.1	29
HKI1	488±17.5	445±32.0	332±15.2	190.28±8.6	193	287±9.67	29
HKI6	482±17.6	465±19.4	346±19.2	204.12±15.3	160	256±4.16	29
HKI12	480±19.4	456±24.5	379±21.4	265.06±47.7	160	281±4.15	29

Table 4-1: Mean values of kinesins' velocity and processivity (mean±sem). (a) Mean velocities from the Gaussian fits to each kinesin's velocity distribution. (b) Processivity as determined from fitting single exponential decay functions to the run length distribution of each kinesin.

CHAPTER 5

CONCLUSION AND FUTURE WORK

5.1 Kinesin's nanotechnology applications

In this dissertation, I presented three kinesin-powered microfluidic devices. Common to these devices is that they do not require external power sources or control system to function properly and achieve their objectives. The first two of these devices efficiently control the direction of microtubules to designated target regions or domains within the device architecture. The third device builds on these of kinesin and microtubule based nanotechnology and has the ability to effectively sort bio-molecules and concentrate them to a specified area. The demonstrations presented here illustrate that molecular motors-powered devices and instruments are now within the reach of applied engineering developments. Integration of technique development within the framework of the research can enhance the functionality of modern analytic and diagnostic instruments, make the highly portable and more efficiency, and therefore hold significant potential to increase the quality of life.

5.1.1 Micropump

Fundamentally, the circular microtubule sorting device performed as designed and expected, however, several additional modifications may enhance the performance and particularly have practical impact of these devices. Device structures that rectify the direction of microtubule movement are ready to be modified to an interesting device: a kinesin-powered micropump. As been shown in Chapter 2, our microtubule direction rectifier has >98% of all microtubules moving with a unique direction along the circular channel. If each of these unidirectional microtubules carries a micrometer-sized piston in a close circular channel, the device immediately becomes a micropump. This concept is similar to that shown in Figure 2-1b (page 20). To achieve this goal, several techniques, including the design and manufacture of the pistons, the crosslink between the pistons and the microtubules, the method to seal an open circular channel to a close channel and the way of characterizing the performance of this pump will need to be improved. Interestingly, theoretical model suggests that such molecular motor-powered micropumps are more efficient than the existing pumping devices(Bull et al., 2005). With the increasing demand for low cost, integrated pumps in diagnostic, microfluidic devices a molecular motor-based design strategy might prove to be highly valuable.

5.1.2 Sorter for multiple molecules

As shown in chapter 2.4, our kinesin-powered molecular sorter is able to sort single analyte species from complex mixtures of molecules. This device has the potential to extend its capabilities to simultaneously sorting multiple molecules and increasing the concentration of these molecules in specified locations. The basic

strategy for a multiple analyte molecular sorter is to modify microtubules with different antibodies such that they capture different target molecules. As long as the different microtubules can be sorted to different designated locations if will be possible to accurately differentiate select analytes. To achieve this goal, we plan to refine the method of labeling microtubules and method to separate them. One strategy we have explored in the past is to use electric fields supplied by tiny external instruments with to physically redirect microtubule motions. This may diminish the advantages of using kinesin to power the microdevices, on the other hand it should be possible to integrate the technology for these external fields into the same device.

5.2 Kinesin's directionality

5.2.1 Convention kinesin with reversed directionality

In chapter 3 I demonstrated that the directionality determinants of minus-end directed kinesin (Ncd) and plus-end directed kinesin-1 may be the C-terminal neck domain and the neck–linker, respectively. To confirm this model, two interesting studies should be performed which finally might allow us to produce kinesin mutants with reversed directionality. The first mutant, a kinesin mutant with reverse neck-linker, can confirm that the neck-linker control kinesin's directionality (Figure 5-1). This mutant motor would need to include additional residues to form an additional β-sheet with the neck-linker or cross-link to the neck-linker by disulfide bonds in order to reverse the orientation of the neck-linker as shown in Figure 5-1. The working hypothesis of the construct is that the zipping of reversed neck-linker will position the

tethered head of kinesin closer to next binding site in the minus direction of the microtubule (Figure 5-2). Therefore, this mutant can not only confirm the mechanism of neck-linker zipping but also the role that the neck-linker in controlling kinesin's directionality.

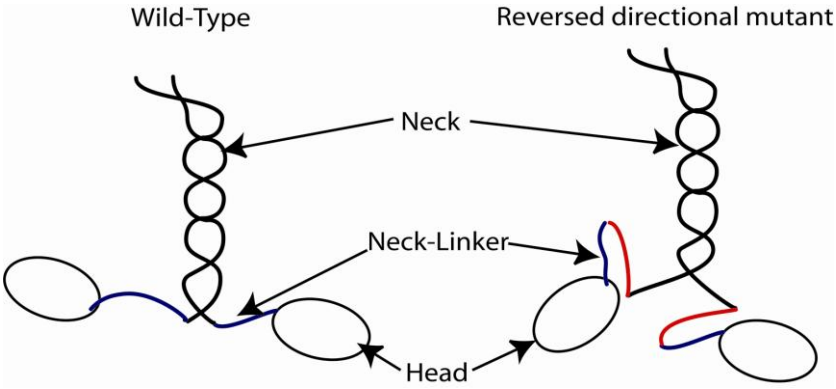

Figure 5-1: Wild-type kinesin and design concept for engineering a kinesin with reversed directionality. Additional residues (red) are added between neck-linker (blue) and neck (black) to cross-link with original neck-linker by disulfide bonds or via a β-sheet structure.

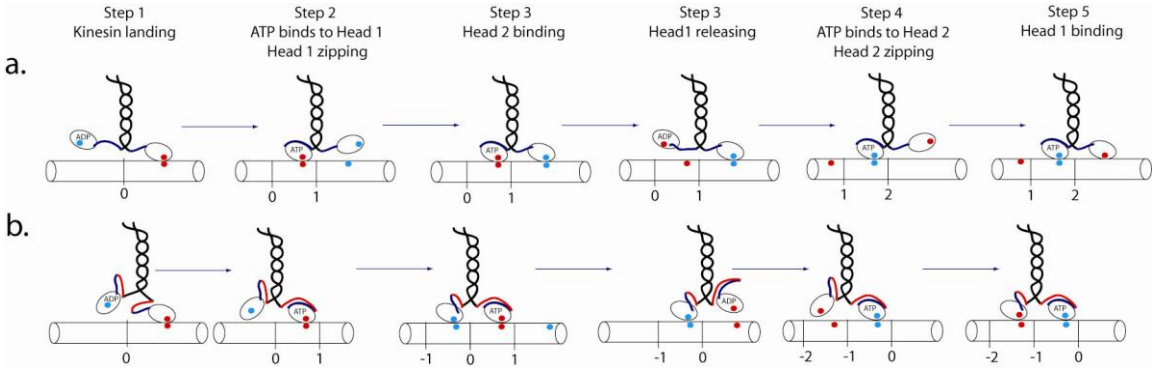

Figure 5-2: Working hypothesis for wild-type and reversed mutant kinesin. a. wild-type kinesin and b. reversed mutant kinesin. When wild-type kinesin' neck-linker zips, the neck-linker moves toward the next binding site in plus end (a: step 3 to step

4) whereas for mutant, the reversed neck-linker will bring kinesin to the next binding site in minus direction (b: step 3 to step 4).

5.2.2 Ncd mutant with reversed direction

I have presented evidence in support of the hypothesis that the C-terminal neck domain may control Ncd's directionality. In addition, one previous report suggests that Ncd uses a power stroke mechanism to move towards the minus-end direction (Endres et al., 2006). These two results indicate that an Ncd mutant with a reversed lever-arm will reverse Ncd's direction. This mutant of Ncd will have an intact C-terminal neck domain and a reversed coiled-coil neck domain and stalk domain. As shown in Figure 5-3b, an Ncd mutant with an additional alpha-helix sequence can generate a reverse-oriented lever-arm and when the intact C-terminal neck domain rotates, this reversed lever-arm will produce a displacement in the opposite direction. I hypothesize that such a reoriented "lever arm" will direct Ncd to plus-end of microtubules. This modification and mechanism are reminiscent to the work of Tsiavaliaris et al. for a myosin motor with a reversed direction(Tsiavaliaris et al., 2004).

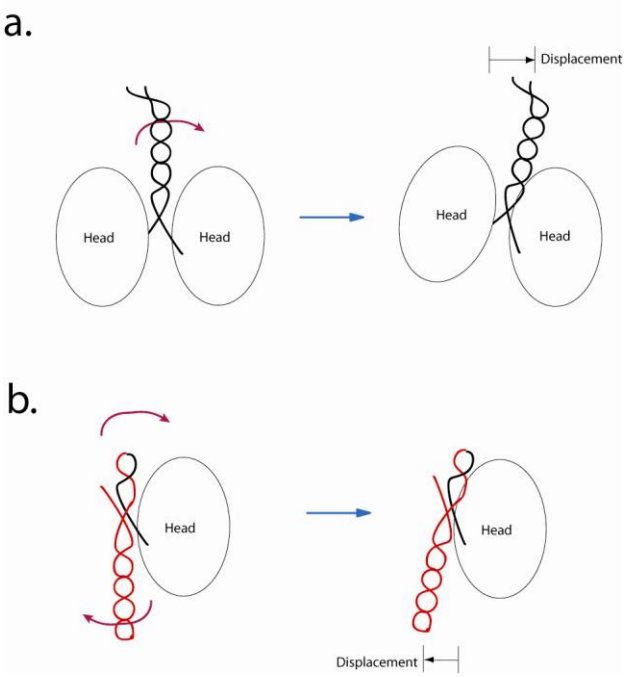

Figure 5-3: Working hypothesis for wild-type Ncd and a proposed Ncd mutant with altered directionality. a. Wild-type Ncd uses a power stroke to rotate its neck relative to microtubule-bound head domain and generate a minus-end directed motion. b. An engineered Ncd (proposed) with reversed directionality also uses a power stroke to rotate the neck region. However, the additional residues (red) in the mutated neck forma "reversed coiled-coil neck" that alters the direction of the power stroke.

5.2.3 C-terminal neck domain of Ncd may also control motor's ATPase

It is clear that the C-terminal neck of Ncd and the neck-linker of conventional kinesin have similar function in controlling the directionality, but the neck-linker may not only control the direction but also appears to be part of a sequence of structural events necessary to stimulate the ATPase activities of the motor. Therefore, it seems that the C-terminal neck of Ncd also plays a similar role in stimulating the ATPase activities as the neck-linker does in the conventional kinesin. To address this issue,

several additional Ncd mutants are required, including some with mutations and truncations in the C-terminal neck domain, and the biophysical and biochemical properties such as multiple motor gliding assays for characterizing their motility, laser trapping assays for measuring the step size and ATPase assays to determine the ATP coupling rate need to be characterized in detail.

5.3 Kinesin's strain coordination

As shown in Chapter 4, mutated kinesins with inserts between their neck and neck-linker do not change their velocity, but their run distances are reduced. This result implies that the reduced strain (due to the inserted neck-linker) between kinesin's two heads does not alter kinesin's speed, and therefore I conclude that the strain does not affect or alter the communication between kinesin's two heads.

This interpolation, however, is based on the assumption that the step size for wild-type and mutated kinesins are identical. If the step sizes for kinesin mutants are different, my conclusion may be inappropriate. Consequently for future studies, it is important to use laser trapping experiments to identify the step sizes of wild-type and mutated kinesins. The result from such laser trapping experiments may or may not immediately affect the conclusions of the strain coordination between two heads, but represent critical information to resolve this important molecular mechanism.

REFERENCES

Aizawa, H., Y. Sekine, R. Takemura, Z. Zhang, M. Nangaku, andN. Hirokawa. 1992. Kinesin family in murine central nervous system. *J Cell Biol* 119(5):1287-1296.

Allen, R.D., J. Metuzals, I. Tasaki, S.T. Brady, andS.P. Gilbert. 1982. Fast axonal transport in squid giant axon. *Science* 218(4577):1127-1129.

Alonso, M.C., D.R. Drummond, S. Kain, J. Hoeng, L. Amos, andR.A. Cross. 2007. An ATP gate controls tubulin binding by the tethered head of kinesin-1. *Science* 316(5821):120-123.

Asbury, C.L., A.N. Fehr, andS.M. Block. 2003. Kinesin moves by an asymmetric hand-over-hand mechanism. *Science* 302(5653):2130-2134.

Asenjo, A.B., Y. Weinberg, andH. Sosa. 2006. Nucleotide binding and hydrolysis induces a disorder-order transition in the kinesin neck-linker region. *Nat Struct Mol Biol* 13(7):648-654.

Bachand, G.D., S.B. Rivera, A. Carroll-Portillo, H. Hess, andM. Bachand. 2006. Active capture and transport of virus particles using a biomolecular motor-driven, nanoscale antibody sandwich assay. *Small* 2(3):381-385.

Bannigan, A., W.R. Scheible, W. Lukowitz, C. Fagerstrom, P. Wadsworth, C. Somerville, andT.I. Baskin. 2007. A conserved role for kinesin-5 in plant mitosis. *J Cell Sci* 120(Pt 16):2819-2827.

Block, S.M. 1998. Kinesin: what gives? *Cell* 93(1):5-8.

Block, S.M., L.S. Goldstein, andB.J. Schnapp. 1990. Bead movement by single kinesin molecules studied with optical tweezers. *Nature* 348(6299):348-352.

Brady, S.T. 1985. A novel brain ATPase with properties expected for the fast axonal transport motor. *Nature* 317(6032):73-75.

Brady, S.T., R.J. Lasek, andR.D. Allen. 1982. Fast axonal transport in extruded axoplasm from squid giant axon. *Science* 218(4577):1129-1131.

Brendza, R.P., L.R. Serbus, J.B. Duffy, andW.M. Saxton. 2000. A function for kinesin I in the posterior transport of oskar mRNA and Staufen protein. *Science* 289(5487):2120-2122.

Bull, J.L., A.J. Hunt, andE. Meyhofer. 2005. A theoretical model of a molecular-motor-powered pump. *Biomed Microdevices* 7(1):21-33.

Carson, J.H., K. Worboys, K. Ainger, andE. Barbarese. 1997. Translocation of myelin basic protein mRNA in oligodendrocytes requires microtubules and kinesin. *Cell Motil Cytoskeleton* 38(4):318-328.

Case, R.B., D.W. Pierce, N. Hom-Booher, C.L. Hart, andR.D. Vale. 1997. The directional preference of kinesin motors is specified by an element outside of the motor catalytic domain. *Cell* 90(5):959-966.

Case, R.B., S. Rice, C.L. Hart, B. Ly, andR.D. Vale. 2000. Role of the kinesin neck linker and catalytic core in microtubule-based motility. *Curr Biol* 10(3):157-160.

Chou, S.Y., P.R. Krauss, W. Zhang, L.J. Guo, andL. Zhuang. 1997. Sub-10 nm imprint lithography and applications. *J. Vac. Sci. Technol. B* 15(6):2897-2904.

Clemmens, J., H. Hess, R. Doot, C.M. Matzke, G.D. Bachand, andV. Vogel. 2004. Motor-protein "roundabouts": microtubules moving on kinesin-coated tracks through engineered networks. *Lab Chip* 4(2):83-86.

Clemmens, J., H. Hess, J. Howard, andV. Vogel. 2003a. Analysis of microtubule guidance in open microfabricated channels coated with the motor protein kinesin. *Langmuir* 19(5):1738-1744.

Clemmens, J., H. Hess, R. Lipscomb, Y. Hanein, K.F. Bohringer, C.M. Matzke, G.D. Bachand, B.C. Bunker, andV. Vogel. 2003b. Mechanisms of microtubule guiding on microfabricated kinesin-coated surfaces: Chemical and topographic surface patterns. *Langmuir* 19(26):10967-10974.

Cochran, J.C., C.A. Sontag, Z. Maliga, T.M. Kapoor, J.J. Correia, andS.P. Gilbert. 2004. Mechanistic analysis of the mitotic kinesin Eg5. *J Biol Chem* 279(37):38861-38870.

Cole, D.G. 1999a. Kinesin-II, coming and going. *J Cell Biol* 147(3):463-466.

Cole, D.G. 1999b. Kinesin-II, the heteromeric kinesin. *Cell Mol Life Sci* 56(3-4):217-226.

Cole, D.G. 2005. Intraflagellar transport: keeping the motors coordinated. *Curr Biol* 15(19):R798-801.

Cole, D.G., S.W. Chinn, K.P. Wedaman, K. Hall, T. Vuong, andJ.M. Scholey. 1993. Novel heterotrimeric kinesin-related protein purified from sea urchin eggs. *Nature* 366(6452):268-270.

Cole, D.G., D.R. Diener, A.L. Himelblau, P.L. Beech, J.C. Fuster, andJ.L. Rosenbaum. 1998. Chlamydomonas kinesin-II-dependent intraflagellar transport (IFT): IFT particles contain proteins required for ciliary assembly in Caenorhabditis elegans sensory neurons. *J Cell Biol* 141(4):993-1008.

Coppin, C.M., J.T. Finer, J.A. Spudich, andR.D. Vale. 1996. Detection of sub-8-nm movements of kinesin by high-resolution optical-trap microscopy. *Proc Natl Acad Sci U S A* 93(5):1913-1917.

Coy, D.L., W.O. Hancock, M. Wagenbach, andJ. Howard. 1999a. Kinesin's tail domain is an inhibitory regulator of the motor domain. *Nat Cell Biol* 1(5):288-292.

Coy, D.L., M. Wagenbach, andJ. Howard. 1999b. Kinesin takes one 8-nm step for each ATP that it hydrolyzes. *J Biol Chem* 274(6):3667-3671.

Dennis, J.R., J. Howard, andV. Vogel. 1999. Molecular shuttles: directed motion of microtubules slang nanoscale kinesin tracks. *Nanotechnology* 10(3):232-236.

Diefenbach, R.J., M. Miranda-Saksena, E. Diefenbach, D.J. Holland, R.A. Boadle, P.J. Armati, andA.L. Cunningham. 2002. Herpes simplex virus tegument protein US11 interacts with conventional kinesin heavy chain. *Journal of Virology* 76(7):3282-3291.

Endow, S.A. 1999. Determinants of molecular motor directionality. *Nat Cell Biol* 1(6):E163-167.

Endow, S.A., S. Henikoff, andL. Soler-Niedziela. 1990. Mediation of meiotic and early mitotic chromosome segregation in Drosophila by a protein related to kinesin. *Nature* 345(6270):81-83.

Endow, S.A., andH. Higuchi. 2000. A mutant of the motor protein kinesin that moves in both directions on microtubules. *Nature* 406(6798):913-916.

Endow, S.A., andK.W. Waligora. 1998. Determinants of kinesin motor polarity. *Science* 281(5380):1200-1202.

Endres, N.F., C. Yoshioka, R.A. Milligan, andR.D. Vale. 2006. A lever-arm rotation drives motility of the minus-end-directed kinesin Ncd. *Nature* 439(7078):875-878.

Felgner, H., R. Frank, andM. Schliwa. 1996. Flexural rigidity of microtubules measured with the use of optical tweezers. *J Cell Sci* 109 (Pt 2):509-516.

Fischer, T., A. Agarwal, andH. Hess. 2009. A smart dust biosensor powered by kinesin motors. *Nat. Nanotechnol.* 4(3):162-166.

Fujiwara, K., andT.D. Pollard. 1976. Fluorescent antibody localization of myosin in the cytoplasm, cleavage furrow, and mitotic spindle of human cells. *J Cell Biol* 71(3):848-875.

Funatsu, T., Y. Harada, H. Higuchi, M. Tokunaga, K. Saito, Y. Ishii, R.D. Vale, andT. Yanagida. 1997. Imaging and nano-manipulation of single biomolecules. *Biophys. Chem.* 68(1-3):63-72.

Gelles, J., B.J. Schnapp, andM.P. Sheetz. 1988. Tracking kinesin-driven movements with nanometre-scale precision. *Nature* 331(6155):450-453.

Gilbert, S.P., M.R. Webb, M. Brune, andK.A. Johnson. 1995. Pathway of processive ATP hydrolysis by kinesin. *Nature* 373(6516):671-676.

Gittes, F., E. Meyhofer, S. Baek, andJ. Howard. 1994. A Simple Piconewton-Scale in-Vitro Force Assay for Kinesin. *Biophys. J.* 66(2):A312-A312.

Goldstein, L.S.B. 2001. Kinesin molecular motors: Transport pathways, receptors, and human disease. *Proceedings of the National Academy of Sciences of the United States of America* 98(13):6999-7003.

Guydosh, N.R., andS.M. Block. 2006. Backsteps induced by nucleotide analogs suggest the front head of kinesin is gated by strain. *Proc Natl Acad Sci U S A* 103(21):8054-8059.

H. Lodish, A.B., P. Matsudaira, C. A.Kaiser, M.Kreger, M. P.Scott, S. L. Zipursky, J. Darnell. 2003. Molcular Cell Biology. W. H. Freeman and Company.

Hackney, D.D. 1995. Highly processive microtubule-stimulated ATP hydrolysis by dimeric kinesin head domains. *Nature* 377(6548):448-450.

Hackney, D.D., M.F. Stock, J. Moore, andR.A. Patterson. 2003. Modulation of kinesin half-site ADP release and kinetic processivity by a spacer between the head groups. *Biochemistry* 42(41):12011-12018.

Hancock, W.O., andJ. Howard. 1999. Kinesin's processivity results from mechanical and chemical coordination between the ATP hydrolysis cycles of the two motor domains. *Proc Natl Acad Sci U S A* 96(23):13147-13152.

Henningsen, U., andM. Schliwa. 1997. Reversal in the direction of movement of a molecular motor. *Nature* 389(6646):93-96.

Hess, H., G.D. Bachand, andV. Vogel. 2004a. Powering nanodevices with biomolecular motors. *Chemistry* 10(9):2110-2116.

Hess, H., G.D. Bachand, andV. Vogel. 2004b. Powering nanodevices with biomolecular motors. *Chemistry-a European Journal* 10(9):2110-2116.

Hess, H., J. Clemmens, C. Brunner, R. Doot, S. Luna, K.H. Ernst, andV. Vogel. 2005. Molecular self-assembly of "nanowires"and "nanospools" using active transport. *Nano Lett* 5(4):629-633.

Hess, H., J. Clemmens, C.M. Matzke, G.D. Bachand, B.C. Bunker, andV. Vogel. 2002. Ratchet patterns sort molecular shuttles. *Appl. Phys. A-Mater. Sci. Process.* 75(2):309-313.

Hess, H., C.M. Matzke, R.K. Doot, J. Clemmens, G.D. Bachand, B.C. Bunker, andV. Vogel. 2003. Molecular shuttles operating undercover: A new photolithographic approach for the fabrication of structured surfaces supporting directed motility. *Nano Letters* 3(12):1651-1655.

Hess, H., andV. Vogel. 2001. Molecular shuttles based on motor proteins: active transport in synthetic environments. *J Biotechnol* 82(1):67-85.

Heuser, J., T. Schroer, E. Steuer, J. Gelles, andM. Sheetz. 1988. Kinesin Structure in the Electron-Microscope. *Cell Motility and the Cytoskeleton* 11(3):202-203.

Higuchi, H., andS.A. Endow. 2002. Directionality and processivity of molecular motors. *Curr Opin Cell Biol* 14(1):50-57.

Hiratsuka, Y., T. Tada, K. Oiwa, T. Kanayama, andT.Q.P. Uyeda. 2001. Controlling the direction of kinesin-driven microtubule movements along microlithographic tracks. *Biophysical Journal* 81(3):1555-1561.

Hirokawa, N. 2000. Stirring up development with the heterotrimeric kinesin KIF3. *Traffic* 1(1):29-34.

Hirokawa, N., andY. Noda. 2008. Intracellular transport and kinesin superfamily proteins, KIFs: structure, function, and dynamics. *Physiol Rev* 88(3):1089-1118.

Hirokawa, N., Y. Noda, andY. Okada. 1998. Kinesin and dynein superfamily proteins in organelle transport and cell division. *Curr Opin Cell Biol* 10(1):60-73.

Hirokawa, N., andR. Takemura. 2004. Kinesin superfamily proteins and their various functions and dynamics. *Exp Cell Res* 301(1):50-59.

Hoff, J.D., L.J. Cheng, E. Meyhofer, L.J. Guo, andA.J. Hunt. 2004. Nanoscale protein patterning by imprint lithography. *Nano Letters* 4(5):853-857.

Hollenbeck, P.J., andJ.A. Swanson. 1990. Radial extension of macrophage tubular lysosomes supported by kinesin. *Nature* 346(6287):864-866.

Howard, J. 1996. The movement of kinesin along microtubules. *Annual Review of Physiology* 58:703-729.

Howard, J., A.J. Hudspeth, andR.D. Vale. 1989. Movement of microtubules by single kinesin molecules. *Nature* 342(6246):154-158.

Howard, J., andA.A. Hyman. 1993. Preparation of marked microtubules for the assay of the polarity of microtubule-based motors by fluorescence microscopy. *Methods Cell Biol* 39:105-113.

Hua, W., E.C. Young, M.L. Fleming, andJ. Gelles. 1997. Coupling of kinesin steps to ATP hydrolysis. *Nature* 388(6640):390-393.

Hunt, A.J., F. Gittes, andJ. Howard. 1994. The force exerted by a single kinesin molecule against a viscous load. *Biophys J* 67(2):766-781.

Hyman, A., D. Drechsel, D. Kellogg, S. Salser, K. Sawin, P. Steffen, L. Wordeman, andT. Mitchison. 1991. Preparation of Modified Tubulins. *Method Enzymol.* 196:478-485.

Ionov, L., M. Stamm, andS. Diez. 2005. Size sorting of protein assemblies using polymeric gradient surfaces. *Nano Lett* 5(10):1910-1914.

Jia, L., S.G. Moorjani, T.N. Jackson, andW.O. Hancock. 2004. Microscale transport and sorting by kinesin molecular motors. *Biomed Microdevices* 6(1):67-74.

Jiang, W., M.F. Stock, X. Li, andD.D. Hackney. 1997. Influence of the kinesin neck domain on dimerization and ATPase kinetics. *J Biol Chem* 272(12):7626-7632.

Johnston, G.C., J.A. Prendergast, andR.A. Singer. 1991. The Saccharomyces cerevisiae MYO2 gene encodes an essential myosin for vectorial transport of vesicles. *J Cell Biol* 113(3):539-551.

Kallipolitou, A., D. Deluca, U. Majdic, S. Lakamper, R. Cross, E. Meyhofer, L. Moroder, M. Schliwa, andG. Woehlke. 2001. Unusual properties of the fungal conventional kinesin neck domain from Neurospora crassa. *Embo J* 20(22):6226-6235.

Kapitein, L.C., E.J. Peterman, B.H. Kwok, J.H. Kim, T.M. Kapoor, andC.F. Schmidt. 2005. The bipolar mitotic kinesin Eg5 moves on both microtubules that it crosslinks. *Nature* 435(7038):114-118.

Kapoor, T.M., T.U. Mayer, M.L. Coughlin, andT.J. Mitchison. 2000. Probing spindle assembly mechanisms with monastrol, a small molecule inhibitor of the mitotic kinesin, Eg5. *Journal of Cell Biology* 150(5):975-988.

Kim, T., L.-J. Cheng, M.-T. Kao, E.F. Hasselbrink, L. Guo, andE. Meyhofer. 2009. Biomolecular motor-driven molecular sorter. *Lab on a Chip* 9(9):1282-1285.

Kim, T., M.T. Kao, E.F. Hasselbrink, andE. Meyhofer. 2007a. Active alignment of microtubules with electric fields. *Nano Letters* 7(1):211-217.

Kim, T., M.T. Kao, E.F. Hasselbrink, andE. Meyhofer. 2008. Nanomechanical model of microtubule translocation in the presence of electric fields. *Biophysical Journal* 94(10):3880-3892.

Kim, T., M.T. Kao, E. Meyhofer, andE.F. Hasselbrink. 2007b. Biomolecular motor-driven microtubule translocation in the presence of shear flow: analysis of redirection behaviours. *Nanotechnology* 18(2).

Kim, T., andE. Meyhofer. 2008. Nanofluidic concentration of selectively extracted biomolecule anattes by microtubules. *Anal. Chem.* 80(14):5383-5390.

Kojima, H., E. Muto, H. Higuchi, andT. Yanagida. 1997. Mechanics of single kinesin molecules measured by optical trapping nanometry. *Biophys J* 73(4):2012-2022.

Kondo, S., R. Sato-Yoshitake, Y. Noda, H. Aizawa, T. Nakata, Y. Matsuura, andN. Hirokawa. 1994. KIF3A is a new microtubule-based anterograde motor in the nerve axon. *J Cell Biol* 125(5):1095-1107.

Kozielski, F., S. De Bonis, W.P. Burmeister, C. Cohen-Addad, andR.H. Wade. 1999. The crystal structure of the minus-end-directed microtubule motor protein ncd reveals variable dimer conformations. *Structure* 7(11):1407-1416.

Kozielski, F., S. Sack, A. Marx, M. Thormahlen, E. Schonbrunn, V. Biou, A. Thompson, E.M. Mandelkow, andE. Mandelkow. 1997. The crystal structure of dimeric kinesin and implications for microtubule-dependent motility. *Cell* 91(7):985-994.

Kull, F.J., E.P. Sablin, R. Lau, R.J. Fletterick, andR.D. Vale. 1996. Crystal structure of the kinesin motor domain reveals a structural similarity to myosin. *Nature* 380(6574):550-555.

Kural, C., H. Kim, S. Syed, G. Goshima, V.I. Gelfand, andP.R. Selvin. 2005. Kinesin and dynein move a peroxisome in vivo: a tug-of-war or coordinated movement? *Science* 308(5727):1469-1472.

Lakamper, S., A. Kallipolitou, G. Woehlke, M. Schliwa, andE. Meyhofer. 2003. Single fungal kinesin motor molecules move processively along microtubules. *Biophys J* 84(3):1833-1843.

Lakamper, S., andE. Meyhofer. 2005. The E-hook of tubulin interacts with kinesin's head to increase processivity and speed. *Biophys J* 89(5):3223-3234.

Lawrence, C.J., R.K. Dawe, K.R. Christie, D.W. Cleveland, S.C. Dawson, S.A. Endow, L.S. Goldstein, H.V. Goodson, N. Hirokawa, J. Howard, R.L. Malmberg, J.R. McIntosh, H. Miki, T.J. Mitchison, Y.

Okada, A.S. Reddy, W.M. Saxton, M. Schliwa, J.M. Scholey, R.D. Vale, C.E. Walczak, andL. Wordeman. 2004. A standardized kinesin nomenclature. *J Cell Biol* 167(1):19-22.

Li-Jing Cheng , M.-T.K., Edgar Meyhöfer, L. Jay Guo. 2005. Highly Efficient Guiding of Microtubule Transport with Imprinted CYTOP Nanotracks. *Small* 11(4):409-414.

Limberis, L., andR.J. Stewart. 2000. Toward kinesin-powered microdevices. *Nanotechnology* 11(2):47-51.

Lin, C.T., M.T. Kao, K. Kurabayashi, andE. Meyhofer. 2006. Efficient designs for powering microscale devices with nanoscale biomolecular motors. *Small* 2(2):281-287.

Lin, C.T., M.T. Kao, K. Kurabayashi, andE. Meyhofer. 2008. Self-contained biomolecular motor-driven protein sorting and concentrating in an ultrasensitive microfluidic chip. *Nano Letters* 8(4):1041-1046.

Lindquist, N.C., A. Lesuffleur, H. Im, andS.-H. Oh. 2009. Sub-micron resolution surface plasmon resonance imaging enabled by nanohole arrays with surrounding Bragg mirrors for enhanced sensitivity and isolation. *Lab on a Chip* 9(3):382-387.

Mabuchi, I., andM. Okuno. 1977. The effect of myosin antibody on the division of starfish blastomeres. *J Cell Biol* 74(1):251-263.

Mandelkow, E., andE.-M. Mandelkow. 2002. Kinesin motors and disease. *Trends in Cell Biology* 12(12):585-591.

Marszalek, J.R., X.R. Liu, E.A. Roberts, D. Chui, J.D. Marth, D.S. Williams, andL.S.B. Goldstein. 2000. Genetic evidence for selective transport of opsin and arrestin by kinesin-II in mammalian photoreceptors. *Cell* 102(2):175-187.

Marszalek, J.R., P. Ruiz-Lozano, E. Roberts, K.R. Chien, andL.S.B. Goldstein. 1999. Situs inversus and embryonic ciliary morphogenesis defects in mouse mutants lacking the KIF3A subunit of kinesin-II. *Proceedings of the National Academy of Sciences of the United States of America* 96(9):5043-5048.

McDonald, H.B., andL.S. Goldstein. 1990. Identification and characterization of a gene encoding a kinesin-like protein in Drosophila. *Cell* 61(6):991-1000.

Meyhofer, E., andJ. Howard. 1995. The force generated by a single kinesin molecule against an elastic load. *Proc Natl Acad Sci U S A* 92(2):574-578.

Nakata, T., andN. Hirokawa. 1995. Point mutation of adenosine triphosphate-binding motif generated rigor kinesin that selectively blocks anterograde lysosome membrane transport. *J Cell Biol* 131(4):1039-1053.

Nicholson, W.V., M. Lee, K.H. Downing, andE. Nogales. 1999. Cryo-electron microscopy of GDP-tubulin rings. *Cell Biochem Biophys* 31(2):175-183.

Nitta, T., andH. Hess. 2005. Dispersion in active transport by kinesin-powered molecular shuttles. *Nano Lett* 5(7):1337-1342.

Nonaka, S., Y. Tanaka, Y. Okada, S. Takeda, A. Harada, Y. Kanai, M. Kido, andN. Hirokawa. 1998. Randomization of left-right asymmetry due to loss of nodal cilia generating leftward flow of extraembryonic fluid in mice lacking KIF3B motor protein. *Cell* 95(6):829-837.

Pazour, G.J., andJ.L. Rosenbaum. 2002. Intraflagellar transport and cilia-dependent diseases. *Trends in Cell Biology* 12(12):551-555.

Purcell, T.J., H.L. Sweeney, andJ.A. Spudich. 2005. A force-dependent state controls the coordination of processive myosin V. *Proc Natl Acad Sci U S A* 102(39):13873-13878.

Qin, H.M., J.L. Rosenbaum, andM.M. Barr. 2001. An autosomal recessive polycystic kidney disease gene homolog is involved in intraflagellar transport in C-elegans ciliated sensory neurons. *Current Biology* 11(6):457-461.

Quirino, J.P., andS. Terabe. 1998. Exceeding 5000-fold concentration of dilute analytes in micellar electrokinetic chromatography. *Science* 282(5388):465-468.

Ramachandran, S., K.H. Ernst, G.D. Bachand, V. Vogel, andH. Hess. 2006. Selective loading of kinesin-powered molecular shuttles with protein cargo and its application to biosensing. *Small* 2(3):330-334.

Rangel, E.C., W.C.A. Bento, M.E. Kayama, W.H. Schreiner, andN.C. Cruz. 2003. Enhancement of polymer hydrophobicity by SF6 plasma treatment and argon plasma immersion ion implantation. *Surface and Interface Analysis* 35(2):179-183.

Ray, S., E. Meyhofer, R.A. Milligan, andJ. Howard. 1993. Kinesin follows the microtubule's protofilament axis. *J Cell Biol* 121(5):1083-1093.

Rice, S., A.W. Lin, D. Safer, C.L. Hart, N. Naber, B.O. Carragher, S.M. Cain, E. Pechatnikova, E.M. Wilson-Kubalek, M. Whittaker, E. Pate, R. Cooke, E.W. Taylor, R.A. Milligan, andR.D. Vale. 1999. A structural change in the kinesin motor protein that drives motility. *Nature* 402(6763):778-784.

Rietdorf, J., A. Ploubidou, I. Reckmann, A. Holmstrom, F. Frischknecht, M. Zettl, T. Zimmermann, andM. Way. 2001. Kinesin-dependent movement on microtubules precedes actin-based motility of vaccinia virus. *Nature Cell Biology* 3(11):992-1000.

Robinson, D.N., andJ.A. Spudich. 2004. Mechanics and regulation of cytokinesis. *Curr Opin Cell Biol* 16(2):182-188.

Rosenfeld, S.S., P.M. Fordyce, G.M. Jefferson, P.H. King, andS.M. Block. 2003. Stepping and stretching. How kinesin uses internal strain to walk processively. *J Biol Chem* 278(20):18550-18556.

Rost, B., G. Yachdav, andJ.F. Liu. 2004. The PredictProtein server. *Nucleic Acids Research* 32:W321-W326.

Ruff, C., M. Furch, B. Brenner, D.J. Manstein, andE. Meyhofer. 2001. Single-molecule tracking of myosins with genetically engineered amplifier domains. *Nat Struct Biol* 8(3):226-229.

Sablin, E.P., R.B. Case, S.C. Dai, C.L. Hart, A. Ruby, R.D. Vale, andR.J. Fletterick. 1998. Direction determination in the minus-end-directed kinesin motor ncd.

Sablin, E.P., F.J. Kull, R. Cooke, R.D. Vale, andR.J. Fletterick. 1996. Crystal structure of the motor domain of the kinesin-related motor ncd. *Nature* 380(6574):555-559.

Sack, S., J. Muller, A. Marx, M. Thormahlen, E.M. Mandelkow, S.T. Brady, andE. Mandelkow. 1997. X-ray structure of motor and neck domains from rat brain kinesin. *Biochemistry* 36(51):16155-16165.

Sakowicz, R., M.S. Berdelis, K. Ray, C.L. Blackburn, C. Hopmann, D.J. Faulkner, andL.S.B. Goldstein. 1998. A marine natural product inhibitor of kinesin motors. *Science* 280(5361):292-295.

Schimmel, P.R., andP.J. Flory. 1967. Conformational Energy and Configurational Statistics of Poly-L-Proline. *Proceedings of the National Academy of Sciences of the United States of America* 58(1):52-&.

Schnitzer, M.J., andS.M. Block. 1997. Kinesin hydrolyses one ATP per 8-nm step. *Nature* 388(6640):386-390.

Schnitzer, M.J., K. Visscher, andS.M. Block. 2000. Force production by single kinesin motors. *Nat Cell Biol* 2(10):718-723.

Schott, D., J. Ho, D. Pruyne, andA. Bretscher. 1999. The COOH-terminal domain of Myo2p, a yeast myosin V, has a direct role in secretory vesicle targeting. *J Cell Biol* 147(4):791-808.

Schuler, B., E.A. Lipman, P.J. Steinbach, M. Kumke, andW.A. Eaton. 2005. Polyproline and the "spectroscopic ruler" revisited with single-molecule fluorescence. *Proceedings of the National Academy of Sciences of the United States of America* 102(8):2754-2759.

Sharp, D.J., K.R. Yu, J.C. Sisson, W. Sullivan, andJ.M. Scholey. 1999. Antagonistic microtubule-sliding motors position mitotic centrosomes in Drosophila early embryos. *Nat Cell Biol* 1(1):51-54.

Shima, T., K. Imamula, T. Kon, R. Ohkura, andK. Sutoh. 2006. Head-head coordination is required for the processive motion of cytoplasmic dynein, an AAA+ molecular motor. *J Struct Biol* 156(1):182-189.

Sindelar, C.V., M.J. Budny, S. Rice, N. Naber, R. Fletterick, andR. Cooke. 2002. Two conformations in the human kinesin power stroke defined by X-ray crystallography and EPR spectroscopy. *Nat Struct Biol* 9(11):844-848.

Sodeik, B. 2000. Mechanisms of viral transport in the cytoplasm. *Trends Microbiol* 8(10):465-472.

Spudich, J.A. 2006. Molecular motors take tension in stride. *Cell* 126(2):242-244.

Stewart, R.J., J.P. Thaler, andL.S. Goldstein. 1993. Direction of microtubule movement is an intrinsic property of the motor domains of kinesin heavy chain and Drosophila ncd protein. *Proc Natl Acad Sci U S A* 90(11):5209-5213.

Stracke, R., K.J. Bohm, L. Wollweber, J.A. Tuszynski, andE. Unger. 2002. Analysis of the migration behaviour of single microtubules in electric fields. *Biochem. Biophys. Res. Commun.* 293(1):602-609.

Svoboda, K., andS.M. Block. 1994. Force and velocity measured for single kinesin molecules. *Cell* 77(5):773-784.

Svoboda, K., C.F. Schmidt, B.J. Schnapp, andS.M. Block. 1993. Direct observation of kinesin stepping by optical trapping interferometry. *Nature* 365(6448):721-727.

Takeda, S., H. Yamazaki, D.H. Seog, Y. Kanai, S. Terada, andN. Hirokawa. 2000. Kinesin superfamily protein 3 (KIF3) motor transports fodrin-associating vesicles important for neurite building. *J Cell Biol* 148(6):1255-1265.

Tanaka, Y., Y. Kanai, Y. Okada, S. Nonaka, S. Takeda, A. Harada, andN. Hirokawa. 1998. Targeted disruption of mouse conventional kinesin heavy chain, kif5B, results in abnormal perinuclear clustering of mitochondria. *Cell* 93(7):1147-1158.

Terada, S., M. Kinjo, andN. Hirokawa. 2000. Oligomeric tubulin in large transporting complex is transported via kinesin in squid giant axons. *Cell* 103(1):141-155.

Thorn, K.S., J.A. Ubersax, andR.D. Vale. 2000. Engineering the processive run length of the kinesin motor. *J Cell Biol* 151(5):1093-1100.

Tomishige, M., andR.D. Vale. 2000. Controlling kinesin by reversible disulfide cross-linking. Identifying the motility-producing conformational change. *J Cell Biol* 151(5):1081-1092.

Tsiavaliaris, G., S. Fujita-Becker, andD.J. Manstein. 2004. Molecular engineering of a backwards-moving myosin motor. *Nature* 427(6974):558-561.

Uemura, S., K. Kawaguchi, J. Yajima, M. Edamatsu, Y.Y. Toyoshima, andS. Ishiwata. 2002. Kinesin-microtubule binding depends on both nucleotide state and loading direction. *Proc Natl Acad Sci U S A* 99(9):5977-5981.

Vale, R.D., T. Funatsu, D.W. Pierce, L. Romberg, Y. Harada, andT. Yanagida. 1996. Direct observation of single kinesin molecules moving along microtubules. *Nature* 380(6573):451-453.

Vale, R.D., andR.A. Milligan. 2000. The way things move: looking under the hood of molecular motor proteins. *Science* 288(5463):88-95.

Vale, R.D., T.S. Reese, andM.P. Sheetz. 1985a. Identification of a novel force-generating protein, kinesin, involved in microtubule-based motility. *Cell* 42(1):39-50.

Vale, R.D., B.J. Schnapp, T. Mitchison, E. Steuer, T.S. Reese, andM.P. Sheetz. 1985b. Different axoplasmic proteins generate movement in opposite directions along microtubules in vitro. *Cell* 43(3 Pt 2):623-632.

Vale, R.D., B.J. Schnapp, T.S. Reese, andM.P. Sheetz. 1985c. Movement of organelles along filaments dissociated from the axoplasm of the squid giant axon. *Cell* 40(2):449-454.

Vale, R.D., B.J. Schnapp, T.S. Reese, andM.P. Sheetz. 1985d. Organelle, bead, and microtubule translocations promoted by soluble factors from the squid giant axon. *Cell* 40(3):559-569.

van den Heuvel, M.G., C.T. Butcher, S.G. Lemay, S. Diez, andC. Dekker. 2005a. Electrical docking of microtubules for kinesin-driven motility in nanostructures. *Nano Lett* 5(2):235-241.

van den Heuvel, M.G., C.T. Butcher, R.M. Smeets, S. Diez, andC. Dekker. 2005b. High rectifying efficiencies of microtubule motility on kinesin-coated gold nanostructures. *Nano Lett* 5(6):1117-1122.

van den Heuvel, M.G.L., C.T. Butcher, R.M.M. Smeets, S. Diez, andC. Dekker. 2005c. High rectifying efficiencies of microtubule motility on kinesin-coated gold nanostructures. *Nano Letters* 5(6):1117-1122.

van den Heuvel, M.G.L., M.P. De Graaff, andC. Dekker. 2006. Molecular sorting by electrical steering of microtubules in kinesin-coated channels. *Science* 312(5775):910-914.

van den Heuvel, M.G.L., andC. Dekker. 2007. Motor proteins at work for nanotechnology. *Science* 317(5836):333-336.

Verhey, K.J., D. Meyer, R. Deehan, J. Blenis, B.J. Schnapp, T.A. Rapoport, andB. Margolis. 2001. Cargo of kinesin identified as JIP scaffolding proteins and associated signaling molecules. *J Cell Biol* 152(5):959-970.

Verma, V., W.O. Hancock, andJ.M. Catchmark. 2009. Nanoscale patterning of kinesin motor proteins and its role in guiding microtubule motility. *Biomed Microdevices* 11(2):313-322.

Visscher, K., M.J. Schnitzer, andS.M. Block. 1999. Single kinesin molecules studied with a molecular force clamp. *Nature* 400(6740):184-189.

Walker, R.A., E.D. Salmon, andS.A. Endow. 1990. The Drosophila claret segregation protein is a minus-end directed motor molecule. *Nature* 347(6295):780-782.

Wang, Z., andM.P. Sheetz. 2000. The C-terminus of tubulin increases cytoplasmic dynein and kinesin processivity. *Biophys J* 78(4):1955-1964.

Watanabe, K., P. Nair, D. Labeit, M.S.Z. Kellermayer, M. Greaser, S. Labeit, andH. Granzier. 2002. Molecular mechanics of cardiac titin's PEVK and N2B spring elements. *Journal of Biological Chemistry* 277(13):11549-11558.

Woehlke, G., A.K. Ruby, C.L. Hart, B. Ly, N. Hom-Booher, andR.D. Vale. 1997. Microtubule interaction site of the kinesin motor. *Cell* 90(2):207-216.

Woehlke, G., andM. Schliwa. 2000a. Directional motility of kinesin motor proteins. *Biochim Biophys Acta* 1496(1):117-127.

Woehlke, G., andM. Schliwa. 2000b. Walking on two heads: the many talents of kinesin. *Nat Rev Mol Cell Biol* 1(1):50-58.

Wong, Y.L., K.A. Dietrich, N. Naber, R. Cooke, andS.E. Rice. 2009. The Kinesin-1 tail conformationally restricts the nucleotide pocket. *Biophys J* 96(7):2799-2807.

Yildiz, A., andP.R. Selvin. 2005. Fluorescence imaging with one nanometer accuracy: application to molecular motors. *Acc Chem Res* 38(7):574-582.

Yildiz, A., M. Tomishige, A. Gennerich, andR.D. Vale. 2008. Intramolecular strain coordinates kinesin stepping behavior along microtubules. *Cell* 134(6):1030-1041.

Yildiz, A., M. Tomishige, R.D. Vale, andP.R. Selvin. 2004. Kinesin walks hand-over-hand. *Science* 303(5658):676-678.

Yokokawa, R., S. Takeuchi, T. Kon, M. Nishiura, K. Sutoh, andH. Fujita. 2004. Unidirectional transport of kinesin-coated beads on microtubules oriented in a microfluidic device. *Nano Letters* 4(11):2265-2270.

Yun, M., C.E. Bronner, C.G. Park, S.S. Cha, H.W. Park, andS.A. Endow. 2003. Rotation of the stalk/neck and one head in a new crystal structure of the kinesin motor protein, Ncd. *Embo J* 22(20):5382-5389.

Zhao, C., J. Takita, Y. Tanaka, M. Setou, T. Nakagawa, S. Takeda, H.W. Yang, S. Terada, T. Nakata, Y. Takei, M. Saito, S. Tsuji, Y. Hayashi, andN. Hirokawa. 2001. Charcot-Marie-Tooth disease type 2A caused by mutation in a microtubule motor KIF1B beta. *Cell* 105(5):587-597.